Forced Periodic Non-isothermal Operation of

Chromatographic Columns

Dissertation
zur Erlangung des akademischen Grades

Doktor rerum naturalium
(Dr. rer. nat.)

von M.Sc. Adnan Hayat

geb. am 10.04.1991 in Swabi, Pakistan

genehmigt durch die Fakultät für Mathematik
der Otto-von-Guericke-Universität Magdeburg, Deutschland

Gutachter: Prof. Dr. Gerald Warnecke
Prof. Dr. Andreas Seidel-Morgenstern
Prof. Dr. Shamsul Qamar

Eingereicht am : 24.10.2023
Verteidigung am: 26.01.2024

Forced Periodic Non-isothermal Operation of

Chromatographic Columns

Dissertation
Submitted for the academic degree

Doctor rerum naturalium
(Dr. rer. nat.)

by: M.Sc. Adnan Hayat
born on: 10.04.1991 in Swabi, Pakistan

approved from the Faculty of Mathematics
Otto-von-Guericke-University, Magdeburg, Germany

Referees: Prof. Dr. Gerald Warnecke
Prof. Dr. Andreas Seidel-Morgenstern
Prof. Dr. Shamsul Qamar

Submitted on: 24.10.2023
Defended on: 26.01.2024

Abstract

Chromatography is a scientific method that allows individual identification of a substance by breaking it down into its components and compounds. One of its many types is High Performance Liquid Chromatography (HPLC), which uses solvents as the mobile phase and small solid particles as the stationary phase. In this process, the strongly retained components may take longer time under isocratic conditions, which lowers productivity and increases eluent consumption. For that reason, gradient operations are used to increase productivity exploiting additional degrees of freedom.

In this work, two different mathematical models, such as the equilibrium model (EM) and the equilibrium dispersive model (EDM), are applied to study the effects of forced temperature gradients generated by an external heat source. The mass balance is related to the applied temperature by a function called the adsorption isotherm, which is assumed to be linear in concentration and nonlinear in temperature.

To illustrate the principle, the column is divided into two segments: Segment I and Segment II. Segment I is kept at reference temperature while segment II is exposed to the aforementioned heat source placed on its conducting walls. The temperature variations in the later segment are introduced step-wise.

As a preliminary case, the EM is coupled with the ideal temperature step gradients, whose analytical solution is derived by a well-known method of characteristics. This method generates solution trajectories which provides ideal and hypothetical but still useful information about retention behavior in different temperature regimes.

The EM is then extended to EDM by introducing dispersion term on the right side of the equation. To obtain more realistic results, this mass balance is coupled with other realistic temperature profiles governed by an energy balance, as well as with its simplified version. The updated models are then solved numerically using the finite volume method (FVM). Because of its reliability in solving conservation laws, the FVM in fluxes form has produced stable solutions. To ensure this stability, the time step restriction is calculated separately for each model.

Using the above models, periodic switching patterns of temperature are formulated for specific elution scenarios to achieve a shorter cycle time compared to the conventional isocratic conditions. The choice of switching times is entirely system specific and may need to be adjusted for each separation problem. Several operating conditions, including injections of a single component as well as a ternary mixture, are considered to validate the model equations and propose a numerical algorithm.

A considerable increase in the column's productivity, ranging from 16% to 20%, is observed. Most of the parameters considered in this study are specific to a particular case study taken from a parallel experimental PhD project [39], the results of which are compared at the end with our theoretical results. A very good agreement is observed in both sets of results.

By considering linear equilibria and step gradients, this study provides a useful tool to predict shorter cycle times in order to make less productive HPLC processes more productive. The study can be extended by considering nonlinear equilibria in concentration and more sophisticated forms of gradients instead of step gradients to deal more real world HPLC problems.

Zusammenfassung

Die Chromatographie ist eine wissenschaftliche Methode, die eine individuelle Identifizierung einer Substanz ermöglicht, indem sie in ihre Bestandteile und Verbindungen zerlegt wird. Eine ihrer vielen Arten ist die Hochleistungsflüssigkeitschromatographie (HPLC), bei der Lösungsmittel als mobile Phase und kleine Feststoffpartikel als stationäre Phase verwendet werden. Bei diesem Verfahren können die stark zurückgehaltenen Komponenten unter isokratischen Bedingungen länger brauchen, was die Produktivität senkt und den Eluentenverbrauch erhöht. Aus diesem Grund werden Gradientenverfahren eingesetzt, um die Produktivität unter Ausnutzung zusätzlicher Freiheitsgrade zu erhöhen.

In dieser Arbeit werden zwei verschiedene mathematische Modelle, wie das Gleichgewichts-Modell (EM) und das Gleichgewichts-Dispersion-Modell (EDM), angewandt, um die Auswirkungen von erzwungenen Temperaturgradienten, die durch eine externe Wärmequelle erzeugt werden, zu untersuchen. Die Massenbilanz wird durch eine Funktion, die so genannte Adsorptionsisotherme, mit der angelegten Temperatur in Beziehung gesetzt, wobei davon ausgegangen wird, dass sie bei der Konzentration linear und bei der Temperatur nichtlinear ist.

Zur Veranschaulichung des Prinzips wird die Säule in zwei Segmente unterteilt: Segment I und Segment II. Das Segment I wird auf Referenztemperatur gehalten, während das Segment II der oben genannten Wärmequelle ausgesetzt wird, die an den leitenden Wänden angebracht ist. Die Temperaturschwankungen im zweiten Segment werden schrittweise eingeführt.

In einem ersten Fall wird das EM mit den idealen Temperaturgradienten gekoppelt, deren analytische Lösung durch eine bekannte Methode der Charakteristiken abgeleitet wird. Diese Methode erzeugt Lösungstrajektorien, die ideale und hypothetische, aber dennoch nützliche Informationen über das Retentionsverhalten in verschiedenen Temperaturregimen liefern.

Das EM wird dann durch Einführung eines Dispersionsterms auf der rechten Seite der Gleichung auf das EDM erweitert. Um realistischere Ergebnisse zu erhalten, wird diese Massenbilanz mit anderen realistischen Temperaturprofilen gekoppelt, die von einer Energiebilanz gesteuert werden, sowie mit ihrer vereinfachten Version. Die aktualisierten Modelle werden dann numerisch mit der Finite-Volumen-Methode (FVM) gelöst. Aufgrund ihrer Zuverlässigkeit bei der Lösung von Erhaltungsgesetzen hat die FVM in Form von Flüssen stabile Lösungen hervorgebracht. Um diese Stabilität zu gewährleisten, wird die Zeitschrittbeschränkung für jedes Modell separat berechnet.

Unter Verwendung der oben genannten Modelle werden periodische Schaltmuster der Temperatur für spezifische Elutionsszenarien formuliert, um eine kürzere Zykluszeit im Vergleich zu den herkömmlichen isokratischen Bedingungen zu erreichen. Die Wahl der Schaltzeiten ist völlig systemspezifisch und muss möglicherweise für jedes Trennproblem angepasst werden. Es werden mehrere Betriebsbedingungen, einschließlich Injektionen einer einzelnen Komponente sowie eines ternären Gemischs, betrachtet, um die Modellgleichungen zu validieren und einen numerischen Algorithmus vorzuschlagen.

iv

Es wird eine beträchtliche Steigerung der Produktivität der Säule beobachtet, die von 16%
bis 20% reicht. Die meisten der in dieser Studie betrachteten Parameter sind spezifisch für
eine bestimmte Fallstudie aus einem parallelen experimentellen Promotionsprojekt [39], dessen
Ergebnisse am Ende mit unseren theoretischen Ergebnissen verglichen werden. Es wird eine sehr
gute Übereinstimmung zwischen den beiden Ergebnissen festgestellt.

Durch die Berücksichtigung linearer Gleichgewichte und Stufengradienten bietet diese Studie
ein nützliches Instrument zur Vorhersage kürzerer Zykluszeiten, um weniger produktive HPLC-
Prozesse produktiver zu machen. Die Studie kann erweitert werden, indem nichtlineare Gle-
ichgewichte in der Konzentration und anspruchsvollere Formen von Gradienten anstelle von
Stufengradienten berücksichtigt werden, um realitätsnähere HPLC-Probleme zu behandeln.

Collaborations and Research Publications

This work represents the theoretical aspect of a comprehensive research project focused on optimizing the productivity of liquid chromatographic columns through temperature gradient operations. This work was carried out in collaboration between the research group "Physical and Chemical Foundations of Process Engineering (PCF)" at the Max Planck Institute for Dynamics of Complex Technical Systems, Magdeburg, and the Institute for Analysis and Numerics (IAN) at Otto von Guericke University (OvGU) Magdeburg.

Thanks to the experimental project, which was essential for our research. In collaboration with Dr. Xinghai An's concurrent PhD thesis, crucial parameters for an actual chromatographic system were determined and experimental results were obtained that are in good agreement with our theoretical predictions. The relevance of our project is greatly enhanced by this harmonious synthesis of theory and practice.

The outcomes and discoveries resulting from this research have been disseminated through two published journal articles. These publications contribute to the existing body of knowledge in this field. They are given below

1. Hayat, A.; An, X.; Qamar, S.; Warnecke, G.; Seidel-Morgenstern, A. Theoretical Analysis of Forced Segmented Temperature Gradients in Liquid Chromatography. *Processes* **2019**, *7*, 846.

   Author contributions: The main work was done and the manuscript was written by Adnan Hayat. Xinghai An helped in determining the relevant parameters. Shamsul Qamar guided in deriving the solutions and implementing them under MATLAB. Gerald Warnecke analyzed and evaluated the consistency of the mathematical model. This study was proposed and supervised by Andreas Seidel-Morgenstern.

   Ref. [37] - Further new results are discussed in Chapter 3.

2. An, X.; Hayat, A.; Lee, J. W.; Qamar, S.; Warnecke, G.; Seidel-Morgenstern, A. Analysis and experimental demonstration of temperature step gradients in preparative liquid chromatography. *Journal of Chromatography A* **2022**, *1665*, 462831.

   Author contributions: Xinghai An led the original draft writing, investigations, and validation. Adnan Hayat developed the methodology, managed software, and curated data. Ju Weon Lee contributed to methodology and manuscript review. Shamsul Qamar and Gerald Warnecke participated in manuscript review. Andreas Seidel-Morgenstern provided conceptualization, supervision, and manuscript review.

   Ref. [38] - The theoretical part of this article is discussed in section 4.1.

List of Figures

List of Tables

List of Symbols

Latin Letters

Symbol	Unit	Designation
A	m^2 or cm^2	Cross-Sectional Area of the Column
a_n	-	Henry Constants of Component n
c	g/L or mol/L	Mobile Phase Concentration
C_p	J/(g.K)	Specific Heat Capacity
$c_{n,\text{inj}}$	g/L or mol/L	Injected n-Concentrations
D$_z$	m^2/s cm^2/min	Axial Dispersion in Concentration
F	-	Phase Ratio
F^c	-	Numerical Flux in Mass Balance
F^T	-	Numerical Flux in Energy Balance
$\Delta H_{A,n}$	kJ/mol or kJ/g	Enthalpy of Adsorption of Component n
J	-	Jacobian Matrix
$\mathring{m}_{L-S}$	g or mol	Mass Flowing From the Liquid to the Solid Phase
$\mathring{m}_{S-L}$	g or mol	Mass Flowing From the Solid to the Liquid Phase
m$_n$	g	Mass of Component n
N_c	-	Number of Components
N_p	-	Number of Theoretical Plates
P$_n$	gh^{-1}L^{-1}	Productivity of Component n
q	g/L or mol/L	Stationary Phase Concentration
R	J/(mol·K) or J/(g·K)	Universal Gas Constant
T_{R}	Kelvin [K]	Reference Temperature
T_{L}	Kelvin [K]	Low Temperature
T_{H}	Kelvin [K]	High Temperature
t_{inj}^p	s or min	Injection p
$t_{n,\text{max}}^p$	s or min	Retention Time of Component n of Injection p
t_0	s or min	Initial Time
t_{dead}	min	Dead Time in the Experiments
t_k	s or min	Dimensional Switching Times
$t_{n,\text{m}}^p$	-	Dimensional Time of Component n of Injection p to Reach z_{m}
Δt_c^p	s or min	Dimensional Cycle Time of Component n of Injection p
t	s or min	Dimensional Time Coordinate
Δt_{saf}^p	s or min	Dimensional Safety Margin for Injection p

Δt	s or min	Dimensional Time Step
Δt_{inj}	s or min	Injection Time or Injection Period
T	Kelvin [K]	Temperature Variable
T_{w}	Kelvin [K]	Wall Temperature
t_{R_0}	s or min	Retention Time of a Non-Retained Component
u	cm/min or m/s	Interstitial Velocity
x	-	Non-Dimensional Space Coordinate
Δx	-	Non-Dimensional Space Step
x_{m}	-	One-Half of the Non-Dimensional Space Coordinate
x_{max}	-	Length of the Non-Dimensional Space Coordinate
z_0	m or cm	Inlet Point of the Column
z_{m}	m or cm	One Half of the Column
z_{max}	m or cm	Length of the Column
Δz	m or cm	Dimensional Space Step
z	m or cm	Dimensional Space Coordinate
z_n^p	-	Trajectory of Component n of Injection p

Superscripts

L	-	Liquid Phase
S	-	Solid Phase

Subscripts

0	-	Initial Value
c	-	Cycle
grad	-	Gradient
H	-	High
hyp	-	Associated Quantity Hypothetically Considered
inc	-	Percent Increase in the Associated Quantity
iso	-	Isocratic
L	-	Low
$L-S$	-	Liquid to Solid
max	-	Maximum
n	-	Associated Quantity for Component n
R	-	Reference
$S-L$	-	Solid to Liquid
w	-	Wall
n, ad	-	Associated Quantity for Adsorption Front of Component n
n, de	-	Associated Quantity for Desorption Front of Component n
n, col	-	Associated Quantity of Component n Collected
n, inj	-	Associated Quantity of Component n Injected
n, m	-	Associated Quantity of Adsorption Front of Component n at Column's Mid

$n, \max$	-	Associated Quantity of Adsorption Front of Component n at Column's Exit
$n, \max, \mathrm{ad}$	-	Associated Quantity of Adsorption Front of Component n at Column's Exit

Greek Letters

Symbol	Unit	Designation
$\alpha_{i,j} = \frac{a_i}{a_j}$	-	Separation Factor Between Components i and j
α_{w}	J/(min.cm^3.K)	Wall Heat Transfer Coefficient
$\lambda_{1,2}$	-	Eigen Values 1 and 2
λ_{z}	m^2/s cm^2/min	Axial Dispersion in Thermal Conductivity
Ω	min	Empirical Adjustment for Calculation of Injection Time
ρ	g/cm^3	Density
σ_i	-	Spatial Cells made of $i+1$ Spatial Points
τ	-	Non-Dimensional Time Coordinate
τ_0	-	Initial Non-Dimensional Time
τ_{inj}^p	-	Non-Dimensional Injection Time of Injection p
τ_{s}	-	A Random Switching Time Selected from τ_k
$\tau_{n,\max}^p$	-	Non-Dimensional Retention Time of Component n of Injection p
$\tau_{n,\mathrm{m}}^p$	-	Non-Dimensional Time of Component n of Injection p to Reach x_{m}
τ_k	-	Non-Dimensional Switching Times
$\Delta\tau$	-	Non-Dimensional Time Step
$\Delta\tau_c^p$	-	Non-Dimensional Cycle Time of Component n of Injection p
$\Delta\tau_{\mathrm{inj}}$	-	Non-Dimensional Injection Time or Injection Period
$\Delta\tau_{\mathrm{saf}}^p$	-	Non-Dimensional Safety Margin for Injection p
ϵ	-	Porosity of the Column

Roman Nuumbers

Number	Designation
I	Segment I of the Column
II	Segment II of the Column
I	Group I of Henry Constants Associated to "Late Eluter" Case
II	Group II of Henry Constants Associated to "Early Eluter" Case
I	Type I: An Early Temperature Change
II	Type II: A Later Temperature Change
I-III	Zones in Space-Time Graph to Explain the Numerical Scheme

Superscript

| I | Associated Quantity in Segment I |
| II | Associated Quantity in Segment II |

Subscript

| I-IV | Selected Times to Show Concentration Profiles Inside the Column |

Indexes

Index	Designation	Nature/Range
n	Number of Components	$1, 2, 3, ..., N_c$
Superscript		
j	Index for Time Discretization Points and Cells	0 - N_τ
P	Number of Injections	$P \in \mathbb{N}$
p	Injection Number	$p = 1, 2, 3, ..., P$
Subscript		
i	Index for Spatial Discretization Points and Cells	0 - N_x
k	Number of Switching Times and Associated Number of Temperatures	$k \in \mathbb{N}_0$

Abbreviations

Abbreviation	Subscription
EE	Energy Equation
EDM	Equilibrium Dispersive Model
EM	Equilibrium Model
FVM	Finite Volume Method
GC	Gas Chromatography
GRM	General Rate Model
HPLC	High Performance Liquid Chromatography
LKM	Lumped Kinetic Model
ODE	Ordinary Differential Equation
PDE	Partial Differential Equation
SEE	Simplified Energy Equation
SMB	Simulated Moving Bed
SG	Step Gradients
TGIC-TD	Temperature Gradient Interaction Chromatography With Triple Detection
TLC	Thin Layer Chromatography
UOP	Universal Oil Products

Contents

Chapter 1

Introduction

This chapter provides an introduction to chromatographic separation techniques and their state of the art. It briefly describes how temperature gradients can be used to increase the productivity of high-performance liquid chromatographic (HPLC) columns. It also summarizes the motivation and objectives of this research and suggests a solution methodology.

1.1 History and Principles of Chromatography

At the beginning of the 20th century, a Russian botanist named Micheal Tswett created chromatography as a preparative method [42]. There were no systematic physical means of analysis at the time. Analytical techniques were mostly focused on sluggish, insensitive chemical processes. He separated precise mixes of plant origin and obtained pure plant pigments. Chromatography was employed to do this, and the fractions that were obtained were then examined offline.

Early in the 1930s, chemists studying natural products [43] and biochemists, who continued to play a crucial role at various stages of development, recognized the significance of chromatography. Examples are the discoveries of paper chromatography [44], gas chromatography [45], size exclusion chromatography [46], and affinity chromatography [47], to name a few.

In the late 1940s, analytical and preparative chromatography split apart due to developments in sensitive detection techniques. The Manhattan Project's purification of rare earths by Spedding's team [8] and the API Project's extraction of pure hydrocarbons from crude oil by Mair *et. al.* [9] were the first significant preparative chromatography operations. Broughton later developed the very productive multi-column simulated moving bed technology for the company UOP (Universal Oil Products) [10].

Principles and Mechanisms: Chromatography is a scientific technique for separating a substance into its various components and compounds for individual identification. It is used in the pharmaceutical and other processing industries for separation and purification purposes. For example, this technique can be successfully applied to separate complex mixtures and to identify very similar target molecules at reasonable production rates and high purity. It has become an important method for chemical analysis and the production of high-purity products on a micro and macro scale. Today it is impossible to imagine pharmacy without it. The rapid development of fine chemistry, pharmaceuticals, and biotechnology over the past years, combined with pressure from regulatory agencies, has resulted in increased emphasis on the manufacturing

of products for use in the pharmaceutical industry. Their efforts have resulted in the production of numerous highly purified chemicals to be used as drugs or pharmaceutical intermediates. They have also identified metabolites of these compounds and completed systematic studies of the toxicological properties of potential drugs and their metabolites prior to their approval. No industrial separation process is more versatile than chromatography. It is well-suited for the rapid production of high-purity products in the milligram to ton range. None has comparable separation performance. In recent years, preparative chromatography has established itself as an industrial process in the pharmaceutical industry [2].

A chromatographic process consists of three building blocks, the mobile phase, the stationary or solid phase and the feed mixture with the molecules to be separated. Depending on the type of contact between the mobile phase and the stationary phase, the chromatographic technique can be divided into different types. Planar chromatography and column chromatography are two of many examples. Planar chromatography is a liquid chromatography in which the stationary phase is arranged in the form of a flat or plane bed and the mobile phase moves by capillary action. Thin Layer Chromatography (TLC) is the most commonly used planar chromatography. In contrast, column chromatography can be performed in a packed column, in which the entire volume of the tube is filled with the porous substance or the stationary phase through which the mobile phase seeps away either by gravity or by an external pressure. However, based on mechanisms, chromatography can be divided into the following types.

- Adsorption Column Chromatography - Separation process in which the compounds (solutes) to be separated are retained or adsorbed on the surface of the adsorbent (solid stationary phase).

- Partition Column Chromatography - It is based on the variance of the partition coefficients of the individual components of the mixture, with both the stationary and mobile phases in the liquid state.

- Gel Column Chromatography - Here, the separation is done by a gel-filled column that has a porous stationary phase. It is also referred to as size exclusion chromatography.

- Ion Exchange Column Chromatography - The basis for separation are the specific charge of the molecules. Separation can occur when certain molecules are specifically attracted to the oppositely charged stationary phase.

- Gas Chromatography (GC) - Uses gas as the mobile phase.

- High Performance Liquid Chromatography (HPLC) - Use solvents as the mobile phase and small solid particles as the stationary phase.

The simplest HPLC setup consists of a solvent container, a pump (desorbent), the column, a selection valve, a detector and one or more valves to collect the waste, see Figure 1.1. The pump must be capable of delivering the required flow rate against the pressure drop of the column. The column is packed with a porous medium. The selection valve switches between eluent and feed. A liquid mixture which contains several solutes is injected into the column by means of the desorbent. This desorbent pumps the feed mixture using the eluent. Both eluent and feed form the mobile phase. When the mobile phase meets the porous medium, each of its solutes distributes differently between the immiscible stationary and mobile phases within the column. During elution, each component is adsorbed differently by the stationary phase due to their different

affinities. This fact leads to different migration rates, resulting in the formation of different composition fronts. These fronts are connected to the courses of the specific adsorption isotherm and lead to a characteristic retention behavior of the components involved. The separated solutes are then collected with the desired purity at regular intervals at the exit of the column.
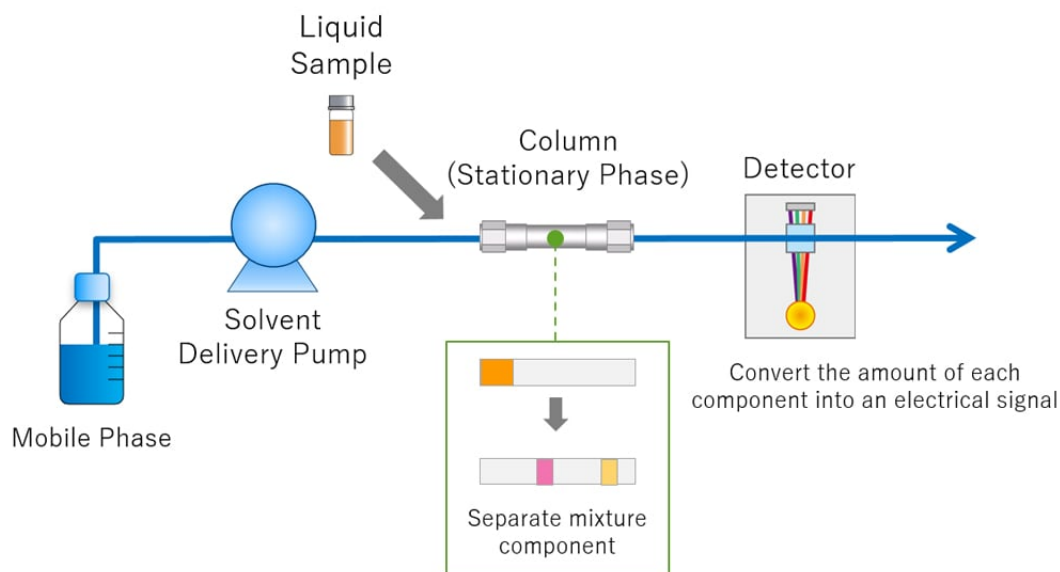
Figure 1.1: Schematic Illustration of an HPLC Process (Source: shimadzu.com [77])

The concept of analytical HPLC was first introduced in the 1960s when stationary phases with high selectivity became available. At the same time, preparative chromatography was greatly advanced by engineers' search for more effective purification techniques. The principle of improving mass transfer by countercurrent flow, combined with the high selectivity of HPLC, greatly improved the performance of preparative chromatography in terms of productivity, eluent consumption, yield, and concentration.

Based on the mode of operation, the concept of chromatographic processes can be classified according to the following types.

1.1.1 Linear and Nonlinear Chromatography

In *linear chromatography*, component's equilibrium concentrations in the stationary and mobile phases are proportionate. The equilibrium isotherms are thus lines that begin at the origin. The sample's composition and volume have no effect on the specific band formation or retention times. The amount of each ingredient in the injected sample directly relates to the peak height. As long as the injected quantities of the sample components are maintained low enough, linear chromatography may be utilized to explain the majority of phenomena seen in analytical applications of chromatography. Let "c" represents the concentration of a solute or component in the mobile phase, while "q" represents the concentration of the same solute in the stationary phase. Then any isotherm may be converted into a second degree polynomial using the formula $q(c) = ac + bc^2$, hence we consider any chromatographic experiment to be carried out under linear

circumstances as long as $bc << a$.

Column chromatography, TLC, and HPLC are frequently used methods that are based on the concepts of linear chromatography. These methods are widely utilized in many different industries, including food testing, environmental monitoring, and pharmaceutical analysis. Good resolution and consistent elution periods make linear chromatography an effective technique for frequent separations.

In *nonlinear chromatography*, the phase equilibrium isotherms are nonlinear. At equilibrium, the component's concentration in the stationary phase is no longer proportional to that in the mobile phase. Any compound's equilibrium isotherm is also influenced by the concentration of all other elements in the solution. Thus, the evolution of the feed concentration at the inlet port of the unit, e.g. the composition of the sample and its amount in the case of an overcharged elution, determines the concentration profiles of all components along the column(s). It also determines the concentration trends at the outlet ports of the chromatographic unit, e.g. the band profile, its height, and retention time in the case of an overcharged elution, etc. This circumstance may be found in almost all preparative applications. The adsorption of certain sugars on ion-exchange resins is a sporadic exception. Over the whole concentration range, their isotherms are almost linear. The interconnectedness of the distinct band profiles and the fact that the quantity of each component adsorbed relies on the concentrations of all species in the solution make nonlinear chromatography issues highly difficult. The distinction between ideal and non-ideal models can help to streamline the study of nonlinear chromatography [1, 2].

Overall, linear chromatography offers predictable separation behavior since it is based on the equilibrium principle. On the other hand, nonlinear chromatography takes into account nonlinearities and competition effects and seeks to enhance separation performance in complicated systems. Nonlinear chromatography is now well understood thanks to recent research, making possible its use for difficult separations, such as protein separations.

1.1.2   Discontinuous and Continuous Processes

A chromatographic process in which the feed mixture is introduced batch-wise to a single column is called a *discontinuous process*. These operations can be performed under different conditions, e.g.

- Isocratic Operation - Chromatographic operations in which the composition of the solvent is not changed during elution or (and) the temperature of the system is kept constant, are referred to as isocratic operations. This method can operate with a simple setup, has a shorter cycle time since the column does not need to be reconditioned, and solvent workup and reuse is easier.

- Gradient Chromatography - Under isocratic conditions, the highly retained components sometimes require a lot of time, leading to a reduction in productivity and high eluent consumption. To improve the productivity, gradient operations are used because they provide additional degrees of freedom [35, 36]. In such a situation, the course of adsorption plays a crucial role by influencing the migration rates through gradients and reducing the cycle time. The following conditions of the process can be changed to achieve the desired improvement:

   1. Mobile phase composition

2. Mobile phase flow rate

3. Temperature

4. Pressure

The first two are classified as solvent gradients. They have a strong effect on elution strength, but require re-equilibration after the chromatogram is completed and cause time delays. In contrast, temperature gradients act instantaneously. However, they have a slower response and they have typically a weaker effect on the elution strength.

It is a fact that solute binding by adsorption is an exothermic process and desorption is an endothermic process; the migration rate in chromatographic columns is temperature dependent. Thermal effects are largely accounted for in gas-phase flows by solid packing [41, 48–52]. However, in liquid chromatography, such effects are usually neglected by (a) assuming that the heat capacities of the two phases are larger than the adsorption enthalpies and (b) assuming a sufficiently large value for the thermal conductivity to maintain a uniform temperature in the column. Solvent gradients are used in most liquid chromatographic procedures to increase productivity. Although most chromatographers assume isocratic conditions when performing liquid chromatography processes. There is experimental evidence of temperature variations in liquid chromatography columns [53, 54].

Note that the expansion of the working range to the nonlinear range of head temperature isotherms is actually the primary distinction between analytical and preparative chromatography. As a result, it is necessary to understand how the individual components and their mixes behave over a broad range of concentrations. Adsorptive equilibrium, like all other phase equilibria, is established by the equality of all interacting components' chemical potentials throughout all phases. In the literature [2, 24], the thermodynamic concepts are described in further detail.

In contrast, a chromatographic process in which the feed mixture is processed continuously in the chromatographic column or usually in several columns is called a *continuous process*. Especially on a preparative scale, continuous processes must be performed to increase productivity and to avoid wasting fresh eluent. Some of the many examples are listed below.

- Column Switching Chromatography – A simple approach to convert batch separation to continuous (or pseudo) separation by switching the injection from one column to another.

- Annular Chromatography – In this type of chromatography, the feed mixture is introduced into a rotating column. The stationary phase is packed between two concentric cylinders, and the liquid moves downward as the column slowly rotates.

- Simulated Moving Bed (SMB) Chromatography – In this concept of chromatography, the stationary phase is circulated at a constant flow rate and in countercurrent to the mobile phase. More efficient separation is achieved by this operation with multiple columns connected. These columns can be connected in series or in parallel. SMB chromatography can be performed under either isocratic or variable process conditions.

The first method involving countercurrent flow was SMB chromatography for large-scale separation in the petrochemical and food processing industries [4]. Recently, countercurrent SMB processes have emerged as key highlights in chromatographic separations. With the goal of increasing productivity and making chromatographic separations more economical, especially for bioproducts, SMB principles are becoming a source for developing new and more flexible processes with a

smaller number of columns. The extreme case here is a proposal for an SMB-like process with only one column, [7]. There are some other studies that report on the trends and suggestions for improving SMB processes, for example [5,6].

A look into the future shows a technology trend towards the use of continuous process flows and downstream processes for chemical and especially biopharmaceutical products. Costs and production capacity need to be examined, and more integrated and efficient approaches should be used. The adaptation of concepts for isolating antibodies from complex fermentation broths in a countercurrent process will enable more cost-effective production of biopharmaceutical products in the coming years.

However, in this work we are concerned with a linear and discontinuous HPLC process associated with a particular system. The process is comparatively run under both isocratic and selected temperature gradients to show how temperature gradients can be used to achieve a better production rate.

1.1.3   Brief Overview of Literature

In the 1980s, the pharmaceutical industry first expressed interest in preparative high-performance chromatography, and in the last 20 years this interest has increased even further [11]. For the extraction and purification of fine compounds, especially those used as pharmaceutical intermediates, chromatography is now an accepted commercial technique.

A chromatographic system based on the idea of a SMB was created and patented by Union Oil in the early 1970s [10, 12, 13]. While streams of the less retained (the "raffinate") and more retained (the "extract") components are continually extracted from the column at fixed flow rates, streams of the mobile phase (the "desorbent") and the feed to be separated are continuously introduced into the column. The places in the columns where these streams enter or exit are regularly changed by the rotary valves. For the selective separation of p-xylene, o-xylene, and ethyl-benzene from the aromatic C7-C8 fraction of light petroleum reformates, for the separation of olefins from keroses in feed mixtures of hydrocarbons with 10 to 14 carbon atoms, and for the separation of fructose and dextrose from corn syrup, production plants have been built and are in operation. It has been demonstrated that forcing the stationary phase to move down the column may transform chromatography, which is typically a batch operation in both the elution and displacement modes, into a continuous process. It is not practicable to move the stationary phase bed physically. However, it is possible to replicate the action of a moving bed, as was done in the Union Oil process by employing a number of columns set up online and coupled to a rotary valve [10]. Practical switches may be made to the positions of the desorbent, extract, feed, and raffinate to enable the machine to run continuously.

Over the past 40 years, proponents of elution have repeatedly made promises of significant improvements for certain separation tasks [14, 15]. However, this strategy has never been used in actual practice in the tightly controlled pharmaceutical sector. It has been shown that the assertion that displacement delivers a 100 percent recovery yield is false since the bands' boxcar elution. The debate has come to an end because of the gradual realization that isocratic elution, whenever possible, leads to faster production rates, higher recoveries, and easier operation, even if it produces more fractions than displacement [16–18]. Because proteins and medium- or large-sized peptides can often not be extracted or purified by isocratic elution, the balance between the benefits and drawbacks of displacement and elution techniques has long been ambiguous. Gradient operations currently seems to be superior. Now that the foundations of nonlinear chromatography

are better known, much research is still being done on the numerous recycling techniques that are currently accessible as well as the simulated moving bed approach.

It has been found that temperature gradients broadly influence the production rate, yield, and efficiency of the column. Some studies suggest that they can reduce viscosity and improve solubility and diffusivity [55, 56]. Both separation and reactions are significantly affected by temperature fluctuations. Only a few contributions are available in the literature dealing with segmented temperature gradients in liquid chromatography [57–65]. One method implemented is Temperature Gradient Interaction Chromatography With Triple Detection (TGIC-TD). The method was suggested by Chang et al. to separate branched polymers according to their molecular weight with a high resolution [66–69].

With the aid of suitable mathematical models, which are typically based on mass, energy, and momentum balances as well as on equations quantifying the thermodynamic equilibria of the distribution of the solutions between the different phases, it is possible to quantitatively describe the band propagation phenomena in chromatography. With respect to model accuracy, the engineering rule is that a good model should not only be as detailed as necessary, but also as simple as possible.

The literature has a variety of models for comprehending the dynamical nature of the transport systems involved in the chromatographic process. Compared to the currently accessible, costly, and time-consuming experimental approaches, these models offer a better and deeper understanding of the associated separation and reaction processes [1, 2].

An important modeling approach for quantifying chromatographic processes is the stochastic theory of chromatography, which is based on the fundamental molecular and dynamic considerations introduced by Giddings and Eyring [25]. There are numerous later developments of this theory, documented for example by [27], [26] and [19].

1.2   Problem Statement

The selection of the chromatographic system and the best process idea, as well as the scaling-up of laboratory-scale trials to economically viable plant sizes, are crucial phases in the design of production-scale chromatographic processes. The amount of time and resources needed for process analysis and optimization can be greatly decreased by predictions based on approximations and numerical simulations. Validated process models may be employed to design plants with the best efficiency and choose the right operational parameters. The clarity produced by process simulation enhances process comprehension and facilitates effective staff training [3]. Because mathematical modeling is used to plan, regulate, and optimize system behavior, it has now become an integral component of chemical engineering.

In chromatography, the influence of temperature on adsorption and thus on process performance is a fact. Therefore, temperature gradients have a potential application in the optimization of separation processes. Examining how induced temperature gradients might increase the performance of liquid chromatographic columns is one of the objectives of this study. If the heat of adsorption is high enough, the system can drastically diverge from isocratic behavior. As a result, the co-occurrence of heat and concentration fronts should be discussed, and the crucial variables that control temperature gradients should be found. To achieve this, a specific forced gradients operation of a liquid chromatographic process is theoretically studied. Particularly, the internal temperature of the column is changed at a specific position through an external heating or cooling

source fixed to the surface of the column wall. Heating accelerates while cooling decelerates the migration speed of the fronts in specific regions of the column.

A chromatographic process involves several interrelated and complex thermodynamic, hydrodynamic, and kinetic phenomena such as dispersion, convection, adsorption-desorption, and mass transfer kinetics. Their mathematical representations are accomplished by taking into account any or all of these phenomena, which results in a range of models with varying degrees of complexity (see, for example, [1, 2, 20–24]). The ideal or equilibrium model (EM), the equilibrium dispersive model (EDM), the general rate model (GRM), the linear driving force model, and the lumped kinetic model (LKM) are some of the models that are now in use.

Despite the widespread belief that the GRM is an effective and accurate model, many factors are involved and the calculations are very complex. For that reason, EM and EDM are the main models in this study because they provide a reasonable approximation with few parameters. The EM is the simplest model and easy to solve, but still a valuable one, as it provides important information, while the latter is the extended version that has a significant impact on the study of chromatographic processes.

Equilibrium theory is incredibly useful for designing and analyzing a variety of complicated processes. Its ability to effectively anticipate, address, and explain the dynamic behavior of such intricate systems is one of its significant strengths. We refer to the [71–73] for in-depth studies on equilibrium theory.

The EM include the linear advection equation, i.e. the axial dispersion of the concentration is neglected in this model, whereas, the EDM comprises system of convection-diffusion partial differential equations (PDEs). When the injected sample is either small in volume or diluted, the equilibrium concentrations of the liquid and solid phases often have a linear relationship, leading to a linear system of equations.

As a preliminary cases, for the EM and EDM, it is assumed that there are no radial gradients and that temperature changes are driven progressively and evenly across the column's cross-sectional area. In order to convey heat across the column, no energy balance is necessary; instead, we give the temperature inside the column as a piece-wise step function. These equations can be analytically solved using the well-known method of characteristics. This method changes the original coordinate system (z, t) to a new coordinate system (z_0, s) to reduce the given partial differential equation (PDE) to an ordinary differential equation (ODE).

If we consider the column's temperature as a real temperature profile described by a detailed energy equation rather than a piecewise function, there is typically a nonlinear relationship between the equilibrium concentrations of the liquid and solid phases, leading to nonlinear differential equations. Analytical solutions to the resultant model are either challenging or perhaps impractical. As a result, effective numerical techniques must be used to produce precise and entropic (physically realistic) solutions.

Since retention time is the crucial factor when it comes to the productivity, the models are initially looked at for individual components to determine how different temperature profiles impact the retention time of a certain component. The models are then expanded to include a mixture that is periodically injected, first under isocratic conditions and subsequently under gradients ones, in order to potentially reduce cycle time, which is essential for determining the performance of the column. Some of the analytical solutions are also compared with the numerical outcomes.

In summary, we want to study the effects of temperature gradients in a discontinuous chromatographic process, especially considering a linear isotherm in concentration. By comparing

the effects of temperature gradients with isocratic conditions, this study focuses on the prediction and optimization of cycle times. The main objective is to investigate how temperature gradients can be used to reduce cycle times and increase productivity. This study is theoretical and uses mathematical modeling and simulations to understand the potential benefits of incorporating temperature gradients into the HPLC process. For the purpose of experimental validation, realistic parameters are utilized, ensuring a practical and accurate representation of the proposed approach.

It is important to carefully select materials that have related parameters such as Henry's constants or (and) adsorption enthalpies. Some systems may not be suitable for the present study. However, in a more systematic research, the analysis of this section can be used to identify accurate criteria to predict the maximum deviation from isocratic behavior and serve as a justification for the final reduction of the model to isocratic behavior.

1.3 Solution Methodology

In the present work, the EM is solved both analytically, while the EDM is analyzed both semi-analytically and numerically for a liquid chromatographic process under isocratic and gradients conditions. For the analytical solution the method of characteristics is used, while for the semi-analytical solution the Laplace transformation and for the numerical solution the upwind finite volume method (FVM) is utilized. Analytical, semi-analytical and numerical results are compared. Some of them are also compared with experimental results of the parallel PhD Project [39]. All the aforementioned techniques helped to calculate formulas for the corresponding cycle and injection times. The effects of varying several key parameters over the temperature profile, influencing the retention times of certain components, are investigated.

1.3.1 Method of Characteristics

The method of characteristics is a mathematical technique used to solve certain types of PDEs. It involves converting a given PDE into a system of ODEs along characteristic curves in the (z, t)-plane, i.e. curves which carry some information and along which the solution of the PDE remains constant in our case. These curves are particularly relevant to the study of equilibrium theory, which is actually the beginning of calculating the solutions in this work. By solving the ODEs, one can determine the solution of the original PDE.

The method of characteristics is particularly useful for linear and quasilinear first order PDEs [74]. It takes advantage of the fact that the characteristics of a PDE are defined by the coefficients of the partial derivatives of the unknown function with respect to the independent variables. By examining the characteristics, one can determine the behavior of the solution.

The method of characteristics has applications in various fields, such as fluid dynamics, optics and transport phenomena. It is a powerful tool for the systematic analysis and solution of partial differential equations [71–73].

1.3.2 Finite Volume Method (FVM)

Due to its ability to accurately represent the behavior of values that are conserved over both space and time, the finite volume approach is frequently employed to solve conservation laws. The fundamental principles of physics, such as the conservation of mass, momentum, and energy,

are described by conservation laws [75]. The finite volume approach is frequently used to solve these conservation laws for the reasons listed below:

1. Conservation property – The finite volume approach is by nature conservative. The domain is discretized into tiny control volumes or cells, and the fluxes of the conserved quantities are calculated at the boundaries of these cells. The technique assures that the overall amount is preserved by adding the fluxes over the control cells.

2. Local and flux conservation – The method maintains local conservation, which ensures that each control cell properly depicts the quantities acquired. By precisely accounting for fluxes of conserved quantities across cell boundaries, it also assures flux conservation.

3. Flexibility in dealing with complex geometries – The solution's discontinuities, irregular meshes and complicated geometries can all be handled using the finite volume approach. It enables modification and improvement in certain areas of interest.

4. Numerical stability – The finite volume method in conjunction with upwind fluxes is reliable for solving conservation laws because it has high numerical stability features. It can manage any discontinuities that the solution may experience, including shocks and contact discontinuities.

The finite volume approach is widely used in computational physics and engineering simulations because it offers an efficient framework for resolving conservation laws, guaranteeing conservation properties, handling complicated geometries, and preserving numerical stability. In the current study, we use the finite volume method to calculate all numerical solutions.

1.4   Objectives and Outline

The main goal of this thesis project is to theoretically analyze forcedly implemented thermal gradients and their role in improving productivity, e.g. performance, in liquid chromatography. In a systematic and summarized form, this is highlighted as follows

1. Solving the EM together with spatially focused temperature step-gradients (see Section 2.4.2) and providing corresponding analytical solutions using the method of characteristics. Estimation of formulas for retention and cycle times, and column's performance under isocratic and gradients conditions.

2. Numerically solving the extended model, the EDM, along with the same temperature step-gradients (see Section 2.4.1) using FVM. Estimation of the same quantities numerically and comparison with the results of the equilibrium model.

3. Providing analytical solutions of the simplified temperature (energy) equation by Laplace transform and subsequent fitting to the EDM for numerical estimation of concentration using the FVM (see Section 2.3). We call this approach semi-analytical analysis.

4. Finally generating numerical solutions of the coupled system of EDM and detailed energy equation (see Section 2.2) using FVM and comparison of the results obtained from this slower temperature changes with the results obtained from the above models with faster temperature changes.

5. Because of the parallel doctoral project [39], comparing the selected theoretical predictions with the experimental results, which are described in more detail in the parallel dissertation. In particular, a comparison is planned for a specific chromatographic separation problem at selected types of temperature gradients.

The remaining parts of the dissertation are organized as follows.

Chapter 2 introduces the concept of gradient chromatography, mathematical models, and the column's production rate. In Chapter 3, the method of characteristics is applied to derive the solution trajectories of EM. Different scenarios are also analyzed for illustration. Chapter 4 performs numerical analysis and studies the stability conditions for each model. A parameter study, results of the theoretical study, and its comparison with the experimental results are presented in Chapter 5. Conclusions are drawn in Chapter 6.

Chapter 2

Gradient Concept and Mathematical Models

This chapter deals with the concept of possible temperature gradients and introduces mathematical models like the Equilibrium Model (EM) and Equilibrium Dispersion Model (EDM). We also discuss energy balance equations in detailed and simple forms to use temperature gradients effectively. By combining these mass and energy balances in different ways, we develop four models for their solutions in the later chapters.

2.1 A Possible Temperature Gradients Concept

Consider some chemical solutes are injected via a moving stream of solvent into a cylindrical chromatographic column of length $z = [z_0, \ z_{\max}]$, where $z_0 = 0$. For illustration of the wider applicable principle of segmented thermal gradients, we divide the z-domain in two equal segments, from z_0 to $z_{\mathrm{m}} = \frac{z_{\max}}{2}$, segment I, and from z_{m} to $z_{\max}$, segment II. We consider that each of the segments behaves like an individual column and that the overall column is described by connecting these two segments. The outlet concentration profiles of segment I are the inlet concentration profiles for segment II.

Let segment I be maintained at a fixed reference temperature T_{R} while the temperature of segment II is changed uniformly via a fixed source placed at the outer surface of the conducting wall. We assume for simplicity that it provides instantaneous heating T_{H} or cooling T_{L} to the whole segment.

To illustrate the effects of the forced periodic regime, we show four different scenarios in Figures 2.1 and 2.2. In the first scenario, see Figure 2.1a, a single solute pulse (showing total concentration in the two phases) is shown eluting in the column. Hereby, it is allowed to face, for example, a lower temperature in segment II. As the pulse starts crossing z_{m}, its right part in segment II decelerates and its left part in segment I is still moving at the larger reference speed. As a result, the profile becomes narrower and more concentrated in segment II. After completely entering into segment II, the whole pulse is migrating at uniform low speed and reaches the column's outlet. The second possible scenario is similar to the first one but now the pulse faces a higher temperature in segment II, see Figure 2.1b. As a result, an opposite effect is observed, that is the pulse becomes broader and less diluted. The third and fourth possible scenarios are more complicated. They refer to the intrinsic goal of chromatography to separate components.
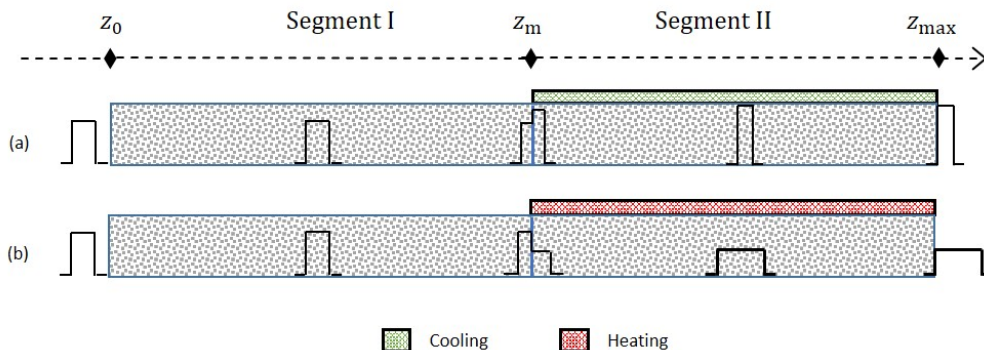
Figure 2.1: Case (**a**) A single-solute pulse is injected one time into the column. The pulse is allowed to face a low temperature in segment II. As a result, the pulse becomes narrower and more concentrated. Case (**b**) Unlike case (**a**), the injected pulse faces a high temperature in segment II. Then, the pulse becomes broader and less concentrated.

For illustrative purposes, the third and fourth scenarios consider a three-component mixture. Suppose the mixture is periodically injected $P-$times into the column under both isothermal and gradient conditions, where $P \in \mathbb{N}$ as shown in Figure 2.2a. In the third scenario, the first two components are assumed to migrate much faster than the third component, which is referred to as "Late Eluter" and is shown in Figure 2.2b, while the fourth scenario in Figure 2.2c, which is referred to as "Early Eluter", describes the situation in which one of the three components elute faster and the other two elute slower. Depending on the individual velocities, each component of the mixture faces temperature changes in the segment II at different times. Figure 2.2d shows the potential of applying well selected temperature gradients to reduce cycle time for both scenarios, that is, the shortest possible time difference between two consecutive injections, in the gradients case, $\Delta t_{c,grad}^p$, compared to the isothermal (isocratic) case, $\Delta t_{c,iso}^p > \Delta t_{c,grad}^p$.

If we choose $p = 1, 2, 3, ..., P \in \mathbb{N}$, then let t_{inj}^p and $t_{n,max}^p$ be the times at which each component n of the pth injection of duration Δt_{inj} enters and leaves the column, respectively. We refer to these times as injection time and retention time, respectively. We assume that $t_{inj}^1 = 0$, $t_{inj}^p < t_{n,max}^p$ for $p = 1, 2, 3, ..., P$. Since the injected concentration remains the same for each pth injection, we do not need a superscript p over c_n. The injection duration Δt_{inj} for each c_n in each injection also remains the same. We estimate the cycle time Δt_c^p at the column exit, which in principle (if no safety margins are considered) should be equal to the difference between two successive injection times, i.e. $t_{inj}^{p+1} - t_{inj}^p$.

In the following section, we will introduce the mathematical models that describe the mass transfer phenomenon in relation to the previously discussed temperature gradients concept.
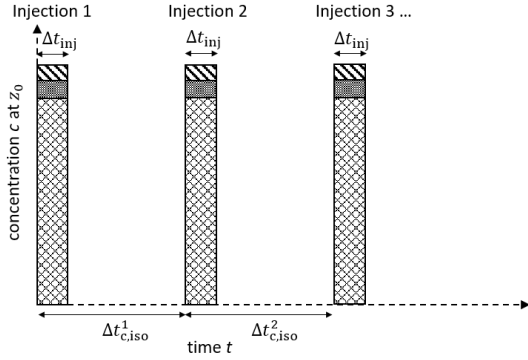
a Illustration of a ternary mixture injected multiple times under isothermal conditions. Each component has a different Henry constant and adsorption enthalpy. The cycle time under isocratic conditions is given as $\Delta t^p_{\mathrm{c,iso}}$.
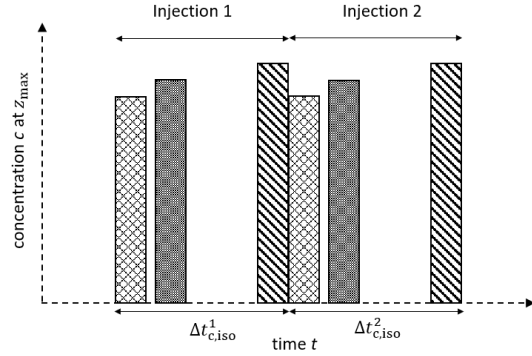
b Case "Late Eluter": Effluent concentrations at z_{max} for isothermal conditions and the corresponding cycle time $\Delta t^p_{\mathrm{c,iso}}$, which should be equal to that at z_0. In this case the retention times of the first two components are similar but smaller than the retention time of the third component.
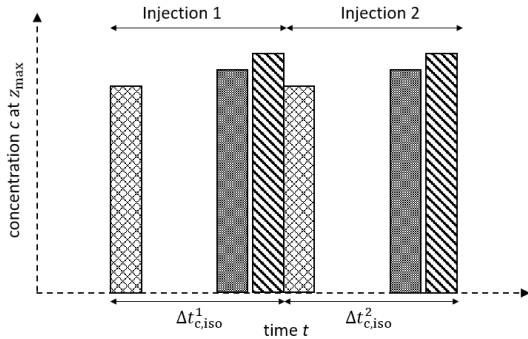
c Case "Early Eluter": In this case the retention times of the last two components are similar but larger than the retention time of the third component.
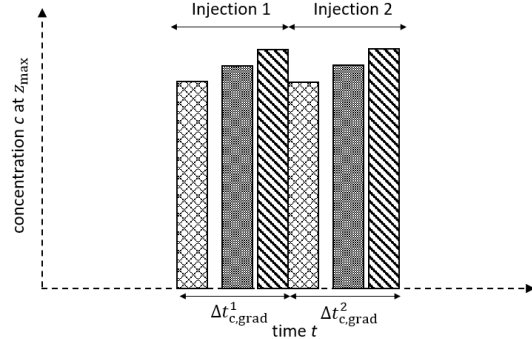
d Collection goal at the outlet of the column: The same mixtures are injected under suitable segmented temperature gradients. The pulses then elute closer to each other, leading to a reduction in the cycle time, that is, $\Delta t^p_{\mathrm{c,grad}} < \Delta t^p_{\mathrm{c,iso}}$.

Figure 2.2: Illustration of the concentration pulses plotted in Figure "a" at the inlet z_0 of the column, while in "b" and "c" they are plotted at z_{max}. The shaded regions indicate the composition of the injected mixture.

2.2   Equilibrium Dispersive Model (EDM) Coupled with Energy Equation

The principles of equilibrium conditions and dispersion effects in mass transport are combined in the equilibrium dispersive model. It integrates the dispersion phenomenon, which is the spreading or mixing of solute in a fluid, and implies quick equilibration. Chemical engineering has extensively explored this concept, which has found use in a number of systems [31, 32]. In the mathematical community, this dispersion term is recognized as diffusion, emphasizing its significance in various mathematical models and applications.

Let the number of solutes injected into the column be $N_c \in \mathbb{N}$, having concentrations c_n in the mobile phase and q_n in the adsorbed phase, such that $n = 1, 2, 3, ..., N_c$. It is assumed that the column is filled with spherical adsorbent particles and that the bed is homogeneous. The evolution of separation is occurs over a time horizon $t = [t_0, \ t_{n,\max}^P]$, where $t_0 = 0$ and $t_{n,\max}^P$ is the time when the last component of the last P^{th} injection exits the column, where $P \in \mathbb{N}$. Further, u represents the interstitial velocity, which is assumed to be constant for all temperatures, and $F = \frac{1-\epsilon}{\epsilon}$ is the phase ratio based on the porosity $\epsilon \in \ ]0, 1[$. For a reliable prediction of concentration profiles, we introduce the apparent dispersion coefficient D_z in the mass balance, which plays a crucial role in characterizing the transport behavior of components in the system. The dispersion term is usually component specific and takes into account molecular diffusion, axial dispersion and mass transfer resistances in its entirety. Our approach simplifies the analysis by neglecting component-specific differences in molecular diffusion and mass transfer resistances and treat D_z as a constant apparent axial dispersion coefficient. We will estimate the value of D_z from the experimentally determined plate number N_p.

Let the indexes L and S be the symbolic representations of liquid and solid phases, respectively, then we define $\mathring{m}_{L-S}$, the mass flowing from the liquid to the solid phase and back, then let the mass balance for a liquid mixture of N_c components in the mobile phase percolating through a cylindrical chromatographic column with a fixed bed be given as

$$\epsilon c_{n_t} + \epsilon u c_{n_z} = \epsilon D_z c_{n_{zz}} + \mathring{m}_{L-S}, \qquad n = 1, 2, 3, ..., N_c \tag{2.1}$$

and in the solid (adsorbed) phase, it is defined as

$$(1 - \epsilon) q_{n_t} = -\mathring{m}_{L-S}. \tag{2.2}$$

For the description of the exchange of mass flow between the two phases, there exist many models. We will not go deeper into them in this thesis. Instead we will assume permanently established equilibrium conditions. Adding (2.1) and (2.2), then dividing both sides by ϵ gives the so-called equilibrium dispersive model (EDM) as

$$c_{n_t} + F q_{n_t} + u c_{n_z} = D_z c_{n_{zz}} . \tag{2.3}$$

Assuming linear equilibria $q(c)$, we will define the Henry constants a_n, which are a function of the temperature T. This temperature dependence is typically expressed via an Arrhenius function incorporating the enthalpy of adsorption $\Delta H_{A,n}$ for each component n and the universal gas constant R. Furthermore, let T_R be any reference temperature. The temperature-dependent Henry constants with respect to the reference Henry constants $a_n(T_R)$ and the actual temperature T are then given as

$$a_n = a_n(T) = a_n(T_{\mathrm{R}}) \exp\left[\frac{-\Delta H_{A,n}}{\mathrm{R}}(\frac{1}{T} - \frac{1}{T_{\mathrm{R}}})\right], \qquad n = 1, 2, 3, ..., N_{\mathrm{c}}. \tag{2.4}$$

The distribution equilibria of the components between the mobile phases and the solid phases under equilibrium conditions are described by a function. It is called, for a given constant temperature, adsorption isotherm. We apply a linear relation in concentration using the above temperature dependent Henry constants $a_n(T)$. Thus the adsorption isotherm equation used in this thesis is linear in concentration and nonlinear in temperature, as expressed below

$$q_n(c_n, T) = a_n(T)c_n = a_n(T_{\mathrm{R}}) \exp\left[\frac{-\Delta H_{A,n}}{R}(\frac{1}{T} - \frac{1}{T_{\mathrm{R}}})\right]c_n, \tag{2.5}$$

Let ρ represent the density per unit volume, C_p the heat capacity, λ_{z} the effective thermal conductivities along the axial direction. The density and heat capacity are assumed not to depend on temperature and composition. Also, let α_{w} and T_{w} represent the overall wall heat transfer coefficient and the wall temperature, respectively. If the enthalpy of mixing is neglected, the energy balance for the temperature T in a differential volume element of a chromatographic column becomes

$$(\rho^L C_{\mathrm{p}}^L + F\rho^S C_p^S)T_t - F\sum_{n=1}^{N_c}(-\Delta H_{A,n}q_{n_t}) + u\rho^L C_{\mathrm{p}}^L T_z = \lambda_z T_{zz} + \alpha_{\mathrm{w}}(T_{\mathrm{w}} - T). \tag{2.6}$$

The combination of the contributions of heat capacity and density from both the liquid phase and the solid phase $\rho^L C_{\mathrm{p}}^L + F\rho^S C_p^S$ provided in the equation defines the storage term. Understanding the dynamics of heat transfer within the system depends heavily on this storage term, which takes into account the combined influence of the two phases.

We know that adsorption is an exothermic and desorption is an endothermic process. This is the context of the term $\sum_{n=1}^{N_c}(-\Delta H_{A,n}q_{n_t})$ in the equation above, which connects the energy equation with the mass balance. It offers insights into the overall dynamics of heat transfer and the energetics of the adsorption-desorption system and provides a thorough description of the net energy exchange associated to the process.

Let $c_{n,\mathrm{inj}}$ be the injected concentrations of components c_n and Δt_{inj} be the corresponding injection time. The initial conditions for (2.3) and (2.6), taking T_{R} as the room or reference temperature, are given as

$$c_n(z, t_0) = 0, \tag{2.7a}$$

$$T(z, t_0) = T_{\mathrm{R}}. \tag{2.7b}$$

We use the Dirichlet boundary condition on the left edge z_0 of the $z-$axis, which is as follows

$$c_n(z_0, t) = \begin{cases} c_{n,\mathrm{inj}}, & t_{\mathrm{inj}}^p \le t \le t_{\mathrm{inj}}^p + \Delta t_{\mathrm{inj}} \\ 0, & t_{\mathrm{inj}}^p + \Delta t_{\mathrm{inj}} < t < t_{n,\mathrm{max}}^p, \end{cases} \qquad \text{for } p = 1, 2, 3, ..., P \in \mathbb{N}. \tag{2.8a}$$

While for the right edge z_{max}, we use the Neumann boundary condition as

$$c_{n_z}(z_{\mathrm{max}}, t) = 0. \tag{2.8b}$$

We use the same set of boundary conditions for the temperature as

$$T(z_0, t) = T_{\mathrm{R}}, \tag{2.8c}$$

$$T_z(z_{\max}, t) = 0. \tag{2.8d}$$

Let us rewrite Eqs. (2.3) and (2.6) in the form

$$c_{n_t} + F q_{n_t}(T) + u c_{n_z} = \mathrm{D_z} c_{n_{zz}}, \qquad n = 1, 2, \cdots, N_{\mathrm{c}}, \tag{2.9}$$

$$T_t + \frac{F \sum_{n=1}^{N_c} \Delta H_{A,n} q_{n_t}(T)}{\rho^L C_{\mathrm{p}}^L + F \rho^S C_p^S} + \frac{u \rho^L C_p^L}{\rho^L C_{\mathrm{p}}^L + F \rho^S C_p^S} T_z = \frac{\lambda_z}{\rho^L C_{\mathrm{p}}^L + F \rho^S C_p^S} T_{zz} + \\ \frac{\alpha_{\mathrm{w}}}{\rho^L C_{\mathrm{p}}^L + F \rho^S C_p^S} (T_{\mathrm{w}} - T). \tag{2.10}$$

For simplicity and numerical computations, we will first de-dimensionalize the time t using the retention time of a non-retained component, t_{R_0}, given as

$$t_{R_0} = \frac{z_{\max}}{u}, \tag{2.11}$$

whereas, the space z is de-dimensionlized using $z_{\max}$. The dimensionless time τ and the normalized space variable x as

$$\tau = \frac{t}{t_{R_0}} \qquad \text{and} \qquad x = \frac{z}{z_{\max}} \in [0, 1]. \tag{2.12a}$$

If Δz and Δt are the spatial and time steps in dimensional form, respectively, then these quantities are written in terms of non-dimensional space and time steps, Δx and $\Delta \tau$, respectively, as

$$\Delta x = \frac{\Delta z}{z_{\max}} \qquad \text{and} \qquad \Delta \tau = \frac{\Delta t}{t_{R_0}}. \tag{2.12b}$$

Also, we define relative middle (the interface) and end positions as

$$x_{\mathrm{m}} = \frac{z_{\mathrm{m}}}{z_{\max}} = \frac{1}{2} \qquad \text{and} \qquad x_{\max} = \frac{z_{\max}}{z_{\max}} = 1. \tag{2.12c}$$

After introducing the above definitions in (2.9) and (2.10), a small simplification and rearrangement yields

$$(c_n + F q_n(T))_\tau = -c_{n_x} + \frac{t_{R_0} \mathrm{D_z}}{z_{\max}^2} c_{n_{xx}}, \qquad n = 1, 2, \cdots, N_{\mathrm{c}}. \tag{2.13}$$

$$\left(T + \frac{F \sum_{n=1}^{N_c} \Delta H_{A,n} q_n(T)}{\rho^L C_{\mathrm{p}}^L + F \rho^S C_p^S} \right)_\tau = -\frac{\rho^L C_p^L}{\rho^L C_{\mathrm{p}}^L + F \rho^S C_p^S} T_x + \frac{\lambda_z t_{R_0}}{z_{\max}^2 (\rho^L C_{\mathrm{p}}^L + F \rho^S C_p^S)} T_{xx} + \\ \frac{\alpha_{\mathrm{w}} t_{R_0}}{\rho^L C_{\mathrm{p}}^L + F \rho^S C_p^S} (T_{\mathrm{w}} - T). \tag{2.14}$$

Now, consider the following abbreviations

$$\mathrm{D}_x = \frac{\mathrm{D}_z}{z_{\max}^2}, \tag{2.15a}$$

$$G_n = \frac{\Delta H_{A,n}}{\rho^L C_p^L + F\rho^S C_p^S}, \qquad n = 1, 2, 3, ..., N_c, \tag{2.15b}$$

$$X_1 = \frac{\rho^L C_p^L}{\rho^L C_p^L + F\rho^S C_p^S}, \tag{2.15c}$$

$$X_2 = \frac{\alpha_w}{\rho^L C_p^L + F\rho^S C_p^S} \tag{2.15d}$$

and

$$X_3 = \frac{\lambda_z}{z_{\max}^2(\rho^L C_p^L + F\rho^S C_p^S)}. \tag{2.15e}$$

In view of the above abbreviations, (2.13) and (2.14) are of the form

$$(c_n + Fq_n(T))_\tau = -c_{n_x} + t_{R_0} D_x c_{n_{xx}}, \tag{2.16a}$$

$$\left(T + F\sum_{n=1}^{N_c} G_n q_n(T)\right)_\tau = -X_1 T_x + t_{R_0} X_3 T_{xx} + t_{R_0} X_2(T_w - T). \tag{2.16b}$$

For simplicity, let us consider now just the elution of a single component, i.e. $N_c = 1$. Then (2.16a) and (2.16b) considering $c_1 = c$, $q_1 = q$, $\Delta H_{A,1} = \Delta H_A$, and $\sum_{n=1}^{1} G_1 = G$ are given as

$$(c + Fq(T))_\tau = -c_x + t_{R_0} D_x c_{xx}, \tag{2.17a}$$

$$(T + GFq(T))_\tau = -X_1 T_x + t_{R_0} X_3 T_{xx} + t_{R_0} X_2(T_w - T). \tag{2.17b}$$

After using (2.5) and applying the chain rule to $q(T) = a(T)c$ in the above equations, we obtain the coupled system of PDEs in non-dimensionalized form as

$$[1 + Fa(T)] c_\tau + cFa(T)_T T_\tau = -c_x + t_{R_0} D_x c_{xx}, \tag{2.18a}$$

$$GFa(T)c_\tau + (1 + cGFa(T)_T) T_\tau = -X_1 T_x + t_{R_0} X_3 T_{xx} + t_{R_0} X_2(T_w - T). \tag{2.18b}$$

The definitions by (2.12a) also transform the initial and boundary conditions (2.7a) to (2.8d), considering $x_0 = \frac{z_0}{z_{\max}} = 0, \tau_0 = \frac{t_0}{t_{R_0}} = 0, \tau_{inj}^p = \frac{t_{inj}^p}{t_{R_0}}$, and $\Delta\tau_{inj} = \frac{\Delta t_{inj}}{t_{R_0}}$, as

$$c_n(x, \tau_0) = 0, \tag{2.19a}$$

$$T(x, \tau_0) = T_R, \tag{2.19b}$$

$$c_n(x_0, \tau) = \begin{cases} c_{n,inj}, & \tau_{inj}^p \leq \tau \leq \tau_{inj}^p + \Delta\tau_{inj} \\ 0, & \tau_{inj}^p + \Delta\tau_{inj} < \tau < \tau_{n,max}^p, \end{cases} \qquad \text{for } p = 1, 2, 3, ..., P \in \mathbb{N}, \tag{2.20a}$$

while, for the right edge, the Neumann boundary condition becomes

$$c_{n_z}(x_{\max}, \tau) = 0. \tag{2.20b}$$

Similarly, for the energy balance, they are given as

$$T(x_0, \tau) = T_{\mathrm{R}}, \tag{2.20c}$$

$$T_z(x_{\max}, \tau) = 0. \tag{2.20d}$$

Equations (2.18a) and (2.18b) can also be written in matrix form as

$$\underbrace{\begin{bmatrix} 1 + Fa(T) & cFa(T)_T \\ GFa(T) & 1 + cGFa(T)_T \end{bmatrix}}_{\mathbf{J}} \underbrace{\begin{bmatrix} c_\tau \\ T_\tau \end{bmatrix}}_{\mathbf{x}} = -\underbrace{\begin{bmatrix} c_x \\ X_1 T_x \end{bmatrix}}_{\mathbf{y}} + \underbrace{\begin{bmatrix} t_{R_0} D_x c_{xx} \\ t_{R_0} X_3 T_{xx} \end{bmatrix}}_{\mathbf{z}} + \underbrace{\begin{bmatrix} 0 \\ t_{R_0} X_2 (T_{\mathrm{w}} - T) \end{bmatrix}}_{\mathbf{s}}$$

$$\tag{2.21}$$

or

$$\mathbf{J}\,\mathbf{x} = -\mathbf{y} + \mathbf{z} + \mathbf{s}. \tag{2.22a}$$

The solution $\mathbf{x}$ could be calculated by inverting the matrix $\mathbf{J}$ to the right side to get

$$\mathbf{x} = \mathbf{J}^{-1}\left(-\mathbf{y} + \mathbf{z} + \mathbf{s}\right). \tag{2.22b}$$

Now we calculate the eigenvalues of the Jacobian matrix $\mathbf{J}$. Let λ_1 and λ_2 be the two eigenvalues of $\mathbf{J}$ and $\mathbf{I}$ be the 2×2 identity matrix, such that $|\mathbf{J} - \lambda_{1,2}\mathbf{I}| = 0$, the well-known characteristic equation, i.e.

$$\lambda_{1,2}^2 - \left(Fa(T) + cGFa(T)_T + 2\right)\lambda_{1,2} + \left(Fa(T) + cGFa(T)_T + 1\right) = 0. \tag{2.23}$$

By employing the factorization method to solve the quadratic equations, the above equation implies

$$\left[\lambda_{1,2} - \left(Fa(T) + cGFa(T)_T + 1\right)\right]\lambda_{1,2} - 1\left[\lambda_{1,2} - \left(Fa(T) + cGFa(T)_T + 1\right)\right] = 0$$

or

$$\left[\lambda_{1,2} - \left(Fa(T) - cGFa(T)_T + 1\right)\right](\lambda_{1,2} - 1) = 0. \tag{2.24}$$

With this we get the two eigenvalues of the Jacobian matrix J as

$$\lambda_1 = 1, \quad \lambda_2 = Fa(T) + cGFa(T)_T + 1, \tag{2.25a}$$

which, in view of (2.4) and (2.15b) look like

$$\lambda_1 = 1, \tag{2.25b}$$

$$\lambda_2 = 1 + \left[1 + \frac{c\Delta H^2}{RT^2(\rho^L C_{\mathrm{p}}^L + F\rho^S C_p^S)}\right] Fa(T_{\mathrm{R}}) \exp\left[\frac{-\Delta H_{\mathrm{A}}}{R}\left(\frac{1}{T} - \frac{1}{T_{\mathrm{R}}}\right)\right]. \tag{2.25c}$$

Now, from (2.25b) and (2.25c), it is clear that both eigenvalues are positive as well as $|\mathbf{J}| = \lambda_1 \lambda_2 = \lambda_2$. Hence, $\mathbf{J}$ is non-singular. Further, the Jacobian matrix $\mathbf{J}$ satisfies the following definition:

Definition 2.1 (M-Matrix)**.** *A matrix $A \in \mathbb{R}^{I \times I}$ for $I \in \mathbb{N}$, is called an M-Matrix, see [34], if*

$$a_{\alpha\alpha} > 0 \qquad \text{for all} \qquad \alpha \in I, \tag{2.26a}$$

$$a_{\alpha\beta} \leq 0 \qquad \text{for all} \qquad \alpha \neq \beta, \tag{2.26b}$$

$$A \text{ is regular and } A^{-1} \geq 0. \tag{2.26c}$$

*Hence, the Jacobian matrix **J** is non-symmetric but positive definite and the evolution problem for our system of PDEs is well-posed.*

This model is solved numerically in Section 4.3.

2.3 EDM Coupled with Simplified Energy Equation

In this valuable simplified model variant, we consider the unchanged mass balance (2.18a) for n components as

$$[1 + Fa_n(T)] c_{n_\tau} + c_n Fa_n(T)_T T_\tau = -c_{n_x} + t_{R_0} D_x c_{n_{xx}}, \qquad n = 1, 2, 3, ..., N_c \tag{2.27}$$

and replace the detailed energy equation with its simplified version. This means that in (2.18b), we neglect the terms containing X_3, and the accumulation term G. The energy balance then reduces to the following form

$$T_\tau = -X_1 T_x + t_{R_0} X_2 (T_w - T) . \tag{2.28}$$

The decision to neglect X_3 and G_n is made to simplify the analytical solvability of the equation. By (2.15e), X_3 incorporates the axial dispersion λ_z in the heat transfer, and by neglecting this term, we assume that the heat transfer within the system is primarily governed by conduction or convection and that the effects of axial mixing or spreading of heat are not important to the specific conditions or system under study.

Similarly, by disregarding the term G, it is assumed that the components' specific enthalpy changes during adsorption and desorption, represented by ΔH_A, have a negligible impact compared to the combined heat capacities of the liquid and solid phases. This simplification allows for a more manageable analysis without compromising the overall understanding of the system.

While these simplifications may introduce certain limitations to the usefulness of the analytical solution, they offer the advantage of making the equation more amenable to mathematical treatment. By focusing on the key terms and disregarding those with minimal impact, the derived analytical solution provides valuable insights into the system's behavior, can serve as a foundation for numerically solving the mass balance equation and facilitates a comprehensive exploration of the system's properties.

The initial and boundary conditions (2.19a) to (2.20c) from the previous model should be considered to solve this model.

We will now calculate the analytical solution of (2.28) and then numerically estimate the concentration solution with (2.27). Thus, we prepare (2.28) for the Laplace transform by

considering $a = -X_1$, $b = -t_{R_0}X_2$, and $c = t_{R_0}X_2T_w$ as intermediate parameters. The Eq. (2.28) can be written as

$$T_\tau = aT_x + bT + c.\qquad(2.29)$$

The Laplace transformation $\mathcal{L}$ maps $T \longrightarrow Y$ and $\tau \longrightarrow s$. Let us apply $\mathcal{L}$ to the above PDE to get

$$\mathcal{L}\{T_\tau\} = \mathcal{L}\{aT_x\} + \mathcal{L}\{bT\} + \mathcal{L}\{c\}.\qquad(2.30a)$$

According to Laplace transform formula, we have

$$\mathcal{L}\{T(\tau)\} = Y(s) = \int_0^\infty e^{-st}T(\tau)\,d\tau,\qquad(2.30b)$$

which results from PDE (2.29) in an ODE of the following form

$$sY - T_R = a\frac{dY}{dx} + bY + \frac{c}{s}\qquad(2.30c)$$

or

$$\frac{dY}{dx} = \frac{s-b}{a}Y - \frac{T_R}{a} - \frac{c}{sa} = AY + B,\qquad(2.30d)$$

such that

$$A = \frac{s-b}{a},\qquad(2.31a)$$

$$B = -\left(\frac{T_R}{a} + \frac{c}{sa}\right)\qquad(2.31b)$$

and

$$\frac{B}{A} = -\frac{T_R}{s-b} - \frac{c}{s(s-b)}.\qquad(2.31c)$$

Now, from Eq. (2.30d), we have

$$\int_{\frac{T_R}{s}}^{Y(x,s)} \frac{dY}{AY+B} = \int_0^1 dx\qquad(2.32a)$$

or

$$\frac{1}{A}\ln\frac{AY(x,s)+B}{A\frac{T_R}{s}+B} = x,\qquad(2.32b)$$

which after a little simplification gives

$$Y(x,s) = -\frac{B}{A} + \left(\frac{T_R}{s} + \frac{B}{A}\right)e^{Ax}.\qquad(2.32c)$$

After putting Eqs. (2.31a) and (2.31c) in above equation, we get

$$Y(x,s) = \frac{T_R}{s-b} + \frac{c}{s(s-b)} + \frac{T_R}{s}e^{(s-b)\frac{x}{a}} - \frac{T_R}{s-b}e^{(s-b)\frac{x}{a}} - \frac{c}{s(s-b)}e^{(s-b)\frac{x}{a}}.$$

After a little simplification and setting $d = bT_R + c, f = \frac{-b}{a}x$ and $g = \frac{x}{a}$, yields

$$Y(x,s) = \frac{T_R}{s-b} + \frac{c}{s(s-b)} - \frac{d}{s(s-b)}e^{f+gs}$$

$$= \frac{T_R}{s-b} + \frac{c}{s(s-b)} - \frac{de^f}{b}\frac{b}{s(s-b)}e^{gs}$$

$$= \frac{T_R}{s-b} + \frac{c}{s(s-b)} - \frac{de^f}{b}\left(-\frac{1}{s} + \frac{1}{s-b}\right)e^{gs}. \tag{2.32d}$$

Let us put back values of d, f and g and $\frac{de^f}{b} = \left(T_R + \frac{c}{b}\right)e^{-\frac{b}{a}x}$ and then do a little simplification to get

$$Y(x,s) = \frac{T_R}{s-b} + \frac{c}{s(s-b)} + \left[\left(T_R + \frac{c}{b}\right)e^{-\frac{b}{a}x}\right]\frac{e^{\frac{x}{a}s}}{s} - \left[\left(T_R + \frac{c}{b}\right)e^{-\frac{b}{a}x}\right]\frac{e^{\frac{x}{a}s}}{s-b} \tag{2.32e}$$

or

$$Y(x,s) = Z_1 + Z_2 + Z_3 + Z_4, \tag{2.32f}$$

where

$$Z_1 : \frac{T_R}{s-b}, \qquad\qquad Z_2 : \frac{c}{s(s-b)},$$

$$Z_3 : \left[\left(T_R + \frac{c}{b}\right)e^{-\frac{b}{a}x}\right]\frac{e^{\frac{x}{a}s}}{s}, \qquad Z_4 : -\left[\left(T_R + \frac{c}{b}\right)e^{-\frac{b}{a}x}\right]\frac{e^{\frac{x}{a}s}}{s-b}. \tag{2.32g}$$

Now we use inverse Laplace transformation, which will transform back $Y \longrightarrow T$ and $s \longrightarrow \tau$. For that we use [76], according to which

$$\frac{1}{s-\alpha} \Leftrightarrow e^{\alpha t}, \qquad\qquad \frac{1}{s(s-\alpha)} \Leftrightarrow \frac{e^{\alpha t}-1}{\alpha},$$

$$\frac{e^{-\alpha s}}{s} \Leftrightarrow \begin{cases} 0 & \text{for } 0 < t < \alpha \\ 1 & \text{for } t > \alpha \end{cases}, \qquad \frac{e^{-\alpha s}}{s+\beta} \Leftrightarrow \begin{cases} 0 & \text{for } t < \alpha \\ e^{-\beta(t-\alpha)} & \text{for } t > \alpha. \end{cases} \tag{2.33}$$

Then, using Eq. (2.33) and taking $\left(T_R + \frac{c}{b}\right)e^{-\frac{b}{a}x} = \frac{de^f}{b}$, the back Laplace transformations of terms in Eq. (2.32g) look like

$$Z_1 : \frac{T_R}{s-b} \Leftrightarrow T_R e^{b\tau}, \qquad\qquad Z_2 : \frac{c}{s(s-b)} \Leftrightarrow \frac{c}{b}\left(e^{b\tau} - 1\right),$$

$$Z_3 : \frac{de^f}{b}\frac{e^{\frac{x}{a}s}}{s} \Leftrightarrow \begin{cases} 0 & \text{for } 0 < \tau < -\frac{x}{a}, a < 0 \\ \frac{de^f}{b} & \text{for } \tau > -\frac{x}{a} \end{cases}, \quad Z_4 : \frac{de^f}{b}\frac{e^{\frac{x}{a}s}}{(s-b)} \Leftrightarrow \begin{cases} 0 & \text{for } \tau < -\frac{x}{a} \\ \frac{de^f}{b}e^{b(\tau+\frac{x}{a})} & \text{for } \tau > -\frac{x}{a}. \end{cases} \tag{2.34}$$

In view of Eq. (2.32f), for $\tau < -\frac{x}{a} = \frac{x}{X_1}$ or $x > X_1\tau$, we get

$$T(x,\tau) = Z_1 + Z_2 \tag{2.35a}$$

or, after using solutions (2.34),

$$T(x,\tau) = T_R e^{b\tau} + \frac{c}{b}\left(e^{b\tau} - 1\right) = -\frac{c}{b} + \left(T_R + \frac{c}{b}\right)e^{b\tau}. \tag{2.35b}$$

Similarly, for $\tau > \frac{x}{X_1}$ or $x < X_1\tau$, we get

$$T(x,\tau) = Z_1 + Z_2 + Z_3 + Z_4 \tag{2.36a}$$

and again using solutions (2.34), we get

$$T(x,\tau) = T_R e^{b\tau} + \frac{c}{b}\left(e^{b\tau} - 1\right) + \frac{de^f}{b} - \frac{de^f}{b}e^{b(\tau+\frac{x}{a})}. \tag{2.36b}$$

Hence, after putting $\frac{c}{b} = -T_w, b = -t_{R_0}X_2, \frac{de^f}{b} = -\left(T_w - T_R\right)e^{-t_{R_0}\frac{X_2}{X_1}x}$ and $a = -X_1$ in Eq. (2.35b) as well as in Eq. (2.36b), we get the final solution of T as

$$T(\tau) = T_w - \left(T_w - T_R\right)e^{-t_{R_0}X_2\tau} \qquad \text{for} \qquad \tau < \frac{x}{X_1} \tag{2.37a}$$

and

$$T(x) = T_w - \left(T_w - T_R\right)e^{-t_{R_0}\frac{X_2}{X_1}x} \qquad \text{for} \qquad x < X_1\tau. \tag{2.37b}$$

We will use this analytical solution in Section 4.2 for the numerical analysis of the mass balance equation given by (2.27). The aim is to establish a comprehensive understanding of the system's behavior under a slower temperature change and its impact on the retention times, distribution of concentration as well as cycle times in comparison to the previous model. Integrating the analytical solution into the numerical analysis allows for a more efficient and accurate evaluation of the mass balance equation.

2.4   Overview of Models Analyzed

In this section, two models are proposed, both of which include an ideal temperature profile known as the temperature step function. Using the step function instead of the energy equation simplifies the analysis by neglecting convective heat transfer, spatial mixing effects, and the heat exchange rate with the source connected to the column. This approach provides an initial, but informative, assessment of the concentration dynamics affected by temperature. The two coupled models with this function are the EDM and EM, that are described below.

2.4.1   EDM Coupled with Ideal Temperature Step Gradients

In this modeling approach, the EDM (2.27) is analyzed in conjunction with an ideal temperature profile known as the temperature step gradient. The term "ideal temperature profile" is used because it assumes that temperature changes at specific switching times happen abruptly when a

certain pulse crosses the point x_m of the column either entirely or partially. Consequently, $T_\tau = 0$ for all τ falling within the closed interval between two consecutive switching times. After this simplification, equation (2.27) can be expressed in the following form.

$$[1 + Fa_n(T)]\, c_{n_\tau} = -c_{n_x} + t_{R_0} D_x c_{n_{xx}}, \qquad n = 1, 2, 3, ..., N_\mathrm{c}. \tag{2.38}$$

The switching times for cooling or heating are denoted in dimensional form by t_k, from which in dimensionless form, according to (2.12a), $\tau_k = \frac{t_k}{t_{R_0}}$ results, where $k \in \mathbb{N}_0$. To each semi-open interval $[\tau_k, \tau_{k+1}[$ and $\tau_k < \tau_{n,\max}^P, P \in \mathbb{N}$, we associate a constant but adjustable temperature for segment II. We take a sequence $T_k \in \{T_\mathrm{R}, T_\mathrm{L}, T_\mathrm{H}\}$, where $T_\mathrm{R}, T_\mathrm{L}$ and T_H are representing reference, low and high temperatures, respectively. With this, we define a specific version of the temperature step function for our theoretical experiment, as

$$T(x, \tau) = \begin{cases} T_\mathrm{R} & \text{for} \quad 0 \leq x \leq x_\mathrm{m}, & \tau \in [0, \tau_{n,\max}^P], \\ T_k & \text{for} \quad x_\mathrm{m} < x \leq x_\max, & \tau \in [\tau_k, \min\{\tau_{k+1}, \tau_{n,\max}^P\}], \\ & & k \in \mathbb{N}_0, \tau_k < \tau_{n,\max}^P. \end{cases} \tag{2.39}$$

Remember that, k only indicates the number of times the temperature of segment II is changed. T_0 means the initial temperature of segment II, T_1 means a first change, whereas, T_2 means, a second change of the temperature, and so on.

It should be kept in mind that for every specific experiment, we will have to consider specific adjusted finite sequences of T_k for each component of a mixture considering the specific migration and separation properties. Also the sequence of the switching times τ_k will depend on the specific migration speeds of the adsorption and desorption fronts.

Once the pulse reaches the middle z_m of the column, it may encounter either a lower or higher temperature immediately or after a slight delay. These temperature changes are referred to as Type I and Type II and are explained in detail in Section 3.3.1. Due to the abrupt change in temperature following the interface, an adjustment is required to account for this discontinuity in the EDM. The specific adjustment is guided by the shock condition, which ensures the consistency of the concentration profiles across the interface. The shock condition provides the necessary information to estimate the amount of concentration in segment II, denoted as c_n^II. This adjustment is applied to the concentration in segment I, denoted as c_n^I. The jump condition for discontinuous solutions with a discontinuity $s = \frac{dx}{d\tau}$ is

$$s\left[\left(1 + Fa_n(T^\mathrm{I})\right)c_n^\mathrm{I} - \left(1 + Fa_n(T^\mathrm{II})\right)c_n^\mathrm{II}\right] + \left[c_n^\mathrm{I} - c_n^\mathrm{II}\right] = 0. \tag{2.40}$$

In Type I, we have $s = 0$. Then the above equation renders

$$c_n^\mathrm{I} = c_n^\mathrm{II}. \tag{2.41}$$

In Type II, we have a stationary jump in temperature with $s = \infty$. Dividing Eq. (2.40) by s and taking $s \to \infty$ yields

$$(1 + Fa_n(T^\mathrm{I}))c_n^\mathrm{I} - (1 + Fa_n(T^\mathrm{II}))c_n^\mathrm{II} = 0$$

or

$$c_n^\mathrm{II} = \frac{1 + Fa_n(T^\mathrm{I})}{1 + Fa_n(T^\mathrm{II})} c_n^\mathrm{I}. \tag{2.42}$$

By incorporating the shock condition, we ensure a smooth transition and a continuous representation of the concentration dynamics, accounting for the temperature-induced jump in the EDM.

This adjustment allows for a more accurate analysis and understanding of the solution's behavior across the interface.

Under constant temperature conditions, the conservation of mass is upheld as long as there is conservation of concentration. This principle extends to the conservation of adsorbed mass, as described by Equation 2.5. However, when there is a jump in temperature, mass conservation can only be maintained if the concentration is adjusted in accordance with Equation 2.42 at the internal boundary where there is a flux due to temperature change.

Due to the aforementioned observation, it becomes necessary to establish separate initial and boundary conditions for each segment as outlined below.

$$c_n^{\mathrm{I}}(x = x_0 \text{ to } x_\mathrm{m}, \tau_0) = 0, \tag{2.43a}$$

$$c_n^{\mathrm{II}}(x = x_\mathrm{m} \text{ to } x_\mathrm{max}, \tau_0) = 0 \tag{2.43b}$$

and for $p = 1, 2, 3, ..., P, P \in \mathbb{N}$, we have

$$c_n^{\mathrm{I}}(x_0, \tau) = \begin{cases} c_{n,\mathrm{inj}}, & \tau_\mathrm{inj}^p \leq \tau \leq \tau_\mathrm{inj}^p + \Delta\tau_\mathrm{inj} \\ 0, & \tau_\mathrm{inj}^p + \Delta\tau_\mathrm{inj} < \tau < \tau_{n,\mathrm{m}}^p, \end{cases} \tag{2.43c}$$

$$c_n^{\mathrm{II}}(x_\mathrm{m}, \tau) = \begin{cases} \frac{1+Fa_n(T^{\mathrm{I}})}{1+Fa_n(T^{\mathrm{II}})} c_n^{\mathrm{I}}(x_\mathrm{m}, \tau_{n,\mathrm{m}}^p), & \tau_{n,\mathrm{m}}^p \leq \tau \leq \tau_{n,\mathrm{m}}^p + \Delta\tau_\mathrm{inj} \\ 0, & \tau_{n,\mathrm{m}}^p + \Delta\tau_\mathrm{inj} < \tau < \tau_{n,\mathrm{max}}^p, \end{cases} \tag{2.43d}$$

where $p = 1, 2, 3, ..., P \in \mathbb{N}$. At the right boundary due to the second order derivative, we have

$$c_{n_x}^{\mathrm{II}}(x_\mathrm{max}, \tau) = 0. \tag{2.43e}$$

This model is solved numerically using FVM in Section 4.1.

2.4.2 Equilibrium Model (EM) Coupled with Ideal Temperature Step Gradients

The last, easily solvable and exploitable model is the so-called equilibrium model. This model disregards molecular diffusion, axial dispersion, and mass transfer resistances in favor of high mass transfer rates. All these facts are summarized in the term $\mathrm{D}_x c_{xx}$, and neglecting this term in (2.38), we obtain the equilibrium model for concentration in the following form

$$[1 + Fa_n(T)] c_{n_\tau} = -c_{n_x}, \qquad n = 1, 2, \cdots, N_\mathrm{c}, \tag{2.44}$$

coupled with the same temperature step gradients profile (2.39)

$$T(x, \tau) = \begin{cases} T_\mathrm{R} & \text{for} \quad 0 \leq x \leq x_\mathrm{m}, \quad \tau \in [0, \tau_{n,\mathrm{max}}^P], \\ T_k & \text{for} \quad x_\mathrm{m} < x \leq x_\mathrm{max}, \quad \tau \in [\tau_k, \min\{\tau_{k+1}, \tau_{n,\mathrm{max}}^P\}], \\ & \qquad\qquad\qquad\qquad k \in \mathbb{N}_0, P \in \mathbb{N}, \tau_k < \tau_{n,\mathrm{max}}^P. \end{cases} \tag{2.45}$$

This model concentrates on obtaining equilibrium conditions, making it possible to analyze concentration behavior more easily. When fast equilibrium attainment is assumed, it offers useful insights into the overall system performance and concentration profiles. When investigating

systems where quick equilibration is anticipated, the equilibrium model is especially helpful in understanding and improving such processes. [37, 40]

Since we plane to solve this model analytically using the method of characteristics, the model is transformed back to its dimensional form. This conversion is facilitated by the equations (2.12a) to (2.12c). Therefore, the equations (2.44) and (2.45) are rewritten in dimensional form as

$$[1 + Fa_n(T)] c_{n_t} = -uc_{n_z}, \qquad n = 1, 2, \cdots, N_\text{c} \tag{2.46}$$

and

$$T(x,t) = \begin{cases} T_\text{R} & \text{for} \quad 0 \leq z \leq z_\text{m}, & t \in [0, t^P_{n,\text{max}}], \\ T_k & \text{for} \quad z_\text{m} < z \leq z_\text{max}, & t \in [t_k, \min\{t_{k+1}, t^P_{n,\text{max}}\}], \\ & & k \in \mathbb{N}_0, P \in \mathbb{N}, t_k < t^P_{n,\text{max}}. \end{cases} \tag{2.47}$$

Like EDM, in the EM also, separate initial and boundary conditions are considered for segment I and segment II, given by (2.43a) to (2.43e). These conditions are given in dimensionlized form as

$$c_n^\text{I}(z = z_0 \text{ to } z_\text{m}, t_0) = 0, \tag{2.48a}$$

$$c_n^\text{II}(z = z_\text{m} \text{ to } z_\text{max}, t_0) = 0, \tag{2.48b}$$

$$c_n^\text{I}(z_0, t) = \begin{cases} c_{n,\text{inj}}, & t^p_\text{inj} \leq t \leq t^p_\text{inj} + \Delta t_\text{inj} \\ 0, & t^p_\text{inj} + \Delta t_\text{inj} < t < t^p_{n,\text{m}}, \end{cases} \tag{2.48c}$$

$$c_n^\text{II}(z_\text{m}, t) = \begin{cases} \frac{1+Fa_n(T^\text{I})}{1+Fa_n(T^\text{II})} c_n^\text{I}(z_\text{m}, t^p_{n,\text{m}}), & t^p_{n,\text{m}} \leq t \leq t^p_{n,\text{m}} + \Delta t_\text{inj} \\ 0, & t^p_{n,\text{m}} + \Delta t_\text{inj} < t < t^p_{n,\text{max}}, \end{cases} \tag{2.48d}$$

with $p = 1, 2, 3, ..., P \in \mathbb{N}$. This model is solved analytically in Chapter 3, while its numerical solution is obtained by solving the EDM given in Section 4.1 for $D_x = 0$.

2.5 Performance of the Chromatographic Process

In chromatography, the column production rate (productivity) is defined as the total mass of each component produced per cycle time. To increase the production rate, the shortest possible cycle time should be determined. In this work, we tried to obtain a higher production rate of the column under gradient conditions, $P_{n,\text{grad}}$, compared to the production rate under isothermal conditions, $P_{n,\text{iso}}$. Before introducing the formulas for the production rate in the above cases, we first define the cycle time.

In HPLC, the cycle time usually refers to the time required for a complete analytical run. It includes injection of the sample into the column, separation of the solutes, and elution of these solutes from the column to the detector. This time is important in determining the productivity of an HPLC system. Let us denote this time variable by Δt_c^p for the case of the planned mixture of n components injected P-times mentioned earlier. We estimate Δt_c^p using the retention time $t^p_{n,\text{max}}$ of the slower component c_n, and the time at which the adsorption front of the fastest component c_1 of the same injection exits the column, i.e., $t^p_{1,\text{max,ad}}$, as follows

$$\Delta t_c^p = t^p_{n,\text{max}} - t^p_{1,\text{max,ad}}, \qquad \text{for} \qquad p = 1, 2, 3, ..., P, P \in \mathbb{N}. \tag{2.49}$$

Now we introduce formulas for production rates in both the isothermal and gradient cases. Let $\Delta t_{c,iso}$ be the cycle time in the earlier case and $\Delta t_{c,grad}^{p}$ be the cycle time in the later case, which one wants to achieve shorter than $\Delta t_{c,iso}$. If $m_{n,total}$ is the mass of each component moving from the column's inlet to the column's outlet, then the production rates in the two cases mentioned above can be written mathematically as

$$P_{n,grad} = \frac{m_{n,total}}{\Delta t_{c,grad}^{p}} \tag{2.50}$$

and

$$P_{n,iso} = \frac{m_{n,total}}{\Delta t_{c,iso}^{p}}, \qquad \text{for} \qquad p = 1, 2, 3, ..., P, P \in \mathbb{N}. \tag{2.51}$$

From both (2.50) and (2.51), it is obvious that the process with shorter cycle time will have higher production rate. In the results, we will divide the values obtained from the above formulas by the volume of the column and convert the time to hours to obtain the productivity in $gh^{-1}L^{-1}$. See Tables 3.6 and 3.10 for instance.

The total mass collected at the outlet of the column can reach the injected amount if there is no overlap between the eluting bands, i.e. $m_{n,total} = m_{n,inj}$. Only this attractive scenario is considered in our study.

Since we consider in this dissertation, the same column volume in both isothermal and gradient operation, we do not touch here on the scale-dependent aspect typically used to evaluate a productivity as the ratio of production rate to column size.

By multiplying the linear velocity, cross-sectional area, porosity factor and injection time, the product represents the volume of the injected sample. This volume is then multiplied by the concentration to obtain the mass of the injected sample in grams. Ensuring that the units are consistent throughout the calculation is crucial for accurate determination of the mass. Hence, the mass injected at the column's inlet z_0, denoting the cross-sectional area of the column by A, is given as

$$m_{n,inj} = uA\epsilon\Delta t_{inj}c_{n,inj}, \qquad n = 1, 2, 3, ..., N_c. \tag{2.52}$$

The mass inside the segments over the distance z at a specific time t^*, denoted total by $m_{n,total}$, is obtained by integrating the sum of concentrations in both the phases over the range from 0 to max z_{max}, i.e.

$$m_{n,total} = A \int_0^{z_{max}} \epsilon c_n(z, t^*) + (1 - \epsilon)a_n(T)c_n(z, t^*)\partial z \tag{2.53}$$

and to obtain it over t for a selected location z^* in the column, we multiply it by the specific velocity of the component at corresponding temperature $\frac{u}{1+Fa_n(T)}$, which is given by

$$m_{n,total} = \frac{u}{1 + Fa_n(T)}A \int_0^{t_{n,max}^{p}} \epsilon c_n(z^*, t) + (1 - \epsilon)a_n(T)c_n(z^*, t)\partial t. \tag{2.54}$$

At z_{max} there in no mass inside solid phase ans hence the collected mass, $m_{n,col}$, is given as

$$m_{n,col} = u\epsilon A \int_0^{t_{n,max}^{p}} c_n(z_{max}, t)\partial t, \qquad n = 1, 2, 3, ..., N_c. \tag{2.55}$$

Here, the various parameters are expressed in their respective units. The interstitial velocity u is measured in centimeters per minute [cm/min], representing the rate at which the solute travels

through the system. The cross-sectional area A is given in square centimeters [cm^2], indicating the size of the column's cross-section. The porosity factor ϵ is a dimensionless quantity that describes the void fraction of the stationary phase. The concentration $c_{n,\mathrm{inj}}$ is measured in grams per liter [g/L], signifying the solute concentration in the injected sample. Finally, the injection time Δt_{inj} is recorded in minutes [min].

Summary of Chapter 2:   In this chapter, a gradient concept for increasing the productivity of liquid chromatographic columns is first proposed. Then four mathematical models have been proposed to theoretically implement this concept. We explored mass balances in the form of EM and EDM coupled with energy balance. This energy balance was introduced in detailed as well as in simplified form. The mentioned mass balances were also presented as coupled with ideal temperature step gradients. These simple models form the foundation for the subsequent analysis and exploration within the study.

The models will be initially tested for single-component injections, enabling the observation of individual concentration and retention behaviors. Subsequently, these models will be subjected to ternary-component mixture injections. Of key relevance will be to evaluate the potential of gradients to reduce the cycle time given by (2.49). This strategic adjustment aims to increase process productivity given by (2.51).

Chapter 3

Equilibrium Model and Method of Characteristics

In this chapter, we will focus on optimizing liquid chromatographic columns using the equilibrium model, also known as the ideal model, coupled with ideal temperature profiles described by step functions. This model is introduced in Section 2.4.2. We will explore the analytical solution of this model achieved through the method of characteristics. Our study will begin with single-component injections, where we will analyze concentration profiles in time and space under different temperature gradients. Building upon this foundation, we will address the challenges posed by ternary component mixtures, specifically the "Late Eluter" and "Early Eluter" cases introduced in Chapter 2. By devising an optimal switching strategy, we aim to improve productivity by optimizing the cycle time under isocratic conditions $\Delta t^p_{c,\text{iso}}$ to obtain the shorter cycle times $\Delta t^p_{c,\text{grad}}$ using gradient operations.

It is noteworthy that a substantial portion of the content in this chapter has been published in [37].

3.1 EM Coupled with Ideal Temperature Step Gradients

To derive the analytical solution using the method of characteristics, we utilize the dimensional versions of the EM and ideal temperature step function. This can be restated from equations (2.46) and (2.47) as

$$[1 + Fa_n(T)]\, c_{n_t} = -uc_{n_z}, \qquad n = 1, 2, \cdots, N_c \tag{3.1}$$

and

$$T(x,t) = \begin{cases} T_R & \text{for} \quad 0 \leq z \leq z_m, & t \in [0, t^P_{n,\max}], \\ T_k & \text{for} \quad z_m < z \leq z_{\max}, & t \in [t_k, \min\{t_{k+1}, t^P_{n,\max}\}], \\ & & k \geq 0, P \in \mathbb{N}, t_k < t^P_{n,\max}. \end{cases} \tag{3.2}$$

According to (3.2), the temperature of segment I is constant, but for segment II it jumps from one constant value to another. Therefore, we use (3.1) in each spatial segment or time interval as

$$c_{n_t} = -\frac{u}{1 + Fa_n(T)} c_{n_z}. \tag{3.3}$$

31

3.2 Analytical Solution

In this section we derive analytical expressions to quantify the transient concentration profiles, generally denoted by $c_n(z, t)$, under the influence of the described segmented temperature gradients. For this we first calculate the trajectories, $z_n(t)$. Then, the method of characteristic is applied to reduce PDE (3.3) to an ODE. As a result, analytical expressions for solution trajectories (paths) are obtained. From the mentioned equation, the characteristic speed of the fronts corresponding to component n, is given as

$$\frac{dz_n}{dt} = \frac{u}{1 + Fa_n(T)} \qquad \text{for } t > t_0 \text{ with } z_n(t_0) = 0. \tag{3.4}$$

The solution of (3.4) provides the trajectories of the solutions. Since the temperature $T(t)$ is piece-wise constant, one can integrate this ODE easily. Furthermore, let $t^p_{n,\mathrm{m}}$ be the time when the adsorption front of component n of an injection p reaches the middle of the column z_{m}, where $p = 1, 2, 3, ..., P \in \mathbb{N}$. We already know that $t^p_{n,\max}$ is the time when the desorption front of the same component reaches $z_{\max}$. For $t \in [0, t^p_{n,\mathrm{m}}]$, after introducing p over z_n, equation (3.4) gives

$$z^p_n(t) = \int_0^t \frac{u}{1 + Fa_n(T_{\mathrm{R}})} dt \;\; = \;\; \frac{ut}{1 + Fa_n(T_{\mathrm{R}})}, \qquad p = 1, 2, 3, ..., P \in \mathbb{N}. \tag{3.5}$$

The above equation gives different space-time positions for each component. Using this equation, we can easily find the time $t^p_{n,\mathrm{m}}$ as

$$t^p_{n,\mathrm{m}} = \frac{1 + Fa_n(T_{\mathrm{R}})}{u} z_{\mathrm{m}}. \tag{3.6}$$

For $t^p_{n,\max} > t > t^p_{n,\mathrm{m}}$, we have $z^p_n(t) \in [z_{\mathrm{m}}, z_{\max}]$. Now, the characteristics speed is affected by the temperature change. This effect depends on the particular switching times $t_k, k \geq 0$, mentioned in Chapter 2. Suppose that we have $t_h, ..., t_{h+l} \in \,]t^p_{n,\mathrm{m}}, t]$ for some $h, l \in \mathbb{N}$. This means that $t_h, ..., t_{h+l}$ are the exploitable switching times in the interval $]t^p_{n,\mathrm{m}}, t]$, which may be different for different components i. Then, Equation (3.5) can be integrated as

$$z^p_n(t) = \int_0^{t^p_{n,\mathrm{m}}} \frac{u}{1 + Fa_n(T_{\mathrm{R}})} dt + \int_{t^p_{n,\mathrm{m}}}^{t_h} \frac{u}{1 + Fa_n(T_{h-1})} dt +$$
$$\sum_{k=h}^{p+l-1} \int_{t_k}^{t_{k+1}} \frac{u}{1 + Fa_n(T_k)} dt + \int_{t_{h+l}}^{t} \frac{u}{1 + Fa_n(T_{h+l})} dt. \tag{3.7}$$

The term $\int_{t^p_{n,\mathrm{m}}}^{t_h} \frac{u}{1 + Fa_n(T_{h-1})} dt$, by setting $T_0 = T_{\mathrm{R}}$, in the above equation tells that the temperature of the pulse stays still T_{R} until the whole pulse enters segment II. This is possible when both the segments are initially kept at the same temperature. Later, in the case studies, we will discuss this scenario as a special case, c.f. Section 3.3.1, (Type II). We neglect this term for the case where both the segments are initially kept at different temperatures, c.f. Section 3.3.1, (Type I).

We denote the time dependent position of the adsorption (ad) front of the pulse by $z^p_{n,\mathrm{ad}}(t)$, while the position of the desorption (de) front by $z^p_{n,\mathrm{de}}(t)$ for component i. The adsorption front enters the column at t_0 while the desorption front enters at $t = t_0 + \Delta t_{\mathrm{inj}}$. With these initial times,

the adsorption and desorption fronts can be explicitly determined. After a simple calculation, the characteristic curve or the space-time trajectory for $z_{n,\mathrm{ad}}(t)$ is obtained from Equation (3.7) as

$$
z^p_{n,\mathrm{ad}}(t) = \begin{cases}
\frac{u}{1+Fa_n(T_\mathrm{R})}t, & \text{for} & t \in [t_0, t^p_{n,\mathrm{m}}[, \\
z^p_{n,\mathrm{ad}}(t_{n,\mathrm{m}}) + \frac{u}{1+Fa_n(T_{h-1})}(t - t_{n,\mathrm{m}}), & \text{for} & t \in [t^p_{n,\mathrm{m}}, t_h[, \\
z^p_{n,\mathrm{ad}}(t_h) + \sum_{k=h}^{h+\ell-1}\frac{u}{1+Fa_n(T_k)}(t_{k+1} - t_k)+ & & \\
\frac{u}{1+Fa_n(T_{h+\ell})}(t - t_{h+\ell}), & \text{for} & t \in [t_{h+\ell}, t_{h+\ell+1}[, \\
& & \ell \in \{0, 1, 2, ..., l-1\}, \\
z^p_{n,\mathrm{ad}}(t_{h+l}) + \frac{u}{1+Fa_n(T_{h+l})}(t - t_{h+l}), & \text{for} & t \in [t_{h+l}, t^p_{n,\mathrm{max}}].
\end{cases}
\tag{3.8a}
$$

Furthermore, we set $z^p_{n,\mathrm{de}}(t) = 0$ for $t \in [0, \Delta t_{\mathrm{inj}}]$ and obtain the trajectories for the desorption fronts as

$$
z^p_{n,\mathrm{de}}(t) = z^p_{n,\mathrm{ad}}(t - \Delta t_{\mathrm{inj}}) \qquad \text{for} \qquad t > \Delta t_{\mathrm{inj}}.
\tag{3.8b}
$$

Consequently, the time $t^p_{n,\mathrm{ad}}(z)$ required for the adsorption front of component n to reach any point in z can be derived as

$$
t^p_{n,\mathrm{ad}}(z) = \begin{cases}
\frac{1+Fa_n(T_\mathrm{R})}{u}z, & \text{for} & z \in [0, z_\mathrm{m}], \\
\frac{1+Fa_n(T_{h-1})}{u}z - \frac{1+Fa_n(T_{h-1})}{u}z^p_{n,\mathrm{ad}}(t_{n,\mathrm{m}}) + t_{n,\mathrm{m}}, & \text{for} & z \in \,]z_\mathrm{m}, z_\mathrm{max}], \\
\frac{1+Fa_n(T_{h+\ell})}{u}z - \frac{1+Fa_n(T_{h+\ell})}{u}z^p_{n,\mathrm{ad}}(t_h) - & & \\
\sum_{k=h}^{h+\ell-1}\frac{1+Fa_n(T_{h+\ell})}{1+Fa_n(T_k)}(t_{k+1} - t_k) + t_{h+\ell}, & \text{for} & z \in \,]z_\mathrm{m}, z_\mathrm{max}], \\
& & \ell \in \{0, 1, 2, ..., l-1\}, \\
\frac{1+Fa_n(T_{h+l})}{u}z - \frac{1+Fa_n(T_{h+l})}{u}z^p_{n,\mathrm{ad}}(t_{h+l}) + t_{h+l}, & \text{for} & z \in \,]z_\mathrm{m}, z_\mathrm{max}]
\end{cases}
\tag{3.8c}
$$

and for the desorption front, where we do not use subscript "de", you get it simply as

$$
t^p_n(z) = t^p_{n,\mathrm{ad}}(z) + \Delta t_{\mathrm{inj}},
\tag{3.8d}
$$

such that

$$
t^p_{n,\mathrm{ad}}(z_\mathrm{m}) =: t^p_{n,\mathrm{m}}, \qquad t^p_n(z_\mathrm{m}) =: t^p_{n,\mathrm{m}} + \Delta t_{\mathrm{inj}}
\tag{3.8e}
$$

and

$$
t^p_{n,\mathrm{ad}}(z_\mathrm{max}) =: t^p_{n,\mathrm{max,ad}}, \qquad t^p_n(z_\mathrm{max}) =: t^p_{n,\mathrm{max}}, \qquad p = 1, 2, 3, ..., P \in \mathbb{N}.
\tag{3.8f}
$$

The above specified trajectories allow calculating the solution for the components' concentration profiles as function of z and t. The solution consists of three parts divided in the time domain by a first state, α, controlled by the reference temperature, a third (final) state, γ, controlled by a different temperature in segment II and an intermediate state, β, which is influenced by both the temperatures via changing migration velocities, c.f. Figure 3.2. The later state gradually transforms the concentration in state α, $c^\alpha_i = c_{n,\mathrm{inj}}$, to the concentration in state γ, c^γ_i, via the concentration in itself, c^β_i. The concentration in each state depends on the difference between the trajectories of the adsorption and desorption fronts (space-bandwidths) in the same state because it varies from state to state. Let Z^α be the space-bandwidth of the pulse in state α, and Z^γ be

the space-bandwidth in state γ. These space-bandwidths are certainly constant because both adsorption and desorption fronts are migrating with same speeds in the corresponding states. But, the space-bandwidth in state β is not constant because, in this state, the desorption front of the pulse is in segment I and the adsorption front is in segment II. So both are migrating with different speeds. As much as, the pulse enters segment II, the space-bandwidth in state β tends to that in state γ. Let us denote this variable space-bandwidth by Z^β, c.f. Figure 3.3. Figures 3.2 and 3.3 will be explained later to illustrate state β graphically. We denote the part of Z^β in segment I, by $Z^{\beta,\mathrm{I}}$ and its part in segment II, by $Z^{\beta,\mathrm{II}}$ so that $Z^\beta = Z^{\beta,\mathrm{I}} + Z^{\beta,\mathrm{II}}$. The concentration obtained from the characteristic curves is the total concentration present in a given volume element and at a given time. However, in order to guarantee the mass conservation via the formulas (2.53) to (2.55), a correct phase-wise distribution of the concentration should be obtained. Since the temperature changes after z_{m} abruptly, the concentration after this point must be adjusted by the ratio suggested by the shock condition in (2.41) and (2.42). Hence, by the conservation of mass, the concentration solutions in the states β and γ are given as

$$
c_n^\beta(z,t) = \begin{cases} 0 & \text{for} \quad z < z_{n,\mathrm{de}}^p(t), \\ \frac{1+Fa_n(T_\mathrm{R})}{1+Fa_n(T_k)}\frac{Z^\alpha}{Z^\beta}c_n^\alpha & \text{for} \quad z_{n,\mathrm{de}}^p(t) \le z \le z_{n,\mathrm{ad}}^p(t), \\ 0 & \text{for} \quad z > z_{n,\mathrm{ad}}^p(t). \end{cases}
\tag{3.9}
$$

and

$$
c_n^\gamma(z,t) = \begin{cases} 0 & \text{for} \quad z < z_{n,\mathrm{de}}^p(t), \\ \frac{1+Fa_n(T_\mathrm{R})}{1+Fa_n(T_k)}\frac{Z^\alpha}{Z^\gamma}c_n^\alpha & \text{for} \quad z_{n,\mathrm{de}}^p(t) \le z \le z_{n,\mathrm{ad}}^p(t), \\ 0 & \text{for} \quad z > z_{n,\mathrm{ad}}^p(t). \end{cases}
\tag{3.10}
$$

In the case of the temperature change of Type I, the factors $\frac{1+Fa_n(T_\mathrm{R})}{1+Fa_n(T_k)}\frac{Z^\alpha}{Z^\beta}$ and $\frac{1+Fa_n(T_\mathrm{R})}{1+Fa_n(T_k)}\frac{Z^\alpha}{Z^\gamma}$ both give the value 1. This is due to the fact that each factor involves the multiplication of two ratios that ultimately cancel each other out. As a result, the mobile phase concentrations c_n^α, c_n^β, and c_n^γ remain unchanged for Type I. This fact is already mentioned in (2.41).

In contrast, in temperature change of Type II, the pulses in both the segments have identical spatial bandwidths whose ratio is equal to 1, so that only the ratio of the retention factors $\frac{1+Fa_n(T_\mathrm{R})}{1+Fa_n(T_k)}$ affects the mobile phase concentration. This is due to the temporal temperature jump , which creates a temperature discontinuity and change the behavior of the ratios. As a result, the mobile phase concentration in the zone β and the zone γ differs from that in the zone α, i.e. $c_n^\alpha \ne c_n^\beta \ne c_n^\gamma$. This is already mentioned in (2.42).

3.3   Illustration and Discussion of Results

After deriving analytical solutions, we evaluate case studies for four different scenarios discussed in Figures 2.1 and 2.2. In the considered case studies, the number of components in the mixture is either 1 (single-component injection) or 3 (ternary-mixture injection).

3.3.1   Analysis of a Single-Component Injection

As explained in Figure 2.1a,b, we first test our analytical solutions for the case where only a single-component ($n = 1$) is injected one time ($P = 1$) as a rectangular pulse into the column. The superscript $P = 1$ is not used in the discussion of single-component injections. As discussed earlier,

upon reaching the midpoint z_{m} of the column, the pulse may immediately or later encounter a temperature change, categorized as Type I and Type II, respectively. In this context, we assign the value $\ell = 0$ for Type I and $\ell = 1$ for Type II, while utilizing (3.8a). This means that the value of ℓ from 1 here represents the number of switchings of the Type II. They are explained below. The relevance will be applied for mixture injection in section 3.3.2. The parameters used in the simulation for single-component tests are listed in Tables 3.1. They represent typical values used in liquid chromatographic processes.

Table 3.1: Typical parameters used in Section 3.3.1 (single-component injections).

Symbol	Quantity	Value Used in Simulation
z_{max}	Length of the column	0.1 m
A	Cross-sectional area of the column	0.0000196 m^2 (diameter d = 0.5 cm)
ϵ	Porosity of the column	0.4
u	Interstitial velocity	0.00167 m/s
Δt_{inj}	Injection period	20 s
$c_{1,\mathrm{inj}}$	Feed concentrations	1 g/L
$\mathrm{m}_{1,\mathrm{inj}}$	Mass injected of c_1	2.62 $\times 10^{-4}$ g
$a_1(T_{\mathrm{R}} = 298 \text{ K})$	Henry constant at reference temperature, T_{R}	0.75
$a_1(T_{\mathrm{L}} = 270 \text{ K})$	Henry constant at lower temperature, T_{L}	1.73
$a_1(T_{\mathrm{H}} = 360 \text{ K})$	Henry constant at higher temperature, T_{H}	0.18
$\Delta H_{A,1}$	Enthalpy of adsorption	-20 kJ/g

Type I: Both segments are initially at different temperatures

In this case, segment I of the column has the reference temperature T_{R} and segment II is maintained either at uniform low or high temperature, that is, $T^{\mathrm{I}}(z_0 \text{ to } z_{\mathrm{m}}, t) = T_{\mathrm{R}}$ and $T^{\mathrm{II}}(z_{\mathrm{m}} \text{ to } z_{\mathrm{max}}, t) = T_{\mathrm{L}}$ or T_{H}. As the adsorption front starts crossing the middle of the column z_{m}, it faces two different temperatures before completely entering segment II, that is, speeds of both the fronts of the pulse are not the same. Figures 3.2 and 3.3 demonstrate the experiment for low temperature T_{L} and Figure 3.4 depicts the experiment for high temperature T_{H}, in segment II. In this case, (3.8a), after removing the superscript p because only one injection is considered, takes the form

$$z_{1,\mathrm{ad}}(t) = \begin{cases} \frac{u}{1+Fa_1(T_{\mathrm{R}})}t & \text{for } t \in [0, t_{1,\mathrm{m}}], \\ z_{1,\mathrm{ad}}(t_{1,\mathrm{m}}) + \frac{u}{1+Fa_1(T_k)}(t - t_{1,\mathrm{m}}) & \text{for } t \in \,]t_{1,\mathrm{m}}, t_{1,\mathrm{max}}]. \end{cases} \tag{3.11}$$

Whereas, the corresponding time variable with respect to the space z is obtained as

$$t_{1,\mathrm{ad}}(z) = \begin{cases} \frac{1+Fa_1(T_{\mathrm{R}})}{u}z, & \text{for} & z \in [0, z_{\mathrm{m}}], \\ \frac{1+Fa_1(T_k)}{u}z - \frac{1+Fa_n(T_k)}{1+Fa_n(T_{\mathrm{R}})}t_{1,\mathrm{m}} + t_{1,\mathrm{m}}, & \text{for} & z \in \,]z_{\mathrm{m}}, z_{\mathrm{max}}]. \end{cases} \tag{3.12}$$

Similarly, we derive the above quantities for the desorption front using the injection period Δt_{inj} as by (3.8b) and (3.8d). The concentration solutions are calculated using (3.9) and (3.10).

All the solutions are plotted in Figures 3.2–3.4. The concentration profiles are plotted along the z-coordinate of the column at specific times and along t-coordinate, they are plotted at different locations, including the most important positions z_m and z_{max}. We call the development of the concentration profiles in time as "t-plot" and in space as "z-plot". The plot of space-time trajectories is also given in the middle of the Figure 3.2 where all the three states α, β and γ (discussed in equations (3.9) and (3.10)) are mentioned. To demonstrate the matching of space-bandwidths and time-bandwidths, z-plot is placed on the left and t-plot is placed below the plot of space-time trajectories. State β is highlighted and demonstrated separately in Figure 3.3. In Figure 3.2, the z-plot shows that across z, the space-bandwidth changes but across t the time-bandwidth between both fronts stays the same. The reason for this is that, although the space-bandwidths between the fronts vary, their speeds also change accordingly. For example, in the z- plot of Figure 3.2, the bandwidth between the fronts decreases and the adsorbed concentration profile becomes more concentrated, although the mobile phase concentration per unit time remains the same. It causes an decrease in the time-bandwidth, but, meanwhile, the speeds of the fronts are also decreased and this smooths the change in the time-bandwidth. So the time-bandwidth inside the two segments stays the same. See t-plot in Figure 3.2. Figure 3.4 tells us the similar story recorded for the higher temperature in the segment II. In this case, the bandwidth does not get narrower but widens, and the profile of the adsorbed phase q_1 is diluted, while the concentration of the mobile phase c_1 remains the same as in segment II. Nevertheless, the mass flow between the phases for both the high and low temperatures is conserved because the area under the pulse $c_1 + q_1$ remains the same in both segments.
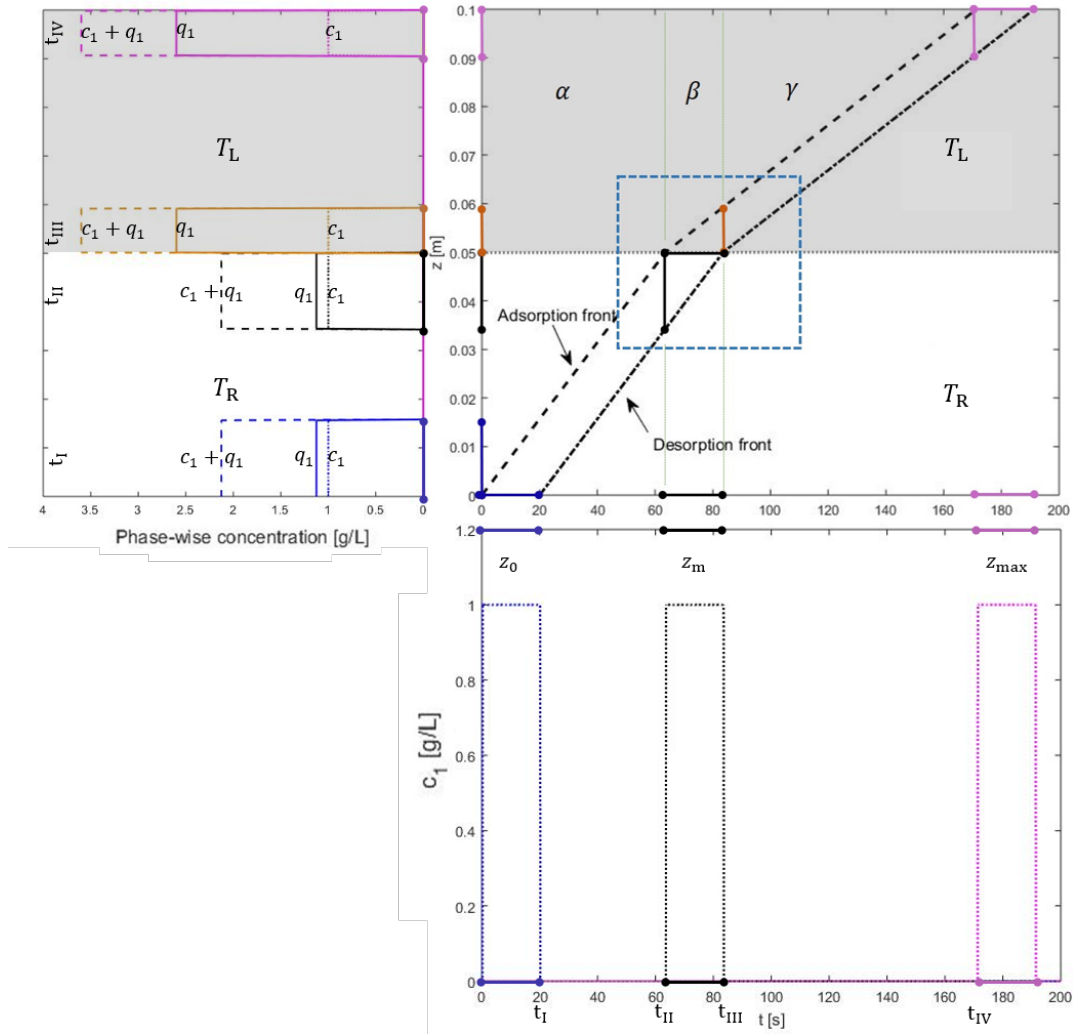
Figure 3.2: Illustration of the solution behavior in α and γ states for cooling of Type I. Switching is done from reference temperature, T_R, to low temperature, T_L. Concentrations, associated with left axes, are plotted along the axial coordinate z at particular times inside the column and plotted against the time coordinate t at different locations in the column. The grey area represents segment II that is kept at a low temperature. Every point in the t-plot corresponds to two points in the z-plot and every point in the z-plot corresponds to two points in the t-plot. The blue profile in t-plot is showing the reaching times of the adsorption and desorption fronts to z_0. Corresponding to it is a blue profile in z-plot at $t_I = \Delta t_{inj} = 20$ s. The black profile in t-plot is showing the profile when the fronts reach z_m. This crossing is plotted in the z-plot at several positions, that is, black one when the adsorption front reaches z_m and orange one when the desorption front reaches z_m. The pink profile in the t-plot is plotted at z_{max}. Whereas, the pink profile in the z-plot illustrates the situation when the adsorption front reaches z_{max}. As β is the crucial state, we have marked the area covering this sate and shown it in Figure 3.3 to delve the transition more clearly.
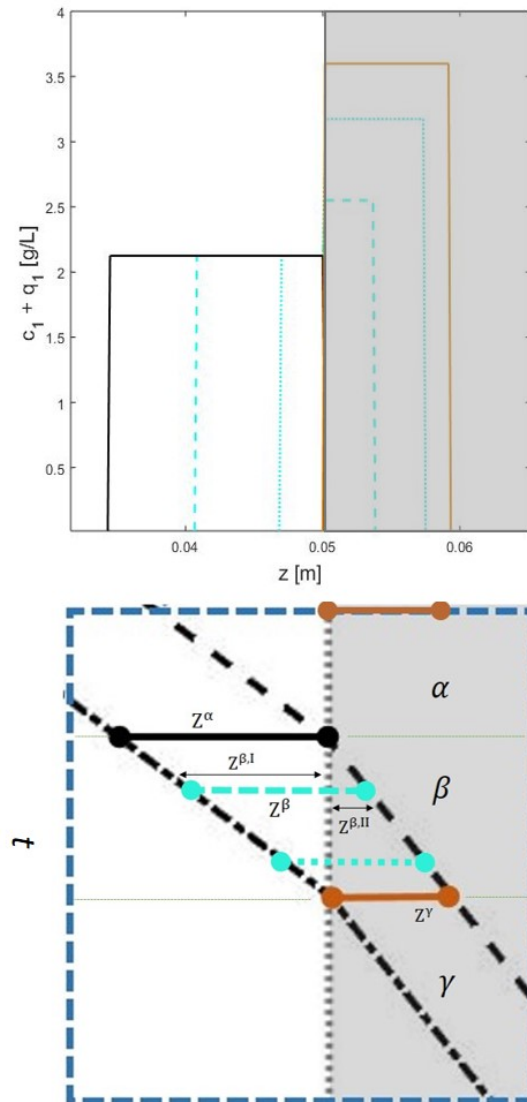
Figure 3.3: Illustration of the solution behavior in the intermediate β state during Type I cooling. This figure refers to the β state, highlighted by the blue dashed boundary in Figure 3.2, and is rotated clockwise along with the corresponding part of the z- plot. The pulse is represented in two places by the color cyan, by a dashed line when most of the pulse is in segment I, and by a dotted line when most of the pulse is in segment II. When the space-bandwidth gradually changes into the β-state, it becomes shorter and shorter and the corresponding concentration also increases correspondingly, while the mass remains conserved. All spatial bandwidths (Z^α, $Z^{\beta,\mathrm{I}}$, $Z^{\beta,\mathrm{II}}$, Z^γ) can be obtained using the equations (3.8a) and (3.8b).
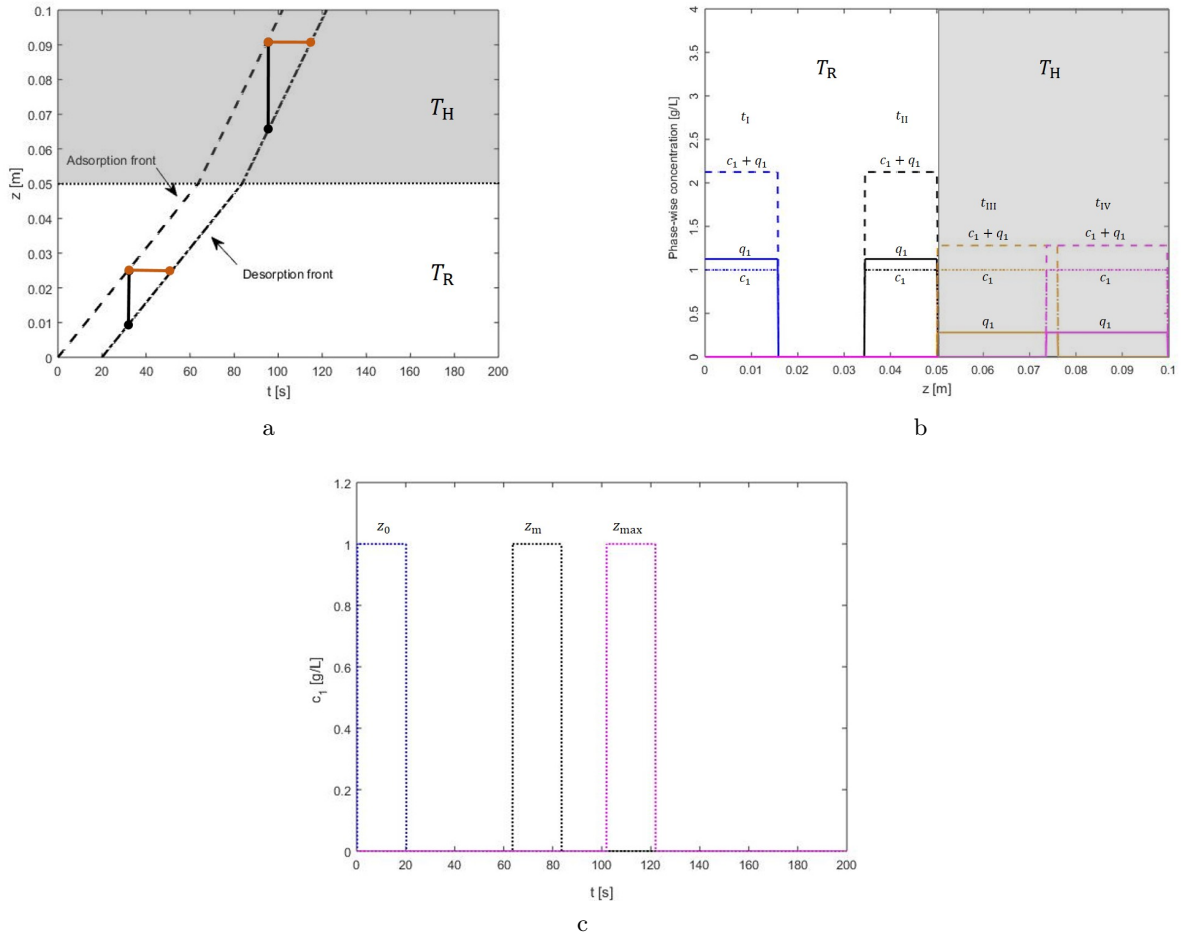
Figure 3.4: Illustration of the solution behavior for heating of Type I. The solution behavior is now showed for a high temperature. In (**a**), the trajectories are drawn for the accelerated pulse. In segment II the space bandwidths become wider and the concentration is diluted compared to that in segment I. The time-bandwidth stays the same as in the previous case. (**b**) The blue color shows the position of the pulse at $t_I = \Delta t_{inj} = 20$ s, in black color when its adsorption front reaches z_m, in orange color when its desorption front reaches z_m, and in pink color when its adsorption front reaches z_{max}. (**c**) The blue color profile is showing the arrival times of both the fronts at z_0, black color, when they reach z_m and the pink color profile is showing when they reach z_{max}.

Type II: Both segments are initially at the same temperature

This special case is discussed to support the understanding of more complex front propagation of mixtures (c.f. Section 3.3.2). Here, segment II is initially at the reference temperature. The temperature changes only when the pulse completely enters this segment, that is, when the desorption front of the pulse also crosses z_m. In this case, $T^I(z = 0$ to $z_m, t) = T_R$ and $T^{II}(z = z_m$ to $z_{max}, 0) = T_R$, but after the time $t_1 = t_{1,m} + \Delta t_{inj}$, $T^{II}(z = z_m$ to $z_{max}, 0) = T_k$. Thus, in contrast to the previous case, both fronts are simultaneously confronted with a sudden

temperature change and migrate at the same speed in the segment II of the column. Figure 3.5 displays the experiment for both the temperatures T_L and T_H. The trajectories in this type, given by Equation (3.8a) for $\ell = 1$, take the form

$$z_{1,\text{ad}}(t) = \begin{cases} \frac{u}{1+Fa_1(T_R)}t & \text{for } t \in [0, t_{1,\text{m}}], \\ z_{1,\text{ad}}(t_{1,\text{m}}) + \frac{u}{1+Fa_1(T_R)}(t-t_{1,\text{m}}) & \text{for } t \in \,]t_{1,\text{m}}, t_1[, \\ z_{1,\text{ad}}(t_1) + \frac{u}{1+Fa_1(T_k)}(t-t_1) & \text{for } t \in [t_1, t_{1,\text{max}}], \end{cases} \tag{3.13}$$

while the concentration solutions are calculated in the same way.

Figures 3.5a,b show that across z_m, unlike the previous case, the space-bandwidths of the profile do not change but the time-bandwidths do, that is, duration between the fronts changes in the time domain. This is due to the fact that both fronts are experiencing the same temperature at the same time and, thus, their speeds change at the same time. This does not allow any change in the space-bandwidths but this allows a change in the time-bandwidth. The graphical results are displayed in Figures 3.5c–f. The solutions behave completely opposite to those in tpye I. The widths in the z-plot remain constant, but they now vary in the t-plot. The concentration c_1 is diluted and q_1 becomes more concentrated for temperature T_L, while the two behave in opposite ways for temperature T_H. In this case as well, the total concentration profile $c_1 + q_1$ remains the same in both segments, thus demonstrating the conservation of mass.
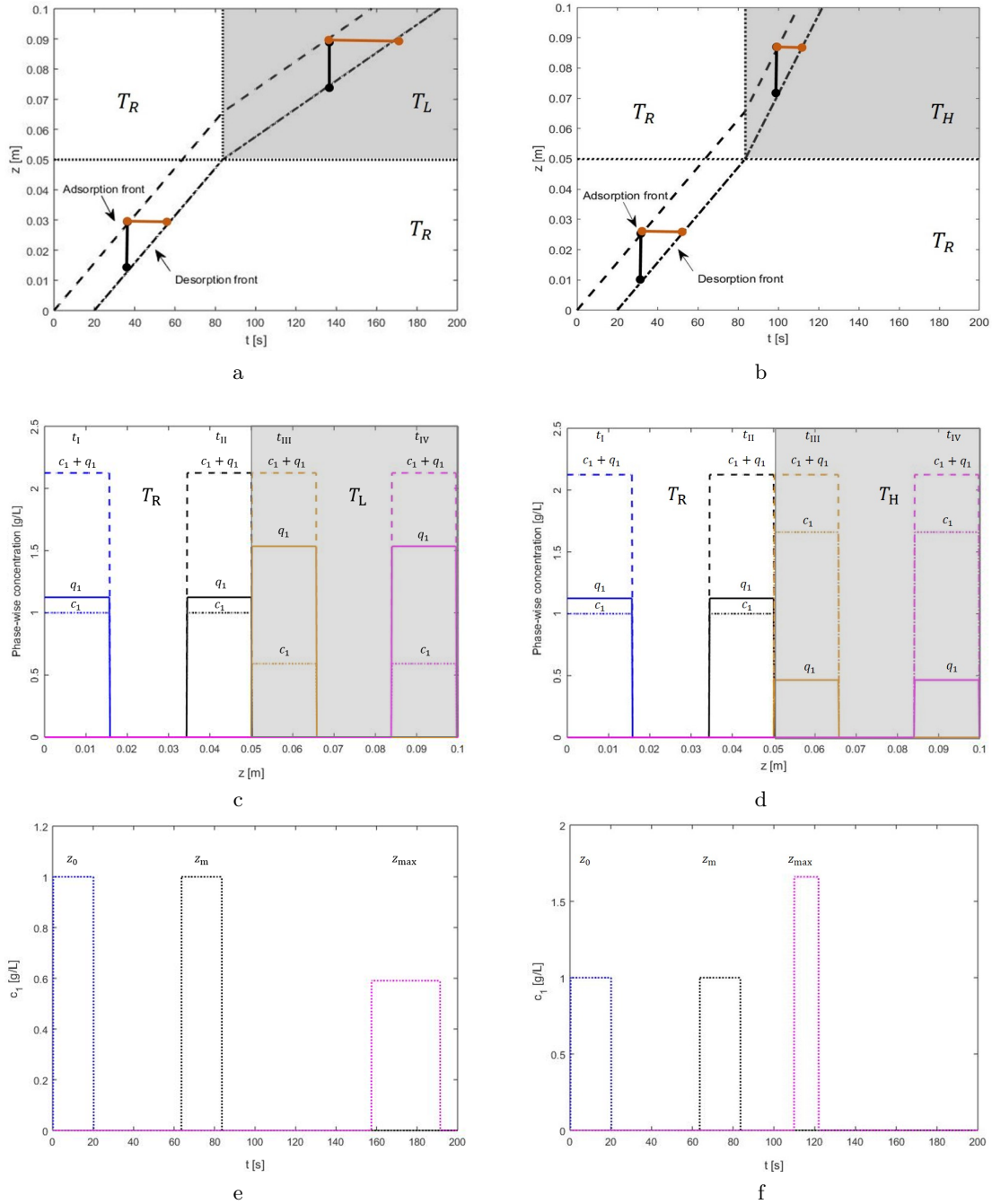
Figure 3.5: Illustration of the solution behavior for both cooling and heating of Type II. (**a**) The grey color is representing segment II with low temperature. The temperature is switched from reference to low at time t_1 when the desorption front of the pulse also enters segment II. The space-bandwidth is marked by black color and stays unchanged. The time-bandwidth of the pulse is marked by orange color which becomes longer. (**b**) Here, the grey color is representing segment II with high temperature. Unlike case (a), here the time-bandwidth decreases. (**c**, **d**) are z-plots for cooling and heating respectively. Whereas, (**e**, **f**) are t-plots for cooling and heating respectively.

3.3.2   Analysis of Consecutive Injections of Ternary Mixture

After the analysis of single-component injections, we extend our analysis to a mixture of three components, i.e. $N_c = 3$, which is injected $p-$times in succession, where $p = 1, 2, 3, ..., P, P \in \mathbb{N}$. We know that the distances between the components within the mixture depend strongly on the corresponding Henry constants $a_n(T)$ of the component n. We define the separation factor between two consecutive Henry constant by $\alpha_{i,j} = \frac{a_i}{a_j}, i < j$ and $i, j = 1, 2, 3$. Based on the typical scenarios in HPLC processes, we choose two groups of Henry constants such that in Group I the migration at the beginning of elution takes a form where two of the three concentrations c_1 and c_2 tend to elute faster. The third c_3 elutes slower, i.e. $\alpha_{1,2} > \alpha_{2,3}$. In contrast, in the Group II only c_1 tends to elute faster and the remaining c_2 and c_3 tend to elute slower, i.e. $\alpha_{1,2} < \alpha_{2,3}$. These scenarios are referred to as the "Late Eluter" and "Early Eluter" cases, respectively, as discussed in Figures 2.2b and 2.2c. The elution pattern in these scenarios could also proceed under isocratic conditions, but would be less productive. In keeping with the objectives of this dissertation, we intend to use the forced periodic temperature modulation of the segment II to achieve improvements in the column's performance as shown in Figure 2.2d. For this purpose, we try to speed up the slower eluting components and slow down the faster eluting components enough to shorten the distance between them and hence reduce the cycle time. Using (3.8e) and (3.8f) for a pth injection, let $t_{n,m}^p$ and $t_{n,\max,\text{ad}}^p$ be the times at which the adsorption fronts of c_n reach the middle of the column at z_m and the end of the column at $z_{\max}$, respectively. Similarly, we already know that $t_{n,\max}^p$ are the times when their desorption fronts reach $z_{\max}$. Since we only need information about the adsorption front at z_m, we omit the suffix "ad" for the associated arrival time, $t_{n,m}^p$. The injection times t_{inj}^p for each pth injection are much more crucial, since injecting the successive mixtures at different times would result in different temperature regimes, which directly affect the cycle time Δt_c^p and thus the productivity of the column. When two pulses or concentrations with different gradient requirements elute simultaneously in the segment II, we must wait for one pulse to leave the segment and then apply the required temperature to the subsequent pulse. Based on a given scenario, we create specific sets of switching times for the periodic modulation of temperature. The first experiment is called a *Conservative Design Concept with Safety Margins* because we allow the repetition of some initial temperature regimes at each successive injection time, which leads to an unnecessary time gap, called the safety margin, Δt_{saf}^p, between them. Due to this limitation, the conservative design concept is not useful compared to the isocratic conditions. Nevertheless, it helps us in finding room for improvement by changing the strategy of switching times for the second injection. We observe the elution of the first injection more closely and find better temperature regimes for the second and later injections, leading to a new *Optimal Design Concept without Safety Margins* with a shorter cycle time. This clearly proves to be more a productive scheme as this leads to $\Delta t_{\text{saf}}^p \approx 0$. In the following we explain these two concepts in detail.

We now shift our attention to optimizing the productivity of mixtures comprising both Group I and Group II components. By developing a targeted strategy, we aim to enhance separation efficiency and overall performance. For this case, the parameters used are listed in Table 3.6. Some important results for both Group I and Group II are shown in Tables 3.10 and 3.14, respectively.

Table 3.6: Reference parameters used in Section 3.3.2

.

Symbol	Quantity	Value Used in Simulation
z_{max}	Length of the column	20 cm
A	Cross-sectional area of the column	0.166 cm^2 (diameter d = 0.46 cm)
ϵ	Porosity of the column	0.555
u	Interstitial velocity	3.26 cm/min
Δt_{inj}	Injection period	1.33 min
$[c_{1,\mathrm{inj}}, c_{2,\mathrm{inj}}, c_{3,\mathrm{inj}}]$	Feed concentrations	[0.95, 0.95, 0.95] g/L
$[\mathrm{m}_{1,\mathrm{inj}}, \mathrm{m}_{2,\mathrm{inj}}, \mathrm{m}_{3,\mathrm{inj}}]$ Eq.(2.52)	Mass injected of $[c_1, c_2, c_3]$	3.8 $\times 10^{-4}$ g
T_{R}	Reference temperature	298.15 K
T_{L}	Low temperature	248.15 K
T_{H}	High temperature	348.15 K
$[\Delta H_{A,1}, \Delta H_{A,2}, \Delta H_{A,3}]$	Adsorption enthalpies	[-8.0,-8.0,-8.0] kJ/g

Henry Constants	$a_1(T_{\mathrm{R}})$	$a_2(T_{\mathrm{R}})$	$a_3(T_{\mathrm{R}})$	Separation Factor $\alpha_{i,j} = \frac{a_i}{a_j}, i, j = 1, 2, 3.$
	4.5	5.0	5.5	$\alpha_{1,2} \approx \alpha_{2,3}$
Group I	4.5	5.0	7.0	$\alpha_{1,2} > \alpha_{2,3}$
	4.5	5.0	9.0 — Gradients	$\alpha_{1,2} >> \alpha_{2,3}$(Late eluter)
	4.5	5.0	5.5	$\alpha_{1,2} \approx \alpha_{2,3}$
Group II	3.0	5.0	5.5	$\alpha_{1,2} < \alpha_{2,3}$
	1.0	5.0	5.5 — Gradients	$\alpha_{1,2} << \alpha_{2,3}$(Early eluter)

Group I This group is characterized by an elution pattern, where two of the three concentrations, namely c_1 and c_2, tend to elute faster, while the third concentration c_3 exhibits a slower elution profile, i.e $\alpha_{1,2} >> \alpha_{2,3}$. By conducting a thorough analysis of the conservative and optimal design concepts in Group I, we can gain valuable insights into their effectiveness and applicability in enhancing separation efficiency and productivity. This preliminary study allows us to establish a baseline understanding of the concepts' performance and their potential impact on the elution behavior of the individual components. By examining key performance metrics, such as cycle time reduction and improved productivity, we aim to assess the advantages and limitations of each scheme within the context of Group I.

Conservative Design Concept with Safety Margins

To begin, we keep segment I at temperature T_{R} and segment II at T_{L}. Then we inject the mixture c_n for $n = 3$, each with an appropriate Henry constant. The initial temperature of the segment II which is set to be T_{L} does not matter before the first component arrives. It is desirable to slow down component c_1 and speed up component c_3. But since at the time of cooling c_1, components c_2 and c_3 also stay in the segment II for a while. They are also slowed down until c_1 leaves the segment II. Then we switch the temperature from T_{L} to T_{H}. The later heating accelerates c_2 and c_3, which helps to shorten the distance between c_1 and c_3. It can be seen that the trajectories

of c_1 contain the temperature T_L and those of c_2 and c_3 contain the temperatures T_L and T_H given by (3.16a) to (3.16c). For each injection p there are two switching times, the first is always heating at time $t_{1,\max}^p$ and the second is always cooling at time $t_{3,\max}^p$. From this, the formula for the switching times of the entire process is given in generalized form, as

$$t_k = \begin{cases} t_{2k} = t_{3,\max}^p & \text{when } T = T_L \quad \text{and } k = 1,2,3,...,P, \\ t_{2k+1} = t_{1,\max}^p & \text{when } T = T_H \quad \text{and } k = 0,1,2,3,...P-1, \ P \in \mathbb{N}. \end{cases} \tag{3.14}$$

Taking into account the equation (3.2), the specific temperature profile of the entire column is thus obtained as

$$T(x,t) = \begin{cases} T_R & \text{for } 0 \leq x \leq x_m, & t \in [t_0, t_{3,\max}^P], \\ T_{2k} = T_L & \text{for } x_m < x \leq x_{\max}, & t \in [t_{2k}, t_{2k+1}[, \\ T_{2k+1} = T_H & \text{for } x_m < x \leq x_{\max}, & t \in [t_{2k+1}, \min\{t_{2k+2}, t_{3,\max}^P\}], \\ & k = 0,1,2,3,...,P, & t_{2k+2} < t_{3,\max}^P. \end{cases} \tag{3.15}$$

The above temperature profile affects the trajectories of all components in the following way.

Let $z_{1,\mathrm{ad}}(t), z_{2,\mathrm{ad}}(t)$ and $z_{3,\mathrm{ad}}(t)$ be the corresponding solution trajectories of the adsorption fronts of c_1, c_2 and c_3, respectively. These trajectories for the adsorption fronts are derived for every p^{th} injection, considering (3.8a) with $l = 0$ (means no Type II switch) for components c_1, while $l = 1$ (means one Type II switch) for components c_2 and c_3, as follows

$$z_{1,\mathrm{ad}}^p(t) = \begin{cases} \frac{u}{1+Fa_1(T_R)}(t - t_{\mathrm{inj}}^p), & \text{for } t \in [t_{\mathrm{inj}}^p, t_{1,\mathrm{m}}^p], \\ z_{1,\mathrm{ad}}^p(t_{1,\mathrm{m}}^p) + \frac{u}{1+Fa_1(T_L)}(t - t_{1,\mathrm{m}}^p), & \text{for } t \in]t_{1,\mathrm{m}}^p, t_{1,\max,\mathrm{ad}}^p], \end{cases} \tag{3.16a}$$

$$z_{2,\mathrm{ad}}^p(t) = \begin{cases} \frac{u}{1+Fa_2(T_R)}(t - t_{\mathrm{inj}}^p), & \text{for } t \in [t_{\mathrm{inj}}^p, t_{2,\mathrm{m}}^p], \\ z_{2,\mathrm{ad}}(t_{2,\mathrm{m}}^p) + \frac{u}{1+Fa_2(T_L)}(t - t_{2,\mathrm{m}}^p), & \text{for } t \in]t_{2,\mathrm{m}}^p, t_{2k+1}[, \\ z_{2,\mathrm{ad}}(t_{2k+1}) + \frac{u}{1+Fa_2(T_H)}(t - t_{2k+1}), & \text{for } t \in [t_{2k+1}, t_{2,\max,\mathrm{ad}}^p], \end{cases} \tag{3.16b}$$

$$z_{3,\mathrm{ad}}^p(t) = \begin{cases} \frac{u}{1+Fa_3(T_R)}(t - t_{\mathrm{inj}}^p), & \text{for } t \in [t_{\mathrm{inj}}^p, t_{3,\mathrm{m}}^p], \\ z_{3,\mathrm{ad}}(t_{3,\mathrm{m}}^p) + \frac{u}{1+Fa_3(T_L)}(t - t_{3,\mathrm{m}}^p), & \text{for } t \in]t_{3,\mathrm{m}}^p, t_{2k+1}], \\ z_{3,\mathrm{ad}}(t_{2k+1}) + \frac{u}{1+Fa_3(T_H)}(t - t_{2k+1}), & \text{for } t \in [t_{2k+1}, t_{3,\max,\mathrm{ad}}^p]. \end{cases} \tag{3.16c}$$

The associated time variables for the adsorption fronts with respect to the space z, one obtains

$$t_{1,\mathrm{ad}}^p(z) = \begin{cases} t_{\mathrm{inj}}^p + \frac{1+Fa_1(T_R)}{u}z, & \text{for } z \in [0, z_m], \\ \frac{1+Fa_1(T_L)}{u}z - \frac{1+Fa_1(T_L)}{1+Fa_1(T_R)}(t_{1,\mathrm{m}}^p - t_{\mathrm{inj}}^p) + t_{1,\mathrm{m}}^p, & \text{for } z \in]z_m, z_{\max}], \end{cases} \tag{3.17a}$$

$$t_{2,\mathrm{ad}}^p(z) = \begin{cases} t_{\mathrm{inj}}^p + \frac{1+Fa_2(T_R)}{u}z, & \text{for } z \in [0, z_m], \\ \frac{1+Fa_2(T_H)}{u}z - \frac{1+Fa_2(T_H)}{1+Fa_2(T_R)}(t_{2,\mathrm{m}}^p - t_{\mathrm{inj}}^p) \\ \quad - \frac{1+Fa_2(T_H)}{1+Fa_2(T_L)}(t_{2k+1} - t_{2,\mathrm{m}}^p) + t_{2k+1}, & \text{for } z \in]z_m, z_{\max}], \end{cases} \tag{3.17b}$$

$$t_{3,\mathrm{ad}}^p(z) = \begin{cases} t_{\mathrm{inj}}^p + \frac{1+Fa_3(T_R)}{u}z, & \text{for } z \in [0, z_m], \\ \frac{1+Fa_3(T_H)}{u}z - \frac{1+Fa_3(T_H)}{1+Fa_3(T_R)}(t_{3,\mathrm{m}}^p - t_{\mathrm{inj}}^p) \\ \quad - \frac{1+Fa_3(T_H)}{1+Fa_3(T_L)}(t_{2k+1} - t_{3,\mathrm{m}}^p) + t_{2k+1}, & \text{for } z \in]z_m, z_{\max}]. \end{cases} \tag{3.17c}$$

Equations (3.16a)–(3.16c) and (3.17a)–(3.17c) also render the trajectories $z_{n,\mathrm{de}}^{p}(t)$ and time variables $t_n^p(z)$ for the desorption fronts of all the injections, respectively, as

$$z_{n,\mathrm{de}}^{p}(t) = z_{n,\mathrm{ad}}^{p}(t - \Delta t_{\mathrm{inj}}) \qquad \text{for} \qquad t > \Delta t_{\mathrm{inj}} \tag{3.18a}$$

and

$$t_n^p(z) = \Delta t_{\mathrm{inj}} + t_{n,\mathrm{ad}}^{p}(z). \tag{3.18b}$$

Furthermore, since in segment I the temperature is always T_{R}, for each corresponding component n in the each pth injection, the following holds

$$t_{n,\mathrm{m}}^{p} = t_{\mathrm{inj}}^{p} + t_{n,\mathrm{m}}^{1} = t_{\mathrm{inj}}^{p} + \frac{1 + Fa_n(T_{\mathrm{R}})}{u}z_{\mathrm{m}}, \qquad \text{for } p = 1, 2, 3, ..., P, P \in \mathbb{N} \text{ and } t_{\mathrm{inj}}^{1} = 0. \tag{3.19}$$

The concentration solutions for all components of the mixtures are obtained from the equations (3.9) and (3.10), taking care to adjust the temperature T_k correctly in the ratio. Note that in case of isocratic operation, the temperatures can be replaced by the reference temperature T_{R} everywhere in above equations to get the solution trajectories.

In particular, we compute the cycle time $\Delta t_{\mathrm{c}}^{p}$ with a conservative bound, which is why we named it a conservative schem. Since the first and last components of each injection have different temperature requirements, each new injection must be initiated so that the adsorption front of its fastest component reaches the middle of the column z_{m} at the same time that the desorption front of the slowest component of the previous injection leaves the column. In this way, we protect these two components from each other's temperature regimes. At this exact time, we switch the temperature of the segment II back to the initial value and repeat the same sequence after every time $t_{3,\mathrm{max}}^{p}$. This time is estimated by jointly (3.17c) and (3.18b) as

$$t_{3,\mathrm{max}}^{p} = \Delta t_{\mathrm{inj}} + \frac{1 + Fa_3(T_{\mathrm{H}})}{u}z_{\mathrm{max}} - \frac{1 + Fa_3(T_{\mathrm{H}})}{1 + Fa_3(T_{\mathrm{R}})}(t_{3,\mathrm{m}}^{p} - t_{\mathrm{inj}}^{p}) - \frac{1 + Fa_3(T_{\mathrm{H}})}{1 + Fa_3(T_{\mathrm{L}})}(t_{2k+1} - t_{3,\mathrm{m}}^{p}) + t_{2k+1} \tag{3.20}$$

and using (3.17a) to estimate $t_{1,\mathrm{m}}^{p}$ as

$$t_{1,\mathrm{m}}^{p} = t_{\mathrm{inj}}^{p} + \frac{1 + Fa_1(T_{\mathrm{R}})}{u}z_{\mathrm{m}}. \tag{3.21}$$

So, according to the planned strategy for injecting the mixtures, we must have the following

$$t_{3,\mathrm{max}}^{p} = t_{1,\mathrm{m}}^{p+1}, \qquad \text{for} \qquad p = 1, 2, ..., P - 1, P \in \mathbb{N}. \tag{3.22a}$$

After applying (3.20) and (3.21) in above formula we get

$$\Delta t_{\mathrm{inj}} + \frac{1 + Fa_3(T_{\mathrm{H}})}{u}z_{\mathrm{max}} - \frac{1 + Fa_3(T_{\mathrm{H}})}{1 + Fa_3(T_{\mathrm{R}})}(t_{3,\mathrm{m}}^{p} - t_{\mathrm{inj}}^{p}) - \frac{1 + Fa_3(T_{\mathrm{H}})}{1 + Fa_3(T_{\mathrm{L}})}(t_{2k+1} - t_{3,\mathrm{m}}^{p}) + t_{2k+1}$$
$$= t_{\mathrm{inj}}^{p+1} + \frac{1 + Fa_1(T_{\mathrm{R}})}{u}z_{\mathrm{m}}. \tag{3.22b}$$

After a small simplification, the time for each next $p + 1^{\text{th}}$ injection considering $t_{\text{inj}}^1 = 0$ and replacing t_{2k+1} by $t_{1,\max}^p$ from (3.14), is given by

$$t_{\text{inj}}^{p+1} = \Delta t_{\text{inj}} + \frac{1 + Fa_3(T_{\text{H}})}{u} z_{\max} - \frac{1 + Fa_3(T_{\text{H}})}{1 + Fa_3(T_{\text{R}})}(t_{3,\text{m}}^p - t_{\text{inj}}^p) - \frac{1 + Fa_3(T_{\text{H}})}{1 + Fa_3(T_{\text{L}})}(t_{1,\max}^p - t_{3,\text{m}}^p)$$
$$+ t_{1,\max}^p - \frac{1 + Fa_1(T_{\text{R}})}{u} z_{\text{m}}, \qquad \text{for } p = 1, 2, ..., P - 1, P \in \mathbb{N}.$$
$$(3.22\text{c})$$

Now we calculate the cycle time Δt_{c}^p. For each pth injection, it is the difference between the times $t_{3,\max}^p$ at which the desorption front of the slowest component of the previous injection reaches $z_{\max}$ and $t_{1,\max,\text{ad}}^p$ when the adsorption front of the faster component of the current injection reaches $z_{\max}$. This calculation also involves adding the safety margin Δt_{saf}^p generated by the concept's limitation. Mathematically, it is written as

$$\Delta t_{\text{c}}^p = t_{3,\max}^p - t_{1,\max,\text{ad}}^p + \Delta t_{\text{saf}}^p. \qquad (3.23\text{a})$$

The safety margin is the difference between the time when the last component of the current injection leaves and the time when the first component of the subsequent injection arrives $z_{\max}$, i.e.

$$\Delta t_{\text{saf}}^p = t_{1,\max,\text{ad}}^{p+1} - t_{3,\max}^p, \qquad \text{for } p = 1, 2, ..., P - 1, P \in \mathbb{N}. \qquad (3.23\text{b})$$

After using (3.17a) and (3.20) in above formula and replacing t_{2k+1} by $t_{1,\max}^p$, we get

$$\Delta t_{\text{saf}}^p = \frac{1 + Fa_1(T_{\text{L}})}{u} z_{\max} - \frac{1 + Fa_1(T_{\text{L}})}{1 + Fa_1(T_{\text{R}})}(t_{1,\text{m}}^{p+1} - t_{\text{inj}}^{p+1}) + t_{1,\text{m}}^{p+1} - \Delta t_{\text{inj}} - \frac{1 + Fa_3(T_{\text{H}})}{u} z_{\max}$$
$$+ \frac{1 + Fa_3(T_{\text{H}})}{1 + Fa_3(T_{\text{R}})}(t_{3,\text{m}}^p - t_{\text{inj}}^p) + \frac{1 + Fa_3(T_{\text{H}})}{1 + Fa_3(T_{\text{L}})}(t_{1,\max}^p - t_{3,\text{m}}^p) - t_{1,\max}^p.$$
$$(3.23\text{c})$$

The formula is introduced to compute the safety margin independently. Since the trajectories of the corresponding components remain the same for each injection under the conservative design concept, we can decompose all terms in (3.23a) using (3.23b) as

$$\Delta t_{\text{c}}^p = t_{\text{inj}}^p + t_{3,\max}^1 - t_{\text{inj}}^p - t_{1,\max,\text{ad}}^1 + t_{\text{inj}}^{p+1} + t_{1,\max,\text{ad}}^1 - t_{\text{inj}}^p - t_{3,\max}^1 \qquad (3.24\text{a})$$

and then delete the same terms with opposite signs to get

$$\Delta t_{\text{c}}^p = t_{\text{inj}}^{p+1} - t_{\text{inj}}^p, \qquad \text{for } p = 1, 2, ..., P - 1, P \in \mathbb{N}. \qquad (3.24\text{b})$$

From this, it is clear that the cycle time is equal to the time interval between two successive injections and is the same for all $p = 1, 2, 3, ..., P \in \mathbb{N}$. After using (3.22c) in the above equation, we obtain as

$$\Delta t_{\text{c}}^p = \Delta t_{\text{inj}} + \frac{1 + Fa_3(T_{\text{H}})}{u} z_{\max} - \frac{1 + Fa_3(T_{\text{H}})}{1 + Fa_3(T_{\text{R}})}(t_{3,\text{m}}^p - t_{\text{inj}}^p)$$
$$- \frac{1 + Fa_3(T_{\text{H}})}{1 + Fa_3(T_{\text{L}})}(t_{1,\max}^p - t_{3,\text{m}}^p) + t_{1,\max}^p - \frac{1 + Fa_1(T_{\text{R}})}{u} z_{\text{m}} - t_{\text{inj}}^p.$$
$$(3.24\text{c})$$

Equation (3.24c) can be used to calculate cycle times $\Delta t_{c,iso}^p$ and $\Delta t_{c,grad}^p$ for both isocratic and the more flexible gradients conditions, because $T_k \in \{T_R, T_L, T_H\}$. If we neglect the safety margin Δt_{saf}^p in (3.23a), we call it a hypothetical cycle time, denoted by $\Delta t_{c,iso,hyp}^p$ and $\Delta t_{c,grad,hyp}^p$ in the aforementioned cases, respectively. The term Δt_{inj} in the expression above shows that longer injections lead to longer cycle times. By (2.50) and (2.51) this means a decrease in productivity.

At this point it is important to mention that in the conservative design concept, as mentioned earlier, all p injections are subjected to the same sequence of temperature regimes. This results in all corresponding components of each injection having the same slope of the trajectories. Therefore, any time variable associated with a particular component, while also computable using eqs. (3.17a) to (3.17c), can simply be computed as a recurrence after each cycle time Δt_c^p, i.e.

$$t_n(z)^{p+1} = \Delta t_c^p + t_n^p(z), \qquad \text{for} \qquad n = 1, 2, 3 \text{ and } p = 1, 2, 3, ..., P-1, P \in \mathbb{N}. \qquad (3.25)$$

It should be noted here that this conservative design concept is not optimum for the segmented gradients case due to the presence of safety margins. The introduction of this type of temperature modulation concept was originally pursued with the intention of reducing cycle time and improving productivity. However, it became clear that this approach did not produce the desired results. Despite the hope that forced periodic operation would serve as a general solution, it became clear that its effectiveness depends on carefully chosen Henry constants, adsorption enthalpy, and well-planned temperature regimes. For this reason, a case-dependent optimal design concept without safety margins is determined based on doing injections earlier but still avoiding remixing. The solution to such an interesting optimization problem is presented below.

Optimal Design Concept without Safety Margins

As mentioned in the previous scheme, as a first attempt to achieve a shorter cycle time compared to the isocratic conditions, different temperature regimes were proposed for the slowest and fastest components of the successive injections, respectively. But we haven't succeeded in that, because an unnecessary time gap, called "safety margin" Δt_{saf}^p, was created. This was an indication that we could achieve a shorter cycle time if we avoid this time gap. For this reason, it is obvious that we must provide analogous temperature regimes for the first and last components of each injection. This is possible if the subsequent injection is performed early enough so that the adsorption front of its first component c_1 could be eluted in the same temperature regime as the last component of the previous injection without being mixed together again. In this way, not only c_1, but also c_2 of the second injection is heated together with c_3 of the previous injection. After the switching time $t_2 = t_{3,max}^1$, i.e. when c_3 of the first injection leaves the column, switching the temperature from T_H to T_L cools the desorption front of c_1. This cooling also affects c_2, since it is still near the end of segment II, and then c_3, since it has now also entered the segment II. This complicated temperature regime of T_L does not help to shorten the cycle time, but it does preserve resolution and protects c_1 as well as c_2 from remixing. Soon c_1 leaves the column. We switch the temperature from T_L back to T_H after the time $t_3 = t_{1,max}^2$. This heats up both c_2 and c_3 and actually contributes to shortening the cycle time. We then allow the repetition of the sequence of these temperature regimes for all the successive injections. This has the effect of avoiding the unnecessary gap created by the conservative design concept, because the component c_1 of the subsequent $p+1^{th}$ injection can now simply be collected immediately after the component c_3 of the previous p^{th} injection for $p \geq 1$. Mathematically, this statement can be expressed as follows

$$t_{3,\max}^{p} = t_{1,\max,\mathrm{ad}}^{p+1}, \qquad \text{for } p = 1, 2, 3, ..., P-1, P \in \mathbb{N}. \tag{3.26}$$

To calculate the above times, we first write the expressions for the trajectories of the second and further injections, and using these expressions we can easily obtain the formulas for the above times. For the first injection $p = 1$, these trajectories are given as in the conservative design concept, i.e. by (3.16a) to (3.16c) and the times are given by (3.17a) to (3.17c). For the adsorption and desorption fronts of the injections $p \geq 2$ and $k \geq 1$, however, they are given as follows

$$z_{1,\mathrm{ad}}^{p}(t) = \begin{cases} \frac{u}{1+Fa_1(T_\mathrm{R})}(t - t_{\mathrm{inj}}^{p}), & \text{for } t \in [t_{\mathrm{inj}}^{p}, t_{1,\mathrm{m}}^{p}], \\ z_{1,\mathrm{ad}}^{p}(t_{1,\mathrm{m}}^{p}) + \frac{u}{1+Fa_1(T_\mathrm{H})}(t - t_{1,\mathrm{m}}^{p}), & \text{for } t \in \,]t_{1,\mathrm{m}}^{p}, t_{1,\max,\mathrm{ad}}^{p}], \end{cases} \tag{3.27a}$$

$$z_{1,\mathrm{de}}^{p}(t) = \begin{cases} \frac{u}{1+Fa_1(T_\mathrm{R})}(t - \Delta t_{\mathrm{inj}} - t_{\mathrm{inj}}^{p}), & \text{for } t \in [t_{\mathrm{inj}}^{p}, t_{1,\mathrm{m}}^{p}], \\ z_{1,\mathrm{ad}}^{p}(t_{1,\mathrm{m}}^{p}) + \frac{u}{1+Fa_1(T_\mathrm{H})}(t - \Delta t_{\mathrm{inj}} - t_{1,\mathrm{m}}^{p}), & \text{for } t \in \,]t_{1,\mathrm{m}}^{p}, t_{2k}[, \\ z_{1,\mathrm{ad}}^{p}(t_{2k}) + \frac{u}{1+Fa_1(T_\mathrm{L})}(t - \Delta t_{\mathrm{inj}} - t_{2k}), & \text{for } t \in [t_{2k}, t_{1,\max}^{p}], \end{cases} \tag{3.27b}$$

$$z_{2,\mathrm{ad}}^{p}(t) = \begin{cases} \frac{u}{1+Fa_2(T_\mathrm{R})}(t - t_{\mathrm{inj}}^{p}), & \text{for } t \in [t_{\mathrm{inj}}^{p}, t_{2,\mathrm{m}}^{p}], \\ z_{2,\mathrm{ad}}^{p}(t_{2,\mathrm{m}}^{p}) + \frac{u}{1+Fa_2(T_\mathrm{H})}(t - t_{1,\mathrm{m}}^{p}), & \text{for } t \in \,]t_{2,\mathrm{m}}^{p}, t_{2k}[, \\ z_{2,\mathrm{ad}}^{p}(t_{2k}) + \frac{u}{1+Fa_2(T_\mathrm{L})}(t - t_{2k}), & \text{for } t \in [t_{2k}, t_{2k+1}[, \\ z_{2,\mathrm{ad}}^{p}(t_{2k+1}) + \frac{u}{1+Fa_2(T_\mathrm{H})}(t - t_{2k+1}), & \text{for } t \in [t_{2k+1}, t_{2,\max,\mathrm{ad}}^{p}], \end{cases} \tag{3.27c}$$

and since the two fronts of c_2 are simultaneously confronted with the same temperature changes, we can simply write

$$z_{2,\mathrm{de}}^{p}(t) = z_{2,\mathrm{ad}}^{p}(t - \Delta t_{\mathrm{inj}}), \tag{3.27d}$$

$$z_{3,\mathrm{ad}}^{p}(t) = \begin{cases} \frac{u}{1+Fa_3(T_\mathrm{R})}(t - t_{\mathrm{inj}}^{p}), & \text{for } t \in [t_{\mathrm{inj}}^{p}, t_{3,\mathrm{m}}^{p}], \\ z_{3,\mathrm{ad}}^{p}(t_{2k}) + \frac{u}{1+Fa_3(T_\mathrm{L})}(t - t_{2k}), & \text{for } t \in \,]t_{3,\mathrm{m}}^{p}, t_{2k+1}[, \\ z_{3,\mathrm{ad}}^{p}(t_{2k}) + \frac{u}{1+Fa_3(T_\mathrm{H})}(t - t_{2k+1}), & \text{for } t \in [t_{2k+1}, t_{3,\max,\mathrm{ad}}^{p}] \end{cases} \tag{3.27e}$$

and as for c_2 we can simply obtain the trajectory of its desorption front as

$$z_{3,\mathrm{de}}^{p}(t) = z_{3,\mathrm{ad}}^{p}(t - \Delta t_{\mathrm{inj}}). \tag{3.27f}$$

Now, using the above trajectories, we obtain the corresponding time expressions for both the fronts of the three components, for $p \geq 2$ and $k \geq 1$, as

$$t_{1,\mathrm{ad}}^{p}(z) = \begin{cases} t_{\mathrm{inj}}^{p} + \frac{1+Fa_1(T_\mathrm{R})}{u}z, & \text{for } z \in [0, z_\mathrm{m}], \\ \frac{1+Fa_1(T_\mathrm{H})}{u}z - \frac{1+Fa_1(T_\mathrm{H})}{1+Fa_1(T_\mathrm{R})}(t_{1,\mathrm{m}}^{p} - t_{\mathrm{inj}}^{p}) + t_{1,\mathrm{m}}^{p}, & \text{for } z \in \,]z_\mathrm{m}, z_{\max}], \end{cases} \tag{3.28a}$$

$$t_{1,\mathrm{de}}^{p}(z) = \Delta t_{\mathrm{inj}} + \begin{cases} t_{\mathrm{inj}}^{p} + \frac{1+Fa_1(T_\mathrm{R})}{u}z, & \text{for } z \in [0, z_\mathrm{m}], \\ \frac{1+Fa_1(T_\mathrm{L})}{u}z - \frac{1+Fa_1(T_\mathrm{L})}{1+Fa_1(T_\mathrm{R})}(t_{1,\mathrm{m}}^{p} - t_{\mathrm{inj}}^{p}) - \\ \frac{1+Fa_1(T_\mathrm{L})}{1+Fa_1(T_\mathrm{H})}(t_{2k} - t_{1,\mathrm{m}}^{p}) + t_{2k}, & \text{for } z \in \,]z_\mathrm{m}, z_{\max}], \end{cases} \tag{3.28b}$$

$$t_{2,\text{ad}}^p(z) = \begin{cases} t_{\text{inj}}^p + \frac{1+Fa_2(T_\text{R})}{u}z, & \text{for } z \in [0, z_\text{m}], \\ \frac{1+Fa_2(T_\text{H})}{u}z - \frac{1+Fa_2(T_\text{H})}{1+Fa_2(T_\text{R})}(t_{2,\text{m}}^p - t_{\text{inj}}^p) - \\ (t_{2k} - t_{2,\text{m}}^p) - \frac{1+Fa_2(T_\text{H})}{1+Fa_2(T_\text{L})}(t_{2k+1} - t_{2k}) + t_{2k+1}, & \text{for } z \in \,]z_\text{m}, z_\text{max}], \end{cases} \tag{3.28c}$$

$$t_{2,\text{de}}^p(z) = \Delta t_{\text{inj}} + t_{2,\text{ad}}^p(z), \tag{3.28d}$$

$$t_{3,\text{ad}}^p(z) = \begin{cases} t_{\text{inj}}^p + \frac{1+Fa_3(T_\text{R})}{u}z, & \text{for } z \in [0, z_\text{m}], \\ \frac{1+Fa_3(T_\text{H})}{u}z - \frac{1+Fa_3(T_\text{H})}{1+Fa_3(T_\text{R})}(t_{3,\text{m}}^p - t_{\text{inj}}^p) - \\ \frac{1+Fa_2(T_\text{H})}{1+Fa_3(T_\text{L})}(t_{2k+1} - t_{3,\text{m}}^p) + t_{2k+1}, & \text{for } z \in \,]z_\text{m}, z_\text{max}]. \end{cases} \tag{3.28e}$$

and

$$t_{3,\text{de}}^p(z) = \Delta t_{\text{inj}} + t_{3,\text{ad}}^p(z). \tag{3.28f}$$

Now for $p = 1$, we have $k = 0$, substituting the value of $t_{3,\text{max}}^1$ from (3.17c) and (3.18b) as well as the value of $t_{1,\text{max,ad}}^2$ from (3.28a) into (3.26), we obtain

$$\Delta t_{\text{inj}} + \frac{1+Fa_3(T_\text{H})}{u}z_\text{max} - \frac{1+Fa_3(T_\text{H})}{1+Fa_3(T_\text{R})}(t_{3,\text{m}}^1 - t_{\text{inj}}^1) - \frac{1+Fa_3(T_\text{H})}{1+Fa_3(T_\text{L})}(t_1 - t_{3,\text{m}}^1) + t_1 = \\ \frac{1+Fa_1(T_\text{H})}{u}z_\text{max} - \frac{1+Fa_1(T_\text{H})}{1+Fa_1(T_\text{R})}(t_{1,\text{m}}^2 - t_{\text{inj}}^2) + t_{1,\text{m}}^2. \tag{3.29a}$$

After applying (3.19), we can replace $t_{1,\text{m}}^2 - t_{\text{inj}}^2$ with $t_{1,\text{m}}^1$ and divide $t_{1,\text{m}}^2$ into $t_{\text{inj}}^2 + t_{1,\text{m}}^1$, so the time for a new injection in this scenario after a small rearrangement is as follows

$$t_{\text{inj}}^2 = \Delta t_{\text{inj}} + \frac{1+Fa_3(T_\text{H})}{u}z_\text{max} - \frac{1+Fa_3(T_\text{H})}{1+Fa_3(T_\text{R})}t_{3,\text{m}}^1 - \frac{1+Fa_3(T_\text{H})}{1+Fa_3(T_\text{L})}(t_1 - t_{3,\text{m}}^1) + t_1 \\ - \frac{1+Fa_1(T_\text{H})}{u}z_\text{max} + \frac{1+Fa_1(T_\text{H})}{1+Fa_1(T_\text{R})}t_{1,\text{m}}^1 - t_{1,\text{m}}^1. \tag{3.29b}$$

Since, in this scheme, the first injection has different temperature conditions than the others, the injection times t_{inj}^3 and the following ones must be calculated differently. To find t_{inj}^3, we estimate the cycle time Δt_c^2 at the exit of the column. This is a sustainable cycle time shorter than that in isocratic operation, since Δt_{saf}^p is omitted in (3.23a). Thus, it is the difference between $t_{3,\text{max}}^2$ and $t_{1,\text{max,ad}}^2$, i.e.

$$\Delta t_\text{c}^2 = t_{3,\text{max}}^2 - t_{1,\text{max,ad}}^2. \tag{3.30a}$$

After substituting the values of (3.28f) and (3.28a) and applying (3.19) as we did above, we get the cycle time as

$$\Delta t_\text{c}^2 = \Delta t_{\text{inj}} + \frac{1+Fa_3(T_\text{H})}{u}z_\text{max} - \frac{1+Fa_3(T_\text{H})}{1+Fa_3(T_\text{R})}t_{3,\text{m}}^1 - \frac{1+Fa_2(T_\text{H})}{1+Fa_3(T_\text{L})}(t_3 - t_{3,\text{m}}^2) + t_3 \\ - \frac{1+Fa_1(T_\text{H})}{u}z_\text{max} + \frac{1+Fa_1(T_\text{H})}{1+Fa_1(T_\text{R})}t_{1,\text{m}}^1 - t_{1,\text{m}}^2, \tag{3.30b}$$

such that

$$t_{\mathrm{inj}}^3 = t_{\mathrm{inj}}^2 + \Delta t_{\mathrm{c}}^2. \tag{3.30c}$$

This means that in this scheme the cycle time Δt_{c}^p is provided for the calculation of productivity starting from the second injection, i.e. $p = 2$, since it is optimal. The injection times t_{inj}^p for the third and further injections can now be written in general form as

$$t_{\mathrm{inj}}^p = t_{\mathrm{inj}}^{p-1} + \Delta t_{\mathrm{c}}^{p-1}, \qquad \text{for} \qquad p = 3, 4, 5, ..., P \in \mathbb{N}. \tag{3.30d}$$

Moreover, the switching times in this scheme are given by the same formula (3.14).

All trajectories and solutions for the Henry constants of the Group II for the isocratic case are shown in Figure 3.7, and for the conservative design concept in Figure 3.8. For the optimal (improved) design concept they are shown in Figure 3.9.

Figure 3.8 shows, for three feed components, the development of the concentration profiles for the conventional isocratic as well as for the forced periodic conservative design concept in segment II. For the isocratic case, only the first and fourth injections are sighted, whereas for the conservative regime, all four injections are given. The minimal cycle time under isocratic conditions, c.f. equation (2.51), is $\Delta t_{\mathrm{c,iso}}^p = 23.46$ min for the parameters used, guarantees that there is no overlap between consecutive cycles and no waste of time by waiting too long before injecting again. On the other hand, in the conservative design concept, if the hypothetical cycle time, i.e. $\Delta t_{\mathrm{c,niso,hyp}}^1 = 13.38$ min, is applied, there is a risk that the bands of component 1 and component 3 in the segment II will be bent again, which may lead to undesired remixing. For this reason the figure illustrates a sample to apply conservative temperature switching regime, which avoids this remixing but it also does not guarantee that the cycle time in the gradients case is shorter than in the isocratic case. It means that if we apply the full cycle time, i.e. $\Delta t_{\mathrm{c,grad}}^1 = 37.6$ min, this is still longer than the isocratic one and of course not useful. That is why, the strategy based on switching in the segment II is changed and a new design concept with optimal switching is applied, which avoid safety margins, c.f. Figure 3.9. There the temperature from low to high and then from high to low at the switching times $t_1 = t_{1,\mathrm{max}}^1 = 39.7$ min and $t_2 = t_{3,\mathrm{max}}^3 = 51.8$ min, respectively, are the same as in the conservative design concept, but the switching at $t_3 = t_{1,\mathrm{max}}^2 = 55$ min is now earlier than in the conservative design concept. The temperature switching now occur periodically, shifted just by cycle time $\Delta t_{\mathrm{c,grad}}^p = 19.8$ min for $p \geq 2$. When this cycle time is used in (2.50), the application of this appropriate strategy corresponds to a 20% increase in the production rate compared to the isocratic case (see also table 3.10).

In the conservative design concept, the switching times were not optimally chosen, resulting in an even larger cycle time compared to the reference isocratic case. This outcome served as a stark reminder that the effectiveness of such strategies is highly case-dependent and requires meticulous consideration of various factors. In response to this setback, we pursued an alternative approach known as the optimal design concept. Through diligent analysis, we discovered a set of switching times and temperature trajectories that proved to be significantly more productive. The optimal design concept demonstrated the potential for shorter cycle times and enhanced productivity, surpassing the results achieved with both the conservative design concept and the isocratic case. This realization highlights the importance of tailored optimization and reinforces the notion that a generalized approach may not always yield the desired outcome. By addressing the limitations of the conservative design concept and introducing the optimal switching strategy,

we have not only showcased the significance of considering specific concentration trajectories but also emphasized the need for well-informed decision-making when designing such processes.

a Trajectories (below) and their corresponding concentration solutions (on the top) under isocratic conditions when $\alpha_{1,2} \approx \alpha_{2,3}$. $t_{inj}^2 = 6.24$ min, $t_{inj}^3 = 12.49$ min, $t_{inj}^4 = 18.7$ min and $\Delta t_c^p = 6.24$ min, $p = 1, 2, 3, 4$.
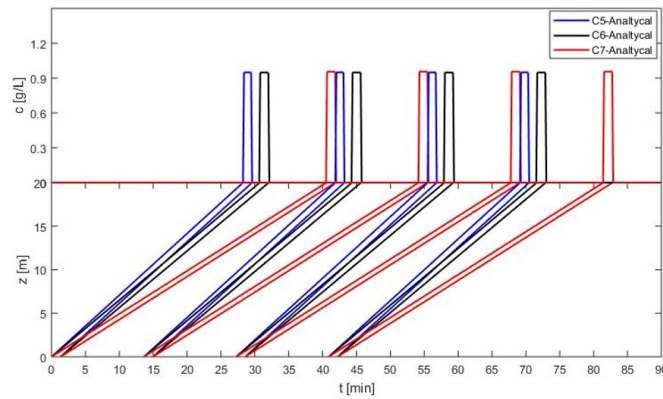
b Trajectories and their corresponding concentration solutions under isocratic conditions when $\alpha_{1,2} > \alpha_{2,3}$. $t_{inj}^2 = 13.62$ min, $t_{inj}^3 = 27.25$ min, $t_{inj}^4 = 40.08$ min and $\Delta t_c^p = 13.62$ min.
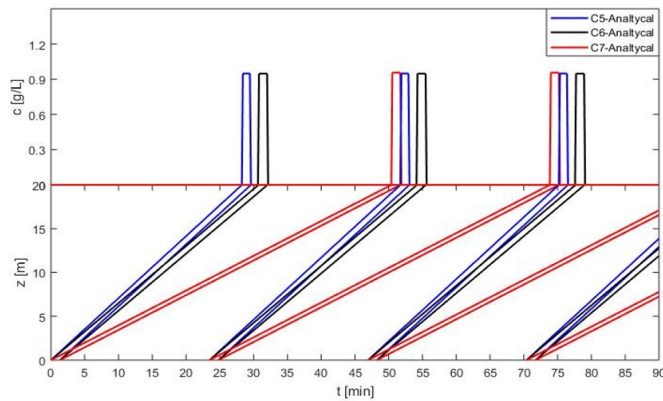
c Trajectories and their corresponding concentration solutions under isocratic conditions when $\alpha_{1,2} >> \alpha_{2,3}$. $t_{inj}^2 = 23.46$ min, $t_{inj}^3 = 46.93$ min, $t_{inj}^4 = 70.39$ min and $\Delta t_c^p = 23.46$ min.

Figure 3.7: Separation scenarios on the basis of the selected Henry constants of Group I under isocratic conditions.
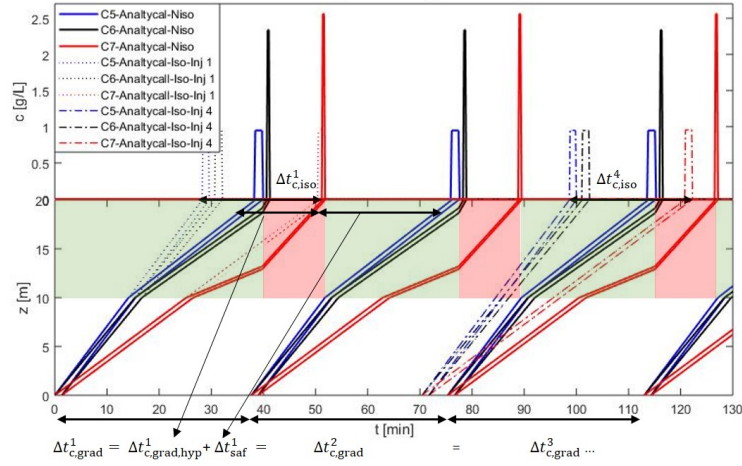
Figure 3.8: Group I conservative design concept with safety margins for "Late Eluter" case–The space-time trajectories and the corresponding concentration solutions. For isocratic conditions, only injection 1 and injection 4 are shown, while for gradient conditions, all four injections are shown. In the gradients case, the first switching of the temperature is done at $t^p_{1,\max}$ and second switching at $t^p_{3,\max}$ and then they shift by $\Delta t^p_{c,\mathrm{grad}}$ alternatively. **Isocratic:** $t^2_{\mathrm{inj}} = 23.46$ min, $t^3_{\mathrm{inj}} = 46.93$ min, $t^4_{\mathrm{inj}} = 70.39$ min and $\Delta t^p_{c,\mathrm{iso}} = 23.46$ min. **Gradients:** $t^2_{\mathrm{inj}} = 37.66$ min, $t^3_{\mathrm{inj}} = 75.33$ min, $t^4_{\mathrm{inj}} = 113$ min and $\Delta t^p_{c,\mathrm{grad}} = 37.66$ min.
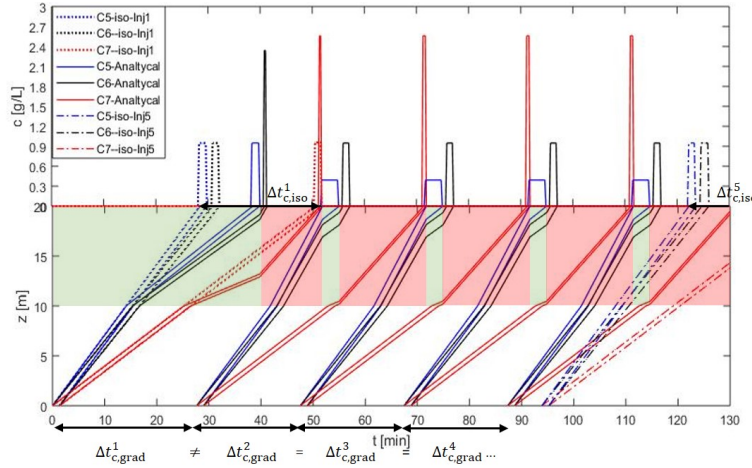
Figure 3.9: Group I Optimal design concept without safety margins for "Late Eluter" case–The space-time trajectories and the corresponding concentration solutions, which are now possible for up to 5 injections to be shown in the given time frame. For isocratic conditions, only injection 1 and injection 5 are shown, while for gradient conditions, all 5 injections are shown. **Isocratic:** All times are the same as in the previous figure. **Gradients:** $t^2_{\mathrm{inj}} = 27.64$ min, $t^3_{\mathrm{inj}} = 47.53$ min, $t^4_{\mathrm{inj}} = 67.42$ min and $\Delta t^1_{c,\mathrm{grad}} = 13.38$ min, $\Delta t^2_{c,\mathrm{grad}} = \Delta t^3_{c,\mathrm{grad}} = \Delta t^4_{c,\mathrm{grad}} = 19.89$ min.

Table 3.10: Results associated to Figures 3.8 and 3.9 (Group I)

Group I		
Symbol	**Quantity**	**Value Obtained**
$t_{c,\text{iso}}^p$	Cycle time in isocratic case (Eq. (3.24c) for $T_H = T_L = T_R$)	23.46 min
$\Delta t_{c,\text{grad}(\text{Conservative})}^p$	Cycle time in gradients conservative design concept (Eq. (3.24c))	37.66 min
$\Delta t_{c,\text{grad,hyp}}^p$	Hypothetical cycle time in gradients conservative design concept (Subtract Eq. (3.23c) from Eq.(3.24c))	13.38 min
Δt_{saf}^p	Safety margin in gradients conservative design concept (Eq. (3.23c))	24.28 min
$\Delta t_{c,\text{grad}(\text{Optimal})}^p$	Cycle time in gradients optimal design concept (Eq. (3.30b))	19.90 min
$m_{1,\text{col}} = m_{2,\text{col}} = m_{3,\text{col}}$	Mass collected of c_1, c_2 and c_3 at $z_{\max}$ (c.f. Eq. (2.55))	3.8×10^{-4} g
$P_{n,\text{iso}}, n = 1, 2, 3.$	Production rate of each component under isocratic conditions (c.f. Eq. (2.51))	0.10 gh^{-1}L^{-1} (avg. of the three)
$P_{n,\text{grad}}, n = 1, 2, 3.$	Production rate of each component under gradients optimal design concept (c.f. Eq. (2.50))	0.12 gh^{-1}L^{-1} (avg. of the three)
P_{inc}	Percent wise increase in the overall production rate by gradients optimal design concept	20% (approx.)

Understanding the elution behavior of each component is crucial in chromatographic separations, as it directly influences the overall performance or productivity. In Group II, the elution tendencies differ from those observed in Group I, where only c_1 tends to elute faster, while c_2 and c_3 exhibit a slower elution profile. This contrast in elution behavior, with $\alpha_{1,2} << \alpha_{2,3}$, presents a little different challenge that requires a careful evaluation of the conservative and optimal design concepts.

Group II After successfully addressing the separation of Group I components using optimized temperature step gradients, the focus now shifts to Group II components (Early Eluter). The objective remains the same: to enhance the separation performance and reduce cycle time. To achieve this, we follow a similar strategy as in Group I, i.e., accelerating the elution of slower components and decelerating the faster ones. However, due to the distinct elution behavior of Group II, involving one faster-eluting and two slower-eluting components, a different switching strategy is required. Nevertheless, we will follow the same conservative and optimal design concepts as for Group I.

Conservative Design Concept with Safety Margins

As foreseen in the strategy, we start cooling component c_1 in segment II. At this point, c_2 and c_3 have not yet entered the segment II and are still in segment I. As c_1 is cooled alone, it leaves the system at time $t_1 = t_{1,\text{max}}^1$. At this time, we change the temperature from T_L to T_H, whereupon c_2 and c_3 enter the heated segment II and their elution is accelerated. This means that all three components in this scenario undergo Type I temperature changes, which is why the trajectories

(3.16a) to (3.16c) can be written even more simply as

$$z_{1,\mathrm{ad}}^{p}(t) = \begin{cases} \frac{u}{1+Fa_1(T_\mathrm{R})}(t - t_{\mathrm{inj}}^{p}), & \text{for } t \in [t_{\mathrm{inj}}^{p}, t_{1,\mathrm{m}}^{p}], \\ z_{1,\mathrm{ad}}^{p}(t_{1,\mathrm{m}}^{p}) + \frac{u}{1+Fa_1(T_\mathrm{L})}(t - t_{1,\mathrm{m}}^{p}), & \text{for } t \in \,]t_{1,\mathrm{m}}^{p}, t_{1,\mathrm{max,ad}}^{p}], \end{cases} \tag{3.31a}$$

$$z_{2,\mathrm{ad}}^{p}(t) = \begin{cases} \frac{u}{1+Fa_2(T_\mathrm{R})}(t - t_{\mathrm{inj}}^{p}), & \text{for } t \in [t_{\mathrm{inj}}^{p}, t_{2,\mathrm{m}}^{p}], \\ z_{2,\mathrm{ad}}(t_{2,\mathrm{m}}^{p}) + \frac{u}{1+Fa_2(T_\mathrm{H})}(t - t_{3,\mathrm{m}}^{p}), & \text{for } t \in \,]t_{2,\mathrm{m}}^{p}, t_{2,\mathrm{max,ad}}^{p}], \end{cases} \tag{3.31b}$$

$$z_{3,\mathrm{ad}}^{p}(t) = \begin{cases} \frac{u}{1+Fa_3(T_\mathrm{R})}(t - t_{\mathrm{inj}}^{p}), & \text{for } t \in [t_{\mathrm{inj}}^{p}, t_{3,\mathrm{m}}^{p}], \\ z_{3,\mathrm{ad}}(t_{3,\mathrm{m}}^{p}) + \frac{u}{1+Fa_3(T_\mathrm{H})}(t - t_{3,\mathrm{m}}^{p}), & \text{for } t \in \,]t_{3,\mathrm{m}}^{p}, t_{3,\mathrm{max,ad}}^{p}]. \end{cases} \tag{3.31c}$$

In a similar manner, one derives the related time variables for the adsorption fronts with respect to space z as

$$t_{1,\mathrm{ad}}^{p}(z) = \begin{cases} t_{\mathrm{inj}}^{p} + \frac{1+Fa_1(T_\mathrm{R})}{u}z, & \text{for } z \in [0, z_\mathrm{m}], \\ \frac{1+Fa_1(T_\mathrm{L})}{u}z - \frac{1+Fa_1(T_\mathrm{L})}{1+Fa_1(T_\mathrm{R})}(t_{1,\mathrm{m}}^{p} - t_{\mathrm{inj}}^{p}) + t_{1,\mathrm{m}}^{p}, & \text{for } z \in \,]z_\mathrm{m}, z_\mathrm{max}], \end{cases} \tag{3.32a}$$

$$t_{2,\mathrm{ad}}^{p}(z) = \begin{cases} t_{\mathrm{inj}}^{p} + \frac{1+Fa_2(T_\mathrm{R})}{u}z, & \text{for } z \in [0, z_\mathrm{m}], \\ \frac{1+Fa_2(T_\mathrm{H})}{u}z - \frac{1+Fa_2(T_\mathrm{H})}{1+Fa_2(T_\mathrm{R})}(t_{2,\mathrm{m}}^{p} - t_{\mathrm{inj}}^{p}) + t_{2,\mathrm{m}}^{p}, & \text{for } z \in \,]z_\mathrm{m}, z_\mathrm{max}], \end{cases} \tag{3.32b}$$

$$t_{3,\mathrm{ad}}^{p}(z) = \begin{cases} t_{\mathrm{inj}}^{p} + \frac{1+Fa_3(T_\mathrm{R})}{u}z, & \text{for } z \in [0, z_\mathrm{m}], \\ \frac{1+Fa_3(T_\mathrm{H})}{u}z - \frac{1+Fa_3(T_\mathrm{H})}{1+Fa_3(T_\mathrm{R})}(t_{3,\mathrm{m}}^{p} - t_{\mathrm{inj}}^{p}) + t_{3,\mathrm{m}}^{p}, & \text{for } z \in \,]z_\mathrm{m}, z_\mathrm{max}]. \end{cases} \tag{3.32c}$$

Whereas, the above parameters for the desorption fronts, are always described by (3.18a) and (3.18b).

As in Group I, we use the same formulas in the current case to calculate switching times, the times of further injections as well as the cycle time. Despite the distinct elution behavior of Group II components, the fundamental principles underlying the calculations remain consistent. By employing these well-established formulas, we can efficiently plan the timing of subsequent injections and optimize the cycle time. The advantage of a fixed sequence of temperature regimes is that the formula (3.14) for calculating the switching times can be consistently applied here as well.

Using (3.22a) under the above time formulas, we obtain the time for each next injection $p+1$ in the conservative design concept as

$$\begin{aligned} t_{\mathrm{inj}}^{p+1} = \Delta t_{\mathrm{inj}} &+ \frac{1+Fa_3(T_\mathrm{H})}{u}z_\mathrm{max} - \frac{1+Fa_3(T_\mathrm{H})}{1+Fa_3(T_\mathrm{R})}(t_{3,\mathrm{m}}^{p} - t_{\mathrm{inj}}^{p}) + t_{3,\mathrm{m}}^{p} \\ &- \frac{1+Fa_1(T_\mathrm{R})}{u}z_\mathrm{m}, \qquad \text{for } p = 1, 2, ..., P-1, P \in \mathbb{N}, \end{aligned} \tag{3.33a}$$

whereas by (3.23a) the unique cycle time for $p = 1, 2, ..., P \in \mathbb{N}$ is given as

$$\Delta t_\mathrm{c}^{p} = \Delta t_{\mathrm{inj}} + \frac{1+Fa_3(T_\mathrm{H})}{u}z_\mathrm{max} - \frac{1+Fa_3(T_\mathrm{H})}{1+Fa_3(T_\mathrm{R})}(t_{3,\mathrm{m}}^{p} - t_{\mathrm{inj}}^{p}) + t_{3,\mathrm{m}}^{p} - t_{1,\mathrm{m}}^{p}. \tag{3.33b}$$

Similar to Group I, the conservative design concept is found to be suboptimal for Group II components as well. In pursuit of an improved approach, we devise again the optimal design concept that eliminates the safety margin and achieves enhanced separation performance. The upcoming section outlines the details of this optimized strategy, tailored specifically to the characteristics of the early eluter case of Group II.

Optimal Design Concept without Safety Margins

As part of this concept, we have carefully analyzed the analytic solution trajectories of equations (3.31a) through (3.31c) at $p = 1$. In this optimized concept, as usually, we plan the first two temperature regimes, T_L and T_H, to be fully applied during the first injection as in the conservative design concept. By strategically initiating the second injection early enough, we ensure efficient heating of the adsorption front of its component c_1, along with c_2 and c_3 of the first injection.

At $t_2 = t_{3,\max}^1$, we strategically switched the temperature from T_H to T_L. Since the second injection is now performed earlier, it effectively heats up the desorption front of c_1 of the second injection. Subsequently, at $t_3 = t_{1,\max}^2$, we return to T_H to affect c_2 and c_3 simultaneously.

Similarly, in the subsequent injections, we repeat the pair of temperature regimes of second injections, maintaining consistent injection and cycle times. By precisely matching the temperature switching times to the elution behavior of the individual components, we have once again succeeded in eliminating the safety margins and achieving efficient elution of the components of the Group II. This optimized strategy of temperature modulation resulted in an acceptable productivity increase also for the constituents of Group II, which is slightly higher than that observed in group I.

The implementation of the distinct temperature strategy resulted in divergent trajectories and time parameters for the second and subsequent injections, in contrast to the conservative design concept where the trajectories remained the same for all injections. However, the first injection retained the same trajectories and times as in the conservative design concept. Here are the trajectories and associated times for second and onwards injections (with $k \geq 1$) obtained through the optimized temperature modulation for Group II components:

$$z_{1,\mathrm{ad}}^p(t) = \begin{cases} \frac{u}{1+Fa_1(T_\mathrm{R})}(t - t_{\mathrm{inj}}^p), & \text{for } t \in [t_{\mathrm{inj}}^p, t_{1,\mathrm{m}}^p], \\ z_{1,\mathrm{ad}}^p(t_{1,\mathrm{m}}^p) + \frac{u}{1+Fa_1(T_\mathrm{H})}(t - t_{1,\mathrm{m}}^p), & \text{for } t \in]t_{1,\mathrm{m}}^p, t_{1,\mathrm{max,ad}}^p], \end{cases} \tag{3.34a}$$

$$z_{1,\mathrm{de}}^p(t) = \begin{cases} \frac{u}{1+Fa_1(T_\mathrm{R})}(t - \Delta t_{\mathrm{inj}} - t_{\mathrm{inj}}^p), & \text{for } t \in [t_{\mathrm{inj}}^p, t_{1,\mathrm{m}}^p], \\ z_{1,\mathrm{ad}}^p(t_{1,\mathrm{m}}^p) + \frac{u}{1+Fa_1(T_\mathrm{H})}(t - \Delta t_{\mathrm{inj}} - t_{1,\mathrm{m}}^p), & \text{for } t \in]t_{1,\mathrm{m}}^p, t_{2k}], \\ z_{1,\mathrm{ad}}^p(t_2) + \frac{u}{1+Fa_1(T_\mathrm{L})}(t - \Delta t_{\mathrm{inj}} - t_{2k}), & \text{for } t \in]t_{2k}, t_{1,\mathrm{max}}^p], \end{cases} \tag{3.34b}$$

$$z_{2,\mathrm{ad}}^p(t) = \begin{cases} \frac{u}{1+Fa_2(T_\mathrm{R})}(t - t_{\mathrm{inj}}^p), & \text{for } t \in [t_{\mathrm{inj}}^p, t_{2,\mathrm{m}}^p], \\ z_{2,\mathrm{ad}}^p(t_{2,\mathrm{m}}^p) + \frac{u}{1+Fa_2(T_\mathrm{H})}(t - t_{1,\mathrm{m}}^p), & \text{for } t \in]t_{2,\mathrm{m}}^p, t_{2,\mathrm{max,ad}}^p] \end{cases} \tag{3.34c}$$

and since both fronts of c_2 are simultaneously exposed to all temperature changes, we can straightforwardly express

$$z_{2,\mathrm{de}}^p(t) = z_{2,\mathrm{ad}}^p(t - \Delta t_{\mathrm{inj}}). \tag{3.34d}$$

Since c_3 is simultaneously heated up with c_2, we observe a similar trajectory for c_3 as well, as

$$z_{3,\text{ad}}^p(t) = \begin{cases} \frac{u}{1+Fa_3(T_\text{R})}(t - t_{\text{inj}}^p), & \text{for } t \in [t_{\text{inj}}^p, t_{3,\text{m}}^p], \\ z_{3,\text{ad}}^p(t_{3,\text{m}}^p) + \frac{u}{1+Fa_3(T_\text{L})}(t - t_{3,\text{m}}^p), & \text{for } t \in]t_{3,\text{m}}^p, t_{3,\text{max,ad}}^p] \end{cases} \tag{3.34e}$$

and the trajectory of its desorption front is given as

$$z_{3,\text{de}}^p(t) = z_{3,\text{ad}}^p(t - \Delta t_{\text{inj}}). \tag{3.34f}$$

Now, utilizing the above trajectories, we can derive the corresponding time expressions for both fronts of the three components as follows

$$t_{1,\text{ad}}^p(z) = \begin{cases} t_{\text{inj}}^p + \frac{1+Fa_1(T_\text{R})}{u}z, & \text{for } z \in [0, z_\text{m}], \\ \frac{1+Fa_1(T_\text{H})}{u}z - \frac{1+Fa_1(T_\text{H})}{1+Fa_1(T_\text{R})}(t_{1,\text{m}}^p - t_{\text{inj}}^p) + t_{1,\text{m}}^p, & \text{for } z \in]z_\text{m}, z_\text{max}], \end{cases} \tag{3.35a}$$

$$t_{1,\text{de}}^p(z) = \Delta t_{\text{inj}} + \begin{cases} t_{\text{inj}}^p + \frac{1+Fa_1(T_\text{R})}{u}z, & \text{for } z \in [0, z_\text{m}], \\ \frac{1+Fa_1(T_\text{L})}{u}z - \frac{1+Fa_1(T_\text{L})}{1+Fa_1(T_\text{R})}(t_{1,\text{m}}^p - t_{\text{inj}}^p)- \\ \frac{1+Fa_1(T_\text{L})}{1+Fa_1(T_\text{H})}(t_2 - t_{1,\text{m}}^p) + t_2, & \text{for } z \in]z_\text{m}, z_\text{max}], \end{cases} \tag{3.35b}$$

$$t_{2,\text{ad}}^p(z) = \begin{cases} t_{\text{inj}}^p + \frac{1+Fa_2(T_\text{R})}{u}z, & \text{for } z \in [0, z_\text{m}], \\ \frac{1+Fa_2(T_\text{H})}{u}z - \frac{1+Fa_2(T_\text{H})}{1+Fa_2(T_\text{R})}(t_{2,\text{m}}^p - t_{\text{inj}}^p) - t_{2,\text{m}}^p, & \text{for } z \in]z_\text{m}, z_\text{max}], \end{cases} \tag{3.35c}$$

$$t_{2,\text{de}}^p(z) = \Delta t_{\text{inj}} + t_{2,\text{ad}}^p(z), \tag{3.35d}$$

$$t_{3,\text{ad}}^p(z) = \begin{cases} t_{\text{inj}}^p + \frac{1+Fa_3(T_\text{R})}{u}z, & \text{for } z \in [0, z_\text{m}], \\ \frac{1+Fa_3(T_\text{H})}{u}z - \frac{1+Fa_3(T_\text{H})}{1+Fa_3(T_\text{R})}(t_{3,\text{m}}^p - t_{\text{inj}}^p) - t_{3,\text{m}}^p, & \text{for } z \in]z_\text{m}, z_\text{max}] \end{cases} \tag{3.35e}$$

and

$$t_{3,\text{de}}^p(z) = \Delta t_{\text{inj}} + t_{3,\text{ad}}^p(z). \tag{3.35f}$$

Having obtained the trajectories and the time variables, we will now calculate the essential parameters, as in the case of the late eluter, for calculating productivity.

The time for the second injection is calculated according to the optimized case of Group I, where the last and the first components of two consecutive injections leave the column one after the other. Thus, (3.26), where (3.32c) is used for the desorption front and $p = 1$ and (3.35a) is used for $p = 2$, replacing $t_{1,\text{m}}^2 - t_{\text{inj}}^2$ with $t_{1,\text{m}}^1$ and divide $t_{1,\text{m}}^2$ into $t_{\text{inj}}^2 + t_{1,\text{m}}^1$, gives the following

$$t_{\text{inj}}^2 = \Delta t_{\text{inj}} + \frac{1 + Fa_3(T_\text{H})}{u}z_\text{max} - \frac{1 + Fa_3(T_\text{H})}{1 + Fa_3(T_\text{R})}t_{3,\text{m}}^1 + t_{3,\text{m}}^1$$
$$- \frac{1 + Fa_1(T_\text{H})}{u}z_\text{max} + \frac{1 + Fa_1(T_\text{H})}{1 + Fa_1(T_\text{R})}t_{1,\text{m}}^1 - t_{1,\text{m}}^1. \tag{3.36a}$$

Similar to the optimal design concept in Group I, in this case, we also calculate t_{inj}^3 due to the distinct cycle times Δt_c^1 and Δt_c^2, which represent the intervals between the first three consecutive injections. To determine t_{inj}^3, we first calculate Δt_c^2, which then allows us to conveniently compute t_{inj}^3. Using (3.35f) and (3.35a) for $p = 2$ in (3.30a), we calculate Δt_c^2 as

$$
\begin{aligned}
\Delta t_c^2 = \Delta t_{inj} &+ \frac{1 + Fa_3(T_H)}{u} z_{max} - \frac{1 + Fa_3(T_H)}{1 + Fa_3(T_R)}(t_{3,m}^2 - t_{inj}^2) - t_{3,m}^2 \\
&- \frac{1 + Fa_1(T_H)}{u} z_{max} + \frac{1 + Fa_1(T_H)}{1 + Fa_1(T_R)}(t_{1,m}^2 - t_{inj}^2) - t_{1,m}^2,
\end{aligned}
\tag{3.37a}
$$

such that

$$
t_{inj}^3 = t_{inj}^2 + \Delta t_c^2 \tag{3.37b}
$$

and

$$
t_{inj}^p = t_{inj}^{p-1} + \Delta t_c^{p-1}, \qquad \text{for} \qquad p = 3, 4, 5, ..., P \in \mathbb{N}. \tag{3.37c}
$$

All trajectories and solutions for the Henry constants of the Group II for the isocratic case are shown in Figure 3.11, and for the conservative design concept in Figure 3.12. For the optimal design concept they are shown in Figure 3.13.

Figure 3.12 presents concentration profiles for three feed components in the early eluter case (Group II) under conventional isocratic conditions and forced periodic conservative design concept of temperature modulation. The isocratic case shows only the first and fourth injections, while the conservative temperature modulation includes all four injections. The minimal cycle time under isocratic conditions is $\Delta t_{c,iso}^p = 23.46$ min, which avoids overlap between consecutive cycles and renders typical production rate. However, applying a shorter hypothetical cycle time of $\Delta t_{c,grad,hyp}^p = 16.18$ min risks undesired remixing of component bands in segment II. To address this issue, the optimal design concept (Figure 3.13) with more quick temperature changes is implemented. The application of this appropriate strategy, using a cycle time of $\Delta t_{c,grad}^p = 19.35$ min for $p \geq 2$, results in a 20% increase in the production rate compared to the isocratic case (see also table 3.14).

a Trajectories (below) and their corresponding concentration solutions (on the top) under isocratic conditions when $\alpha_{1,2} \approx \alpha_{2,3}$. $t_{inj}^2 = 6.24$ min, $t_{inj}^3 = 12.49$ min, $t_{inj}^4 = 18.7$ min and $\Delta t_c^p = 6.24$ min, $p = 1, 2, 3, 4$.
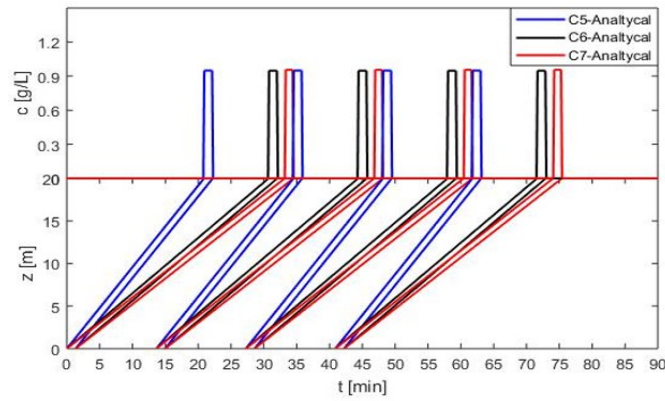
b Trajectories and their corresponding concentration solutions under isocratic conditions when $\alpha_{1,2} < \alpha_{2,3}$. $t_{inj}^2 = 13.62$ min, $t_{inj}^3 = 27.25$ min, $t_{inj}^4 = 40.08$ min and $\Delta t_c^p = 13.62$ min.
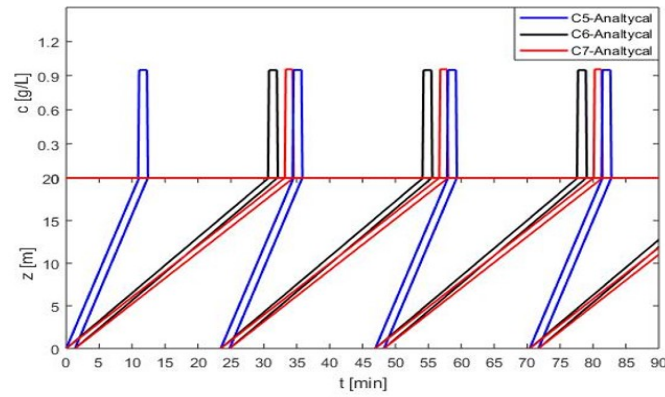
c Trajectories and their corresponding concentration solutions under isocratic conditions when $\alpha_{1,2} << \alpha_{2,3}$. $t_{inj}^2 = 23.46$ min, $t_{inj}^3 = 46.93$ min, $t_{inj}^4 = 70.39$ min and $\Delta t_c^p = 23.46$ min.

Figure 3.11: Separation scenarios on the basis of the selected Henry constants of Group II under isocratic conditions.
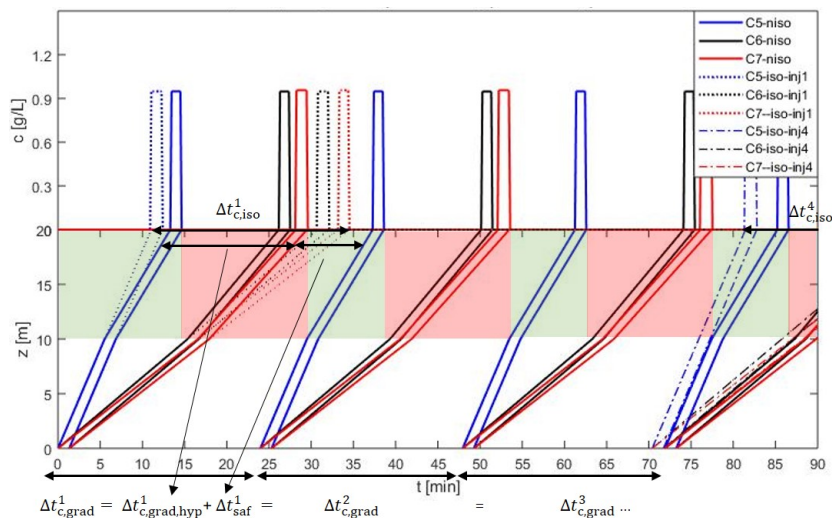
Figure 3.12: Group II conservative design concept with safety margins for "Early Eluter" case – In isocratic conditions, as in Group I, only Injection 1 and Injection 4 are shown, while in gradient conditions all four injections are shown. **Isocratic:** As in Group I. **Gradients:** $t_{inj}^2 = 23.97$ min, $t_{inj}^3 = 47.94$ min, $t_{inj}^4 = 71.913$ min and $\Delta t_{c,grad}^p = 23.97$ min.
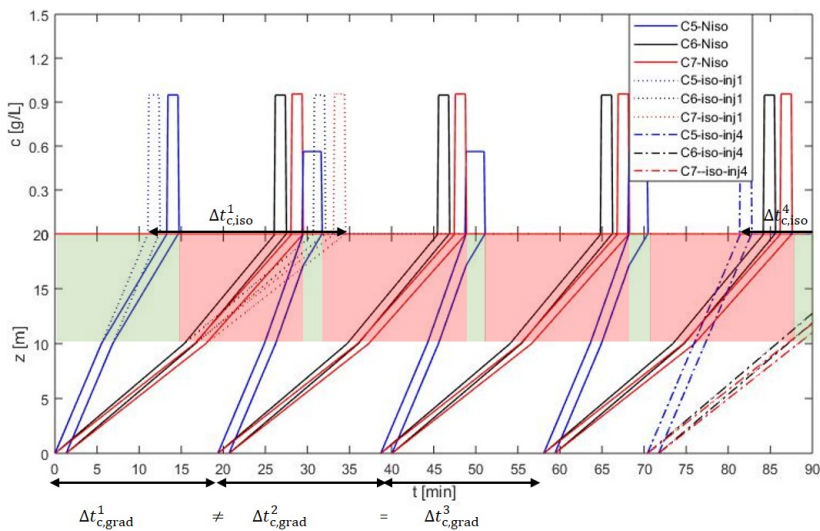
Figure 3.13: Group II Optimal design concept without safety margins for "Early Eluter" case– For isocratic conditions, again only injection 1 and injection 4 are shown, while for gradient conditions, all four injections are shown. **Isocratic:** All times are the same as in Group I. **Gradients:** $t_{inj}^2 = 19.35$ min, $t_{inj}^3 = 38.71$ min, $t_{inj}^4 = 58.07$ min and $\Delta t_{c,grad}^1 = 16.18$ min, $\Delta t_{c,grad}^2 = \Delta t_{c,grad}^3 = \Delta t_{c,grad}^4 = 19.35$ min.

Table 3.14: Results of productivity gain in Group II

Group II		
Symbol	**Quantity**	**Value Obtained**
$\Delta t^p_{c,\text{grad}(\text{Conservative})}$	Cycle time in gradients conservative design concept (Eq. (3.33b))	23.97 min
$\Delta t^p_{c,\text{grad,hyp}}$	Hypothetical cycle time in gradients conservative design concept (Subtract Eq. (3.23b) from Eq. (3.33b))	16.18 min
Δt^p_{saf}	safety margin in gradients conservative design concept (Eq. (3.23b))	7.78 min
$\Delta t^p_{c,\text{grad}(\text{Optimal})}$	Cycle time in gradients optimal design concept (c.f. Eq. (3.37a))	19.35 min
$P_{n,\text{iso}}, n = 1, 2, 3.$	Production rate of each component under isocratic conditions (c.f. Eq. (2.51))	0.10 gh^{-1}L^{-1} (avg. of the three)
$P_{n,\text{grad}}, n = 1, 2, 3.$	Production rate of each component under gradients optimal design concept (c.f. Eq. (2.50))	0.12 gh^{-1}L^{-1} (avg. of the three)
P_{inc}	Percent wise increase in the overall production rate by gradients optimal design concept	20% (approx.)

Summery of the Chapter 3: In this chapter, we explored the equilibrium model, also known as the ideal model, coupled with an ideal temperature profile as a step function. We analytically solved the model using the method of characteristics for obtaining generalized trajectory solutions. These solutions were then applied to single-component injections, allowing us to analyze concentration profiles over time (chromatograms) and space under various temperature gradients.

Building upon this foundation, we planned multi-injections of a ternary mixture, considering the elution patterns in two scenarios: "Late Eluter" and "Early Eluter" cases based on Henry constant combinations in Group I and Group II, respectively. However, the initially pursued conservative design concept of temperature modulation considering safety margins proved to be suboptimal for both groups.

To overcome this limitation, we devised an optimal design concept, eliminating safety margins and achieving efficient elution of components. This optimized approach led to an acceptable productivity gains, increasing by up to 20% for both Group I and Group II, surpassing the isocratic case.

To conclude, the primary objective of this chapter was to provide an analytical estimation of cycle times under strategically planned temperature gradients, which are notably shorter in comparison to those experienced under isocratic conditions. Key formulas derived from both conservative and optimal design concepts are presented. For the late eluter case of Group I, these formulas are represented by equations (3.24c) and (3.30b), respectively. Similarly, for the early eluter scenario of Group II, the corresponding formulas in both design concepts are expressed by equations (3.33b) and (3.37a).

Chapter 4

Numerical Methods

In this chapter, we will explore the use of numerical techniques to solve the remaining mathematical models presented in Chapter 2. We start with the EDM, coupled with ideal temperature gradients (section 2.4.1). We proceed in the opposite direction to the detailed model with the EDM coupled with the energy equation (section 2.2). In contrast to the previous chapter, some of the parameters used in this chapter are determined experimentally, which allows for a more realistic approach to the simulations. We will use the finite volume upwind scheme for the advective terms and central discretization for the second-order dispersion terms in the numerical solutions. Additionally, we investigate new properties of the coupled mass and energy equations. We also solve the EDM for a large plate number N_p to compare the results with EM, which was solved analytically in the previous chapter. Furthermore, we perform stability analysis for all the models to ensure stable and accurate solutions.

Discretization

To numerically solve the mathematical models, we need to discretize the differential equations. This involves defining a mesh over the rectangular domain $\Omega = [0, x_{\max}] \times [0, \tau^P_{n,\max}]$, where $\tau^P_{n,\max}$ is the time at which the last component of the process exits the column. Let x_i for $i \in \mathbb{N}_0$ be the number of grid points, Δx be the spatial step size and N_x be the number of cells which is chosen to be an even natural number depending upon the desired resolution of the solution, such that

$$x_i = i\Delta x, \qquad \text{for } i = 0, 1, 2, ..., N_x, \qquad \text{with} \qquad \Delta x = \frac{x_{\max} = 1}{N_x}. \tag{4.1}$$

All grid points x_i correspond to cells σ_i, c.f. Figure 4.1. At the left boundary, we have $\sigma_0 = [0, \frac{\Delta x}{2}]$, at the right boundary, $\sigma_{N_x} = [1 - \frac{\Delta x}{2}, 1]$ and in the interior, we have $\sigma_i = [x_i - \frac{\Delta x}{2}, x_i + \frac{\Delta x}{2}]$ for $n = 1, 2, 3, ..., N_x - 1$. Let $N_{x_2} = \frac{N_x}{2}$ be the index of the grid point at the middle of the column. Then, numerically, the grid points x_0 to $x_{N_{x_2}}$ form segment I, whereas, $x_{N_{x_2}}$ to x_{N_x} form segment II. The point $x_{N_{x_2}}$ is the common boundary point at the interface of both the segments. It means that each end point of the segments has a grid point with $x_{N_{x_2}}$ as the most important one. Corresponding to this point, we have a cell $\sigma_{N_{x_2}} = [x_{N_{x_2}} - \frac{\Delta x}{2}, x_{N_{x_2}} + \frac{\Delta x}{2}]$, which lies half in segment I and half in segment II. Now we define, for the time step $\Delta \tau$, the number of time discretization points as $N_\tau = \text{rd}\left(\frac{\tau^P_{n,\max}}{\Delta \tau}\right)$. In order to get a stable solution, we will have to estimate $\Delta \tau$ by doing a proper stability analysis for every specific system of PDE's.
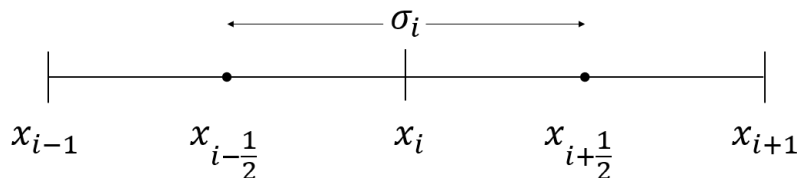
Figure 4.1: Grid points and corresponding cells for defining the fluxes

4.1   EDM Coupled with Ideal Temperature Step Gradients

To tackle the EDM via the FVM, our initial step involves discretization of the governing partial differential equations (PDEs) that describe solute transport and dispersion in porous media. By partitioning the domain into finite control volumes, we approximate the continuous PDE solution. Upon completing the numerical simulation, we perform a comparative analysis between the FVM results and analytical solutions of the EM to validate accuracy and reliability. Note that the results obtained from this model are already published in the article [38].

Let us reconsider Eqs. (2.38), (2.39) and (2.43a)–(2.43e), i.e.

$$[1 + Fa_n(T)]\, c_{n_\tau} = -c_{n_x} + t_{R_0} D_x c_{n_{xx}}, \qquad n = 1, 2, 3, ..., N_c, \tag{4.2}$$

$$T(x,\tau) = \begin{cases} T_R & \text{for} \quad 0 \le x \le x_m, \quad \tau \in [0, \tau^P_{n,\max}], \\ T_k & \text{for} \quad x_m < x \le x_{\max}, \quad \tau \in [\tau_k, \min\{\tau_{k+1}, \tau^P_{n,\max}\}], \\ & \qquad\qquad\qquad\qquad k \in \mathbb{N}_0, \tau_k < \tau^P_{n,\max}, \end{cases} \tag{4.3}$$

such that

$$c_n^I(x_0 \text{ to } x_m, \tau_0) = 0, \quad c_n^{II}(x_m \text{ to } x_{\max}, \tau_0) = 0, \tag{4.4a}$$

whereas, for $p = 1, 2, 3, ..., P$ with $P \in \mathbb{N}$, the following boundary conditions are considered

$$c_n^I(x_0, \tau) = \begin{cases} c_{n,\text{inj}}, & \tau^p_{\text{inj}} \le \tau \le \tau^p_{\text{inj}} + \Delta\tau_{\text{inj}}, \\ 0, & \tau^p_{\text{inj}} + \Delta\tau_{\text{inj}} < \tau < \tau^p_{n,m}, \end{cases} \tag{4.4b}$$

$$c_n^{II}(x_m, \tau) = \begin{cases} \frac{1 + Fa_n(T^I)}{1 + Fa_n(T^{II})} c_n^I(x_m, \tau^p_{n,m}), & \tau^p_{n,m} \le \tau \le \tau^p_{n,m} + \Delta\tau_{\text{inj}}, \\ 0, & \tau^p_{n,m} + \Delta\tau_{\text{inj}} < \tau < \tau^p_{n,\max}. \end{cases} \tag{4.4c}$$

At the right boundary for the second order derivative, we have to take the Neumann boundary condition, i.e.

$$c_{n_x}^{II}(x_{\max}, \tau) = 0. \tag{4.4d}$$

In our numerical approach to solve the EDM, we opt for the explicit finite volume method, which is a popular scheme for discretizing partial differential equations involving transport phenomena. This method is well-suited for simulating solute transport and dispersion in porous media.

To apply the explicit FVM for solving the EDM, we rearrange the (4.2) to isolate the time derivative on the left side and move all spatial derivatives with respect to x to the right side. This allows for efficient explicit time-stepping numerical integration, making the method

computationally straightforward and practical for simulating solute transport and dispersion in porous media. Hence we write the equation as

$$c_{n_\tau} = -\frac{1}{1 + Fa_n(T)} c_{n_x} + \frac{t_{R_0} D_x}{1 + Fa_n(T)} c_{n_{xx}}. \tag{4.5}$$

4.1.1 Discretization of Single-Component Injection

Let us examine the elution of a single component, represented by $N_c = 1$. By applying these simplifications to equation (4.5), where we take $c_1 = c$, $q_1 = q$, $c_{1,\text{inj}} = c_{\text{inj}}$, $\tau^p_{1,\text{max}} = \tau_{\text{max}}$, and $\Delta H_{A,n} = \Delta H_A$, the equation can be expressed in the following form

$$c_\tau = -\frac{1}{1 + Fa(T)} c_x + \frac{t_{R_0} D_x}{1 + Fa(T)} c_{xx}, \tag{4.6}$$

where

$$a(T) = a(T_R) \exp\left[\frac{-\Delta H_A}{R}\left(\frac{1}{T} - \frac{1}{T_R}\right)\right]. \tag{4.7}$$

The initial and boundary conditions then become

$$c^{\text{I}}(x_0 \text{ to } x_{\text{m}}, \tau_0) = 0, \tag{4.8a}$$

$$c^{\text{II}}(x_{\text{m}} \text{ to } x_{\text{max}}, \tau_0) = 0 \tag{4.8b}$$

and neglecting "p" as we do only one injection of a single solute, the boundary conditions are given as

$$c^{\text{I}}(x_0, \tau) = \begin{cases} c_{\text{inj}}, & \tau_{\text{inj}} \leq \tau \leq \tau_{\text{inj}} + \Delta\tau_{\text{inj}}, \\ 0, & \tau_{\text{inj}} + \Delta\tau_{\text{inj}} < \tau < \tau_{\text{m}}, \end{cases} \tag{4.8c}$$

$$c^{\text{II}}(x_{\text{m}}, \tau) = \begin{cases} \frac{1 + Fa(\tau_{\text{I}})}{1 + Fa(\tau_{\text{II}})} c^{\text{I}}(x_{\text{m}}, \tau_{\text{m}}), & \tau_{\text{m}} \leq \tau \leq \tau_{\text{m}} + \Delta\tau_{\text{inj}}, \\ 0, & \tau_{\text{m}} + \Delta\tau_{\text{inj}} < \tau < \tau_{\text{max}}, \end{cases} \tag{4.8d}$$

$$c^{\text{II}}_x(x_{\text{max}}, \tau) = 0. \tag{4.8e}$$

To externally impose temperature changes in this model, we follow the similar approach as in the equilibrium theory, which involves two types of temperature changes: Type I and Type II.

In Type I, we maintain segment I of the system at a reference temperature T_R, while segment II is set either at T_L or T_H. As a result, T_0 becomes a set of possible temperatures T_L, T_H. So, in this case, there are no switching times τ_k until time τ_{max}. This means that the only value of k that exists is 0. As a consequence, the temperature profile, considering equation (4.3), can be expressed as follows.

$$T(x,t) = \begin{cases} T_R & \text{for } 0 \leq x \leq x_{\text{m}}, & \tau \in [0, \tau_{\text{max}}], \\ T_0 & \text{for } x_{\text{m}} < x \leq x_{\text{max}}, & \tau \in [0, \tau_{\text{max}}]. \end{cases} \tag{4.9}$$

In Type II, the initial period from $\tau_0 = 0$ to τ_1, involves both segments maintained at the reference temperature $T_0 = T_R$. The value of τ_1 is estimated in experiments or based on specific

requirements. After τ_1, we switch the temperature of segment II to either $T_1 = T_L$ or $T_1 = T_H$. As there is only one planned switching event, we have $k = 0, 1$. As a result, the temperature profile for this Type II scenario can be described as follows

$$T(x,t) = \begin{cases} T_R & \text{for} \quad 0 \leq x \leq x_m, & \tau \in [0, \tau_{max}], \\ T_0 & \text{for} \quad x_m < x \leq x_{max}, & \tau \in [0, \tau_1[, \\ T_1 & \text{for} \quad x_m < x \leq x_{max}, & \tau \in [\tau_1, \tau_{max}]. \end{cases} \qquad (4.10)$$

In the explicit finite volume upwind method, we handle the time advancement using a forward difference scheme, which means that the concentration values are updated at each time step based on information from the previous time step. This explicit nature makes the numerical integration straightforward and computationally efficient. For the convection terms, we employ a backward difference scheme. This approach allows us to account for the transport of solutes with respect to the direction of flow, ensuring accuracy in modeling advection-dominated phenomena. Additionally, to approximate the dispersion terms in (4.6), we use a central difference scheme of order two. This central differencing provides higher accuracy in capturing the dispersion effects while minimizing numerical artifacts associated with numerical diffusion.

By combining the forward difference, backward difference, and central difference schemes, we obtain a robust and accurate numerical method for solving the EDM. After introducing these differences in (4.6), the resulting discrete form given by (4.11) demonstrates the numerical implementation of the explicit finite volume method for the Equilibrium Dispersive Model (EDM). This equation captures the concentration update at cell i and time step $j + 1$, while considering the influence of the equilibrium isotherm through the factor $Fa(T)$, i.e.

$$\frac{c_i^{j+1} - c_i^j}{\Delta \tau} = -\frac{1}{1 + Fa(T)} \frac{c_i^j - c_{i-1}^j}{\Delta x} + \frac{t_{R_0} D_x}{1 + Fa(T)} \frac{c_{i-1}^j - 2c_i^j + c_{i+1}^j}{\Delta x^2} \qquad (4.11)$$

or

$$c_i^{j+1} = c_i^j - \frac{\Delta \tau}{1 + Fa(T)} \frac{c_i^j - c_{i-1}^j}{\Delta x} + \frac{\Delta \tau t_{R_0} D_x}{1 + Fa(T)} \frac{c_{i-1}^j - 2c_i^j + c_{i+1}^j}{\Delta x^2}. \qquad (4.12)$$

For simplicity, let us use the following abbreviations

$$b(T) = \frac{1}{1 + Fa(T)}, \qquad d(T) = \frac{t_{R_0} D_x}{1 + Fa(T)} \frac{1}{\Delta x}. \qquad (4.13)$$

Then (4.12), after rearranging the terms, yields

$$c_i^{j+1} = c_i^j - \frac{\Delta \tau}{\Delta x} \left[\left\{ b(T) \left(c_i^j \right) - d(T) \left(c_{i+1}^j - c_i^j \right) \right\} - \left\{ b(T) \left(c_{i-1}^j \right) - d(T) \left(c_i^j - c_{i-1}^j \right) \right\} \right]. \qquad (4.14)$$

We introduce the symbols $\Delta_{\pm} c_i^j$ to denote the differences in the above equations, so that

$$\Delta_{\pm} c_i^j = \pm \left(c_{i\pm 1}^j - c_i^j \right). \qquad (4.15)$$

So, in view of the above notation, (4.14) takes the form

$$c_i^{j+1} = c_i^j - \frac{\Delta \tau}{\Delta x} \left[\left\{ b(T) c_i^j - d(T) \Delta_+ c_i^j \right\} - \left\{ b(T) c_{i-1}^j - d(T) \Delta_- c_i^j \right\} \right]. \qquad (4.16)$$

To make sure there is no loss in mass, we define fluxes $\mathrm{F}^c_{i+\frac{1}{2}}$ and $\mathrm{F}^c_{i-\frac{1}{2}}$ in each cell σ_i as

$$\mathrm{F}^c_{i+\frac{1}{2}} = \mathrm{b}(T)c^j_i - \mathrm{d}(T)\Delta_+ c^j_i, \qquad \mathrm{F}^c_{i-\frac{1}{2}} = \mathrm{b}(T)c^j_{i-1} - \mathrm{d}(T)\Delta_- c^j_i, \tag{4.17}$$

which are called right and left fluxes, respectively. In view of these fluxes, (4.14) looks like

$$c^{j+1}_i = c^j_i - \frac{\Delta\tau}{\Delta x}\left(\mathrm{F}^c_{i+\frac{1}{2}} - \mathrm{F}^c_{i-\frac{1}{2}}\right). \tag{4.18}$$

The last term $-\frac{\Delta\tau}{\Delta x}\left(\mathrm{F}^c_{i+\frac{1}{2}} - \mathrm{F}^c_{i-\frac{1}{2}}\right)$ of above PDE represents a spatial discretization. It calculates the change in concentration due to flux differences at cell interfaces ($i+\frac{1}{2}$ and $i-\frac{1}{2}$). Fluxes F^c represent the flow of the concentration between neighboring grid points.

The FVM in the flux form is widely used for numerical simulations of transport phenomena in various scientific and engineering applications. By transforming partial differential equations into integral conservation equations for each control volume, FVM ensures mass and other conserved quantities are accurately preserved within the discretized domain. This approach offers flexibility in handling complex geometries, achieves high spatial accuracy, and exhibits robustness in dealing with non-uniform grids. Moreover, FVM's conservative nature and suitability for parallel computing contribute to its computational efficiency [33, 75].

Stability condition: Stability analysis plays a crucial role in numerical simulations of mathematical models, particularly when employing numerical methods to solve partial differential equations (PDEs) or other iterative algorithms. Ensuring the stability of a numerical scheme is essential to produce reliable and accurate results. A stable numerical method guarantees that small errors at each step of the computation do not grow uncontrollably over time, preventing the simulation from converging or producing unrealistic outcomes. By analyzing the stability of a numerical method, researchers and engineers can determine appropriate time step sizes and other parameters that maintain numerical stability throughout the simulation. Moreover, stability analysis provides insights into the behavior and limitations of the numerical scheme under different conditions, allowing users to select appropriate methods for specific applications. In the context of the EDM, a thorough stability analysis ensures that the time step size and spatial discretization are carefully chosen to ensure the reliability of predictions and accurate representations of solute transport and dispersion in porous media.

We derive a generalized stability condition for the time step $\Delta\tau$ that holds for all N_c components, denoted by c_n with $n = 1, 2, \cdots, N_\mathrm{c}$. To determine the stability constraint, we make full use of the corresponding Henry constants $a_n(T)$ for each component c_n, where $T = T_k$ are the available temperatures. By Equation (2.4), as the provided temperatures T_k form a monotonic sequence, the corresponding Henry constants, which are inversely proportional to these temperatures, also follow a monotonic pattern. Consequently, we always have a maximum and minimum value of $a_n(T)$. We define $a_{\min}(T)$ as the smallest Henry constant, which can be determined by considering the available temperature options. The stability condition for the time step $\Delta\tau$ is formulated based on $a_{\min}(T)$ for all the available temperatures T, to ensure accurate and stable numerical simulations in all injection scenarios. So, let us say that

$$a_{\min}(T) = \min\left\{a_1(T), a_2(T), ..., a_{N_c}(T)\right\}. \tag{4.19}$$

Now using (4.13), the above Henry constant, consequently, produces largest advection coefficient $b_{\max}(T)$ and largest dispersion coefficient $d_{\max}(T)$, given as

$$b_{\max}(T) = \frac{1}{1 + Fa_{\min}(T)} \qquad \text{and} \qquad d_{\max}(T) = \frac{t_{R_0}D_x}{1 + Fa_{\min}(T)}\frac{1}{\Delta x}. \tag{4.20}$$

As mentioned earlier, N_x is chosen arbitrarily, so Δx is always available as $\frac{x_{\max}}{N_x}$. We calculate $\Delta\tau$ from Δx by using the Discrete Maximum Principle (DMP), [70]. Let $\bar{c}_i^j$ is the solution of concentration obtained from (4.14), then we must have

$$\min(c_{i-1}^j, c_i^j, c_{i+1}^j) \leq \bar{c}_i^{j+1} \leq \max(c_{i-1}^j, c_i^j, c_{i+1}^j). \tag{4.21}$$

For a well-posed problem, we must also have $\bar{c}_i^{j+1} \geq 0$. Using this fact in (4.14), we seek

$$\bar{c}_i^{j+1} = \left(1 - \frac{\Delta\tau}{\Delta x}\left(b_{\max}(T) + 2d_{\max}(T)\right)\right)c_i^j + \frac{\Delta\tau}{\Delta x}d_{\max}(T)c_{i+1}^j + \tag{4.22}$$

$$\frac{\Delta\tau}{\Delta x}\left(b_{\max}(T) + d_{\max}(T)\right)c_{i-1}^j \geq 0, \tag{4.23}$$

which implies the restrictions

$$0 \leq 1 - \frac{\Delta\tau}{\Delta x}\left(b_{\max}(T) + 2d_{\max}(T)\right), \frac{\Delta\tau}{\Delta x}d_{\max}(T), \frac{\Delta\tau}{\Delta x}\left(b_{\max}(T) + d_{\max}(T)\right) \leq 1 \tag{4.24}$$

or

$$1 - \frac{\Delta\tau}{\Delta x}\left(b_{\max}(T) + 2d_{\max}(T)\right) \geq 0. \tag{4.25}$$

The above inequality can also be written as

$$\frac{\Delta\tau}{\Delta x}\left(b_{\max}(T) + 2d_{\max}(T)\right) \leq 1,$$

giving the following stability restriction on our time steps

$$\Delta\tau \leq \frac{\Delta x}{b_{\max}(T) + 2d_{\max}(T)}. \tag{4.26}$$

With this, we define the time vector, for $N_\tau = \frac{\tau_{\max}}{\Delta\tau}$, as

$$\tau_j = j\Delta\tau \qquad \text{for } j = 0, 1, 2, ..., N_\tau. \tag{4.27}$$

We will utilize the time step as defined by (4.26) not only in single-component tests but also in the experiments involving ternary mixture injections.

Coding in MATLAB (R2017a): Let τ_s be the switching time that was used in the experiments with which we want to compare our numerical results. We want to run computations with one change of temperature in segment II at the time τ_s. Let τ_m be the time at which the front of the pulse having concentration c_m^j reaches x_m, i.e. when $c_m^j > 0$ for the first time, such that $\tau_m \leq \tau_s < \tau_{\max}$. In Type I, we have $\tau_s = \tau_m$, while, in Type II, $\tau_s = \tau_1$, the time when the pulse

is somewhere inside segment II and we switch its temperature suddenly. Remember that in Type II, the value of τ_s is a predetermined value taken in the experiments. Based on this selection of τ_s, we could write the code for both Type I and Type II concertedly. Note that the time τ_m is calculated from the code itself and all the τ_k are chosen appropriately. Let us explain the code using space-time graphs given in Figure 4.2.
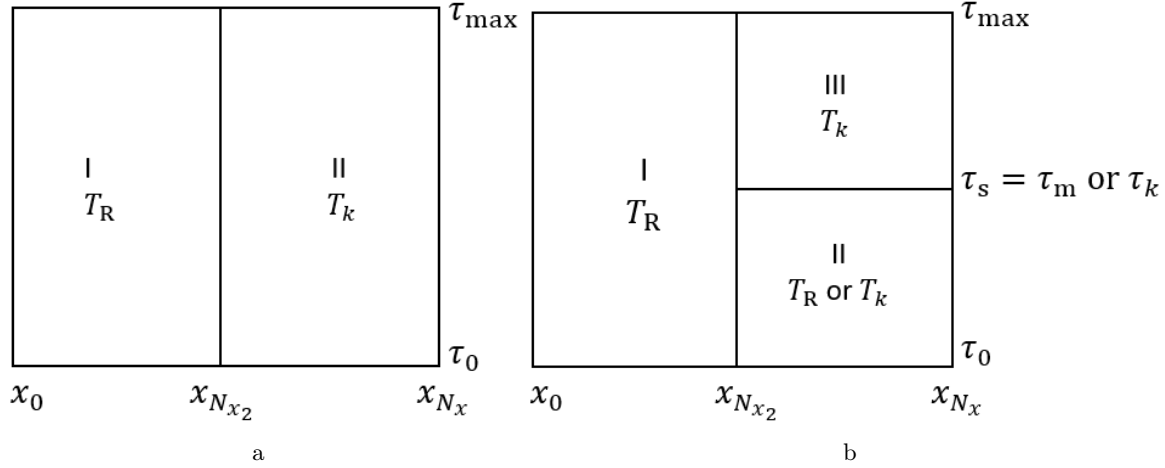
Figure 4.2: Figure (a) corresponds to Type I temperature change, where the space-time plane is divided into two zones, in which Zone I corresponds to segment I and cells $[\sigma_0, \ \sigma_{N_{x_2}}]$, while Zone II corresponds to segment II and cells $[\sigma_{N_{x_2}+1}, \ \sigma_{N_x}]$. On the other hand, Figure (b) is associated with Type II that has three zones. Zone I corresponding to segment I and Zone II as well as Zone III forming segment II. In a single-component experiment, we normally have T_R in the Zone II, while in a multicomponent experiment we have T_k in this zone. The line of τ_s in (b), which is flexible between τ_m and τ_{max}, is a type of border between Zone II and Zone III.

As we have noticed in the characteristics solution in Chapter 3, the estimation of concentrations in segment II of the chromatographic column requires the multiplication of two ratios: the ratio of retention factors under different temperatures $\frac{1+Fa(T_R)}{1+Fa(T_k)}$ and the ratio of space bandwidths in the two segments. In Type I temperature change, the two ratios turn out to be reciprocals of each other, smoothing out each other. This means that the mobile phase concentration remains unaffected in Type I. The reason for this is that in Type I temperature change, there is no jump in temperature over time, and the continuity in temperature conditions keeps the ratios reciprocal. On the other hand, in Type II, the space bandwidths in the two segments are the same and their ratio gives value of 1, leaving only the ratio of retention factors that affects the mobile phase concentration. This is because Type II involves a temperature jump over time, leading to discontinuity in temperature conditions, which affects the behavior of the ratios. Hence, in Type II, we perform the multiplication of the latter ratio to accurately estimate the concentration in segment II.

To ensure the well-posedness of the problem, we impose boundary conditions on the half cells at the edges. The left boundary cell (σ_0) follows the left boundary condition (4.8c) which establishes the concentration value at the very left edge of the spatial domain. Similarly, the right boundary cell (σ_{N_x}) adheres to the right boundary condition (4.8e), setting the concentration

value at the extreme right of the domain, which, after getting split by central difference implies

$$\frac{c_{N_x+1}^{j+1} - c_{N_x-1}^{j+1}}{2\Delta x} = 0 \tag{4.28a}$$

or

$$c_{N_x+1}^{j+1} = c_{N_x-1}^{j+1}. \tag{4.28b}$$

For the rest of the cells, we use a zone-wise division of the code as given below.

In Type I, corresponding to Figure 4.2a, Zone I maintains temperature T_R, while Zone II has temperature $T_k \in \{T_R, T_L, T_H\}$. Therefore, in Zone I, i.e. for cells $[\sigma_1, \ \sigma_{N_{x_2}}]$ and for all times j, using (4.14), the PDE has the following appearance

$$c_i^{j+1} = c_i^j - \frac{\Delta\tau}{\Delta x}\left[\left\{b(T_R)c_i^j - d(T_R)\Delta_+ c_i^j\right\} - \left\{b(T_R)c_{i-1}^j - d(T_R)\Delta_- c_i^j\right\}\right], \tag{4.29}$$

while for Zone II corresponding to cells $[\sigma_{N_{x_2}+1}, \ \sigma_{N_x-1}]$, it is given as

$$c_i^{j+1} = c_i^j - \frac{\Delta\tau}{\Delta x}\left[\left\{b(T_k)c_i^j - d(T_k)\Delta_+ c_i^j\right\} - \left\{b(T_k)c_{i-1}^j - d(T_k)\Delta_- c_i^j\right\}\right]. \tag{4.30}$$

The scenario of the Type II, shown in the figure 4.2b, implies that zones I and II remain at temperature T_R, since both segments are initially kept at the reference temperature and this is changed at time τ_s only for the segment II. The concentration in these two zones is defined by the PDE (4.29). However, as discussed earlier, the calculation of concentration in Zone III requires an adjustment after the switching time τ_s due to the sudden temperature change in our model at this specific time. In Zone III, the index j starts from ℓ, which is the lowest index where $\tau_j \geq \tau_s$. When $\tau_\ell \geq \tau_s > \tau_{\ell-1}$, the concentration must be multiplied by the ratio demanded by the jump condition (2.42), which is given by

$$\frac{1 + Fa(T_R)}{1 + Fa(T_k)} = \frac{b(T_k)}{b(T_R)}. \tag{4.31}$$

So, the concentration entering Zone III from Zone II through line τ_s is given as

$$c_n^\ell = \frac{b(T_k)}{b(T_R)}c_n^\ell. \tag{4.32}$$

The computation of the right-hand side in the above equation is based on (4.29), and the resulting values are used as the initial conditions for the subsequent time step. This effectively employs the boundary condition (4.8d) to ensure a consistent and smooth transition between time steps, ensuring the accuracy and stability of the numerical solution.

So, at the boundary between Zone I and III there is a cell $\sigma_{N_{x_2}} = [x_{N_{x_2}} - \frac{\Delta x}{2}, x_{N_{x_2}} + \frac{\Delta x}{2}]$, which is half in Zone I and half in Zone III. Therefore, the right flux corresponds to the temperature T_k and the left flux corresponds to the temperature T_R. The left flux is adjusted by the ratio (4.31) and consequently, the concentration in this cell is defined as

$$c_i^{j+1} = c_i^j - \frac{\Delta\tau}{\Delta x}\left[\left\{b(T_k)c_i^j - d(T_k)\Delta_+ c_i^j\right\} - \frac{b(T_k)}{b(T_R)}\left\{b(T_k)c_{i-1}^j - d(T_k)\Delta_- c_i^j\right\}\right]. \tag{4.33}$$

And finally, the concentration throughout Zone III, looks like

$$c_i^{j+1} = c_i^j - \frac{\Delta\tau}{\Delta x}\left[\left\{b(T_k)c_i^j - d(T_k)\Delta_+ c_i^j\right\} - \left\{b(T_k)c_{i-1}^j - d(T_k)\Delta_- c_i^j\right\}\right]. \tag{4.34}$$

Calculation of Important Times: We know that calculating the arrival times at the interface x_{m} and the column exit $x_{\max}$ holds significant importance as these times play a crucial role in determining the retention times for each component. This information enables us to determine the most appropriate injection times for consecutive injections of multicomponent mixtures. Additionally, the cycle times, representing the time interval between consecutive injections, can be accurately determined, contributing to the optimization of column productivity and separation efficiency.

In the MATLAB code, associated to x_{m} and $x_{\max}$, we use concentration arrays, representing the concentrations of a particular component at these locations during all the process time, respectively. We use the ''`find`'' function to locate the indices in these arrays, where the concentration values meet a specific threshold. This calculation is given step by step below.

Step 1: *Finding Non-zero Concentrations at x_{m} and $x_{\max}$*
In the MATLAB code, we have a concentration matrix ''`c`'' representing the concentrations of a particular component at all time-space mesh points. The variables `Nx2` and `Nx` are the indexes representing the locations of the interface x_{m} and column's exit $x_{\max}$, respectively. We use the ''`find`'' function to locate the indices in the array `c(Nx2,:)` and `c(Nx,:)` where the concentration values are greater than `10^(-2)`. This means we are looking for the time steps at which the concentration of the component at the aforementioned locations becomes significant, considering a threshold of `10^(-2)` as significant.

Step 2: *Extracting Time Information*
The function returns column vectors ''`fm`'' at x_{m} and ''`fmax`'' at $x_{\max}$ containing the row positions where the condition is met. Each element of ''`fm`'' and ''`fmax`'' represents a time index where the concentration at x_{m} and $x_{\max}$, respectively, is greater than `10^(-2)`. The first element of ''`fm`'' represents the earliest time at which the adsorption front of the component reaches x_{m} and the last element of ''`fmax`'' represents the latest time at which the desorption front of the component reaches $x_{\max}$.

Step 3: *Finding the Times at x_{m} and $x_{\max}$*
The next lines of code ''`tm`'' and ''`tmax`'' extracts the time information. The line ''`tm`'' takes the first element of ''`fm`'' (i.e. the earliest time index where the concentration is greater than `10^(-2)` at x_{m}) and the line ''`tmax`'' takes the last element of ''`fmax`'' (i.e. the latest time index where the concentration is greater than `10^(-2)` at $x_{\max}$). The ''`round`'' function rounds the values to the nearest integer (as time indices are discrete), and then accesses the corresponding time value from the time array τ. The result are stored in the variables ''`tm`'' and ''`tmax`''.

The MATLAB code for these calculations is given below.

```
fm=find (c(Nx2,:)>10^(-2));    % Non-zero array of c at xm
tm=t(round(fm(1)));            % time for c to reach xm
fmax=find (c(Nx,:)>10^(-2));   % Non-zero array of c at xmax
tmax=t(round(fmax(end)));      % time for c to cross xmax
```

Calculation of Mass at Column's Outlet: Maintaining accurate mass balance is fundamental in the FVM as it ensures the conservation of mass during numerical simulations. This

accuracy is of paramount importance for various applications, including chemical engineering, especially in the field of chromatography. By adhering to mass balance principles, the FVM's results can be validated against experimental data or analytical solutions, instilling confidence in the reliability of the simulations for a wide range of practical and scientific investigations. The FVM's precise mass balance capability contributes to optimizing transport processes and effectively predicting solute behavior in porous media systems, making it a robust and invaluable tool in tackling real-world challenges in chemical engineering and chromatography.

To determine the mass at $x = x_{\max}$, we utilize (2.55), but a direct application is not possible due to the need for a discrete version of the integral. An inherent challenge arises in obtaining precisely the injected mass, as $\Delta\tau_{\text{inj}}$ may not align perfectly with $\Delta\tau$, potentially resulting in a slight surplus or deficit. To address this, we manually adjust $\Delta\tau_{\text{inj}}$ to ensure it is a multiple of $\Delta\tau$ and then subtract any excess mass from the original formula. Introducing a time variable $\bar{\tau}_j$ for $j = 0, 1, 2, ..., N\tau$, with $\bar{\tau}_0 = 0$, allows us to modify the formulas (2.53) to (2.55) for all j such that $\tau_j \le \Delta\tau_{\text{inj}}$ as follows:

$$\bar{\tau}_{j+1} = \bar{\tau}_j + \Delta\tau \qquad \text{for} \qquad j = 0, 1, 2, ..., N_\tau. \tag{4.35}$$

The mass adjustment at any time τ_j and location x_i is given by $c_{\text{inj}}(\bar{\tau}_j - \Delta\tau_{\text{inj}})$. Therefore, expressing (2.53) to (2.55) in its discrete sum form for $n = 1$ and $\text{m}_n = \text{m}$, we obtain the correct mass for any $j^* \in [0, N_\tau]$ as follows

$$\text{m}_{\text{total}} = A\left[\epsilon + (1 - \epsilon)a_n(T)\right] \sum_{j=0}^{N_x} \left[c_i^{j^*} - c_{\text{inj}}(\bar{\tau}_j - \Delta\tau_{\text{inj}})\right] \Delta x, \tag{4.36a}$$

for any $i^* \in [0, N_x]$

$$\text{m}_{\text{total}} = \frac{u}{1 + Fa_n(T)} A\left[\epsilon + (1 - \epsilon)a_n(T)\right] \sum_{j=0}^{N_\tau} \left[c_{i*}^{j} - c_{\text{inj}}(\bar{\tau}_j - \Delta\tau_{\text{inj}})\right] \Delta\tau, \tag{4.36b}$$

while, for $i = N_x$, it is given as

$$\text{m}_{\text{col}} = u\epsilon A \sum_{j=0}^{N_\tau} \left[c_{N_x}^{j} - c_{\text{inj}}(\bar{\tau}_j - \Delta\tau_{\text{inj}})\right] \Delta\tau. \tag{4.36c}$$

The above newly derived formulas for mass calculation are not only applicable to single-component injections but also play a crucial role in handling multicomponent injections. As we move forward to consider scenarios involving multiple solute components, the adjustment technique remains consistent and ensures accurate mass calculations.

4.1.2   Analysis of Consecutive Injections of Ternary Mixture

In the previous chapter, we explored two groups, Group I and Group II, each comprising three distinct scenarios based on the relative migration rates of the components. In this section, we will only focus on the last scenario that resembles the late eluter case of Group I, i.e. $\alpha_{1,2} >> \alpha_{2,3}$. This is also because in the experimental project mentioned at the beginning, this scenario was considered. To this end, we will use experimentally determined Henry constants and real system parameters to improve the accuracy and representativeness of our numerical simulations. In this

way, we hope to gain deeper insights into the performance of the column and explore ways to improve its productivity.

Our primary focus remains on reducing the cycle time $\Delta\tau_c$ while maintaining the integrity of the numerical solution to validate its accuracy against experimental data.

Let us recall the scenario when $\alpha_{1,2} >> \alpha_{2,3}$, where a multicomponent mixture with concentrations c_1, c_2, and c_3 is consecutively injected P-times at specific injecting times τ_{inj}^p where $p = 1, 2, ..., P \in \mathbb{N}$. We use the equations given by (4.2) and (4.3), where $N_c = 3$ and $\tau_{3,\text{max}}^P$ is the final time of the experiment when the last component of last injection exit the column, i.e.

$$[1 + Fa_n(T)]\, c_{n_\tau} = -c_{n_x} + t_{R_0} \mathrm{D}_x c_{n_{xx}}, \qquad n = 1, 2, 3, \tag{4.37}$$

$$T(x, \tau) = \begin{cases} T_R & \text{for} \quad 0 \le x \le x_m, \quad \tau \in [0, \tau_{3,\text{max}}^P], \\ T_k & \text{for} \quad x_m < x \le x_{\text{max}}, \quad \tau \in [\tau_k, \min\{\tau_{k+1}, \tau_{3,\text{max}}^P\}], \\ & \qquad\qquad\qquad\qquad k \in \mathbb{N}_0, \tau_k < \tau_{3,\text{max}}^P. \end{cases} \tag{4.38}$$

Now, let's extend the initial and boundary conditions, previously established for a single component in (4.8), to encompass the n-component scenario, where $n = 1, 2, 3$ and $p = 1, 2, 3, ..., P, P \in \mathbb{N}$, i.e.

$$c_n^{\mathrm{I}}(x_0 \text{ to } x_m, \tau_0) = 0, \tag{4.39a}$$

$$c_n^{\mathrm{II}}(x_m \text{ to } x_{\text{max}}, \tau_0) = 0, \tag{4.39b}$$

$$c_n^{\mathrm{I}}(x_0, \tau) = \begin{cases} c_{n,\text{inj}}, & \tau_{\text{inj}}^p \le \tau \le \tau_{\text{inj}}^p + \Delta\tau_{\text{inj}}, \\ 0, & \tau_{\text{inj}}^p + \Delta\tau_{\text{inj}} < \tau < \tau_{n,m}^p, \end{cases} \tag{4.39c}$$

$$c_n^{\mathrm{II}}(x_m, \tau) = \begin{cases} \dfrac{1 + Fa_n(T^{\mathrm{I}})}{1 + Fa_n(T^{\mathrm{II}})} c_n^{\mathrm{I}}(x_m, \tau_{n,m}^p), & \tau_{n,m}^p \le \tau \le \tau_{n,m}^p + \Delta\tau_{\text{inj}}, \\ 0, & \tau_{n,m}^p + \Delta\tau_{\text{inj}} < \tau < \tau_{n,\text{max}}^p, \end{cases} \tag{4.39d}$$

$$c_{n_x}^{\mathrm{II}}(x_{\text{max}}, \tau) = 0. \tag{4.39e}$$

Recall that the injected concentration remains constant for each pth injection, which is why we do not use a superscript p for each c_n. We also know that the injection time $\Delta\tau_{\text{inj}}$ for each c_n remains unchanged in each injection.

Associated to each component, we also determine the times $\tau_{1,m}^p, \tau_{2,m}^p$, and $\tau_{3,m}^p$ corresponding to when the fronts of c_1, c_2 and c_3 reach the middle of the column x_m during the pth injection. Additionally, we calculate $\tau_{1,\text{max}}^p, \tau_{2,\text{max}}^p$, and $\tau_{3,\text{max}}^p$ as the times when these components have just exited the column. While we previously calculated these times analytically using trajectories, in the numerical analysis we estimate them using computational methods explained in three steps previously.

In this numerical study, we will apply both the conservative and optimal design concepts to calculate the injection times t_{inj}^p and cycle times Δt_c^p in the multicomponent mixture system. The objective is to examine now the numerically estimated solutions to determine if either of these concepts can generate shorter cycle times compared to the isothermal case. Having previously

found that only the optimal design concept without safety margins can achieve shorter cycle times given arbitrary parameters, we will now re-examine both the concepts in the context of experimentally determined parameters. By comparing the results from both the concepts, we aim to identify the most effective approach for reducing the cycle time and increasing the productivity of the chromatographic column. As these schemes are extensively explained in Section 3.3.2, we will provide a concise overview here.

Conservative Design Concept with Safety Margins

We start with the same idea of keeping segment I at the reference temperature T_R and segment II at T_L. After the the injection of the mixture c_n, each with a corresponding experimentally determined Henry constant, migration takes the form of the late eluter case mentioned earlier. In the segment II with temperature T_L, we aim to slow down the fast eluting component c_1, but by the time it leaves the column, c_2 and c_3 also enter the segment II and are slowed down. At the point where c_1 has just left the column, that is, at the time $\tau_1 = \tau_{1,\mathrm{max}}^1$, we change the temperature from T_L to T_H. Concentrations c_2 and c_3 which elute somewhere in segment II, get accelerated by T_H due to which the gap between all the three components is reduced, i.e. $\alpha_{1,2} \approx \alpha_{2,3}$. We keep the temperature until c_2 and c_3 both leave the column. Then we switch back the temperature from T_H to T_L at time $\tau_2 = \tau_{3,\mathrm{max}}^1$ and repeat the same sequence of the temperature regimes for the successive injections.

With this understanding in mind, we can now introduce the formula for switching times τ_k, which was already utilized in dimensional form during the analytical analysis in Chapter 3, equation (3.14). This formula is now given by (4.40) in non-dimensional form which defines the switching times $\tau_k = \frac{t_k}{t_{R_0}}$ corresponding to the changes in temperature during each injection. As observed, the cooling of segment II continues after times τ_{2k} and heating occurs after τ_{2k+1}, where $k \in \mathbb{N}_0$ and $\tau_0 = 0$. Consequently, the formula for all the switching times remains unchanged compared to the one provided by the analytical solution, i.e.

$$\tau_k = \begin{cases} \tau_{2k} = \tau_{3,\mathrm{max}}^p & \text{when } T = T_\mathrm{L} \quad \text{and } k = 1, 2, 3, ..., P, \\ \tau_{2k+1} = \tau_{1,\mathrm{max}}^p & \text{when } T = T_\mathrm{H} \quad \text{and } k = 0, 1, 2, 3, ...P - 1, \ P \in \mathbb{N}. \end{cases} \tag{4.40}$$

After introducing the switching times and the associated sequence of temperature regimes, we can effectively formulate the temperature profile of the entire column, as demonstrated in equation (4.38), as

$$T(x, \tau) = \begin{cases} T_\mathrm{R} & \text{for} \quad 0 \leq x \leq x_\mathrm{m}, & \tau \in [0, \tau_{n,\mathrm{max}}^p], \\ T_{2k} = T_\mathrm{L} & \text{for} \quad x_\mathrm{m} < x \leq x_\mathrm{max}, & \tau \in [\tau_{2k}, \tau_{2k+1}[, \\ T_{2k+1} = T_\mathrm{H} & \text{for} \quad x_\mathrm{m} < x \leq x_\mathrm{max}, & \tau \in [\tau_{2k+1}, \min\{\tau_{2k+2}, \tau_{n,\mathrm{max}}^p\}], \\ & \quad k \in \mathbb{N}_0, \tau_{2k+2} < \tau_{n,\mathrm{max}}^p. \end{cases}$$
$$\tag{4.41}$$

The injection times in this design concept are consistently determined from $\tau_{3,\mathrm{max}}^p$ and $\tau_{1,\mathrm{m}}^{p+1}$. This ensures that a successive injection takes place at a time that allows the concentration c_1 of the succeeding injection to reach the interface x_m precisely when the concentration c_3 of the preceding injection leaves the column. Mathematically, we establish the relationship between $\tau_{3,\mathrm{max}}^p$ and $\tau_{1,\mathrm{m}}^{p+1}$ as follows

$$\tau_{3,\mathrm{max}}^p = \tau_{1,\mathrm{m}}^{p+1}, \qquad \text{where } p = 2, 3, 4, ..., P. \tag{4.42a}$$

Alternatively, utilizing (3.19) enables us to obtain the time for the next injection without the need for complicated simplifications, yielding

$$\tau_{\text{inj}}^{p+1} = \tau_{3,\text{max}}^{p} - \tau_{1,\text{m}}^{1}. \tag{4.42b}$$

Similarly, considering the arrival time of the adsorption fronts of component c_1 at x_{max} in the pth injection, denoted as $\tau_{1,\text{max,ad}}^{p}$, and introducing a safety margin $\Delta\tau_{\text{saf}}^{p}$ between two consecutive injections, the cycle time $\Delta\tau_{\text{c}}$ (previously introduced in (3.23a)) is determined as follows

$$\Delta\tau_{\text{c}} = \tau_{3,\text{max}}^{p} - \tau_{1,\text{max,ad}}^{p} + \Delta\tau_{\text{saf}}^{p}, \qquad \text{for } p = 1, 2, ..., P, P \in \mathbb{N}, \tag{4.43a}$$

where

$$\Delta\tau_{\text{saf}}^{p} = \tau_{1,\text{max,ad}}^{p+1} - \tau_{3,\text{max}}^{p}, \qquad \text{for } p = 1, 2, ..., P-1, P \in \mathbb{N}. \tag{4.43b}$$

In our numerical analysis, we follow a similar approach to the conservative design concept explained in chapter 3, i.e. the cycle time $\Delta\tau_{\text{c}}$ is determined for calculating productivity starting from the first injection ($p = 1$). This cycle time remains constant for all injections, making it a critical parameter for evaluating the overall performance of the chromatographic column.

The abbreviations (4.13) and (4.15) in the case of multicomponent injection are used as follows

$$b_n(T) = \frac{1}{1 + Fa_n(T)}, \qquad d_n(T) = \frac{t_{R_0}D_x}{1 + Fa_n(T)}\frac{1}{\Delta x}, \qquad \text{for } n = 1, 2, 3, \tag{4.44}$$

$$\Delta_{\pm}c_{n,i}^{j} = \pm\left(c_{n,i\pm1}^{j} - c_{n,i}^{j}\right). \tag{4.45}$$

In conclusion, having established the switching times and the corresponding temperature sequences, we discretize the PDEs governing the behavior of the three eluting components under different temperature regimes, following the conservative design concept.

$\mathbf{c_1}$:

As c_1 undergoes a Type I cooling, its corresponding PDE can be illustrated as shown in Figure 4.2a. In both zones, the PDE for c_1 is represented by the following expression

$$c_{1,i}^{j+1} = c_{1,i}^{j} - \frac{\Delta\tau}{\Delta x}\left[\left\{b_1(T_{\text{R}})c_{1,i}^{j} - d_1(T_{\text{R}})\Delta_{+}c_{1,i}^{j}\right\} - \left\{b_1(T_{\text{R}})c_{1,i-1}^{j} - d_1(T_{\text{R}})\Delta_{-}c_{1,i}^{j}\right\}\right], \tag{4.46a}$$

$$c_{1,i}^{j+1} = c_{1,i}^{j} - \frac{\Delta\tau}{\Delta x}\left[\left\{b_1(T_{\text{L}})c_{1,i}^{j} - d_1(T_{\text{L}})\Delta_{+}c_{1,i}^{j}\right\} - \left\{b_1(T_{\text{L}})c_{1,i-1}^{j} - d_1(T_{\text{L}})\Delta_{-}c_{1,i}^{j}\right\}\right]. \tag{4.46b}$$

$\mathbf{c_2}$:

The component in the middle, c_2, undergoes two temperature changes, initially experiencing cooling of Type I and then heating of Type II. As a result, we have switching times $\tau_{\text{s}} = \{\tau_{2,\text{m}}, \tau_1\}$. Figure 4.2b represents this scenario, and the concentration c_2 in its Zone I is described by the following PDE

$$c_{2,i}^{j+1} = c_{2,i}^{j} - \frac{\Delta\tau}{\Delta x}\left[\left\{b_2(T_{\text{R}})c_{2,i}^{j} - d_2(T_{\text{R}})\Delta_{+}c_{2,i}^{j}\right\} - \left\{b_2(T_{\text{R}})c_{2,i-1}^{j} - d_2(T_{\text{R}})\Delta_{-}c_{2,i}^{j}\right\}\right]. \tag{4.46c}$$

In Zone II, it is given as

$$c_{2,i}^{j+1} = c_{2,i}^{j} - \frac{\Delta\tau}{\Delta x}\left[\left\{b_2(T_{\text{L}})c_{2,i}^{j} - d_2(T_{\text{L}})\Delta_{+}c_{2,i}^{j}\right\} - \left\{b_2(T_{\text{L}})c_{2,i-1}^{j} - d_2(T_{\text{L}})\Delta_{-}c_{2,i}^{j}\right\}\right]. \tag{4.46d}$$

As shown in (4.32), then for $j = \ell$ as the lowest index with $\tau_j \geq \tau_1$ and $\tau_\ell \geq \tau_1 > \tau_{\ell-1}$, the temperature jumps from T_L to T_H. So we have

$$c_{2,i}^\ell = \frac{b_2(T_H)}{b_2(T_L)} c_{2,i}^\ell. \tag{4.46e}$$

Consequently, this adjustment affects the left flux at the cell $\sigma_{N_{x_2}} = [x_{N_{x_2}} - \frac{\Delta x}{2}, x_{N_{x_2}} + \frac{\Delta x}{2}]$. Thus, the concentration in this cell is calculated as

$$c_{2,i}^{j+1} = c_{2,i}^j - \frac{\Delta\tau}{\Delta x} \left[\left\{ b_2(T_H)c_{2,i}^j - d_2(T_H)\Delta_+ c_{2,i}^j \right\} - \frac{b_{22}(T_H)}{b_2(T_R)} \left\{ b_2(T_R)c_{2,i-1}^j - d_2(T_R)\Delta_- c_{2,i}^j \right\} \right]. \tag{4.46f}$$

Hence, the concentration in the onwards cells $[\sigma_{N_{x_2}+1}, \sigma_{N_x-1}]$ is calculated as

$$c_{2,i}^{j+1} = c_{2,i}^j - \frac{\Delta\tau}{\Delta x} \left[\left\{ b_2(T_H)c_{2,i}^j - d_2(T_H)\Delta_+ c_{2,i}^j \right\} - \left\{ b_2(T_H)c_{2,i-1}^j - d_2(T_H)\Delta_- c_{2,i}^j \right\} \right]. \tag{4.46g}$$

c_3 :
The last component, c_3, is also subject to Type I and Type II temperature variations in the same sequence as c_2. Since c_3 enters segment II at time $\tau_{3,m}$, therefore, we have $\tau_s = \{\tau_{3,m}, \tau_1\}$. The scheme remains unchanged from c_2, which is why we reconsider Equations (4.46c) to (4.46g) for c_3.

Keep in mind that in the last cell σ_{N_x}, we utilize the right boundary condition for all three components using the central difference scheme. As a result, the concentration in the final cell is obtained as follows

$$c_{n,N_x+1}^{j+1} = c_{n,N_x-1}^{j+1}. \tag{4.46h}$$

In a similar way, we can write the scheme for the components of the succeeding injections.

As mentioned earlier, the conservative design concept takes into account safety margins between the elution of component c_3 from the previous injection and the elution of component c_1 from the following injection to avoid back-mixing. However, due to the existence of these safety margins, this concept has not demonstrated promising results and has not improved productivity compared to the isocratic case. This is because, in this design concept, we are unable to do every $p + 1^{th}$ injection earlier than that in isothermal case. This leads to a larger cycle time and loss in productivity. Therefore, in the next section, we will study the optimal design concept, which omits safety margins between consecutive injections and helps achieve higher productivity gains compared to the isocratic conditions.

Optimal Design Concept without Safety Margins

In this design concept, we maintain the same temperature regimes and switching times for the first injection as in the conservative design concept. However, we introduce a crucial modification for the second injection to omit the safety margins. Here, we initiate the second injection earlier, allowing the adsorption front of component c_1 to experience heating together with the last component of the preceding injection before the time $\tau_2 = \tau_{3,max}^1$. Subsequently, the temperature is switched to T_L, cooling the desorption front of component c_1 of the second injection. Although this intricate temperature profile does not directly reduce the cycle time, it plays a vital role in

preserving resolution and preventing remixing of components c_1 and c_2. The acceptable reduction in cycle time is achieved then by heating the last two components, c_2 and c_3, of the second injection after the time $\tau_3 = \tau_{1,\mathrm{max}}^2$. We allow the repetition of the sequence of these temperature regimes, for the consecutive injections. This has the effect of avoiding the safety margins created by the conservative design concept, where we applied unanimous temperature regimes to every injection. By omitting safety margins between consecutive injections and intelligently utilizing the temperature profiles, the optimal design concept yielded a substantial productivity gains that we failed to achieve in the conservative design concept. In this case, we are now able to do every $p + 1^{\mathrm{th}}$ injection earlier than that in isothermal case. This actually leads to a shorter cycle time and gain in productivity.

We also know from our analytical studies in the previous chapter, that in the optimal design concept, the calculation of injection times τ_{inj}^p differs from the conservative design concept. The goal in the optimal design concept is to ensure that the adsorption front of the component c_1 in the successive injection reaches x_{max} at the same time as the desorption front of the component c_3 from the previous injection leaves x_{max}. Unlike the conservative design concept, where elution times were known in advance due to the same temperature regimes for all the injections, the optimal design concept requires a different approach. In contrast to the analytical solution for the optimal design concept, the calculation of the time for the second injection in our numerical approach takes a more empirical route. We adopt a method where each τ_{inj}^2 is determined by adjusting $\tau_{1,\mathrm{max}}^1$ with a small time quantity Ω. This choice of Ω is crucial as it directly influences the level of remixing between the tails of c_3 and c_1. The formula for second injection is given as follows

$$\tau_{\mathrm{inj}}^2 = \tau_{1,\mathrm{max}}^1 \pm \Omega. \tag{4.47}$$

Once the second injection is completed, we find the cycle time using the same approach as in the previous studies of optimal design concept, i.e.

$$\Delta\tau_{\mathrm{c}}^2 = \tau_{3,\mathrm{max}}^2 - \tau_{1,\mathrm{max,ad}}^2. \tag{4.48}$$

Starting from τ_{inj}^3, we calculate all the successive injection times based on the cycle times previously calculated at the column's outlet. This iterative process allows us to determine the injection times for all subsequent injections, enabling us to perform multiple injections in a more efficient and productive manner. Mathematically, τ_{inj}^3 can be calculated as

$$\tau_{\mathrm{inj}}^3 = \tau_{\mathrm{inj}}^2 + \Delta\tau_{\mathrm{c}}^2 \tag{4.49}$$

and in its generalized form, we can express the injection time for each new injection as given in (4.50). This approach ensures that the injections are scheduled at optimal intervals, leading to a shorter cycle time and higher productivity for the chromatographic process.

$$\tau_{\mathrm{inj}}^p = \tau_{\mathrm{inj}}^{p-1} + \Delta\tau_{\mathrm{c}}^{p-1}, \qquad p = 3, 4, ..., P \in \mathbb{N}. \tag{4.50}$$

By carefully adjusting the injection times, we can achieve better resolution and productivity in our numerical simulations, making the optimal design concept more applicable to real-world scenarios.

In this scheme, the cycle time $\Delta\tau_{\mathrm{c}}$ is provided for the calculation of productivity starting from the second injection, i.e. $p = 2$, since it is the optimal one. Moreover, the switching times in this scheme are given by the same formula (4.40).

Consequently, the PDEs in this scheme would be similar to those in the conservative design concept, e.g. equations (4.46a) to (4.46h). The main difference lies in fitting the correct temperatures and ratios at the respective places, which are now influenced by the optimized injection and switching times. As a result, we do not need to rewrite the PDEs for this concept.

In conclusion, the optimal design concept has proven to be productive, surpassing the conservative design concept by omitting the safety margins without compromising on remixing prevention. The success of this approach is attributed to the careful analysis of each component's Henry constants, adsorption enthalpies and the available temperature range etc., allowing us to craft a suitable gradient operation strategy. By selecting precise switching and injection times, we can achieve the shortest possible cycle time enhancing the performance of liquid chromatographic columns.

A detailed explanation of the results from this model can be found in Chapter 5, specifically in Sections 5.2.1 and 5.3.1.

To this point, the distinction between the conservative design concept, which includes safety margins, and the optimal design concept, which omits them, has been clearly established. The purpose of presenting both concepts is to highlight the critical role of switching strategies in chromatographic processes and to demonstrate how the inclusion or omission of safety margins can significantly impact the results. This underscores the specificity of this study and suggests that outcomes may vary under different conditions. Given that the optimal design concept has shown improvement compared to isocratic conditions in our study, we do not see the necessity of further investigating the conservative design concept in the subsequent sections.

4.2   EDM Coupled with Simplified Energy Equation

In this modeling approach, we replace the ideal temperature gradients with a simplified energy equation (2.28). We have already solved this simplified energy equation analytically using Laplace transform in Section 2.3. The solution is given in two forms by (2.37a) and (2.37b). Based on this analytical solution, we will now estimate the concentration solution using FVM as in the previous section. For this purpose, we consider again (2.27) together with the aforementioned solution of T, i.e.

$$[1 + Fa_n(T)]\, c_{n_\tau} + c_n Fa_n(T)_T T_\tau = -c_{n_x} + t_{R_0} \mathrm{D}_x c_{n_{xx}}, \qquad n = 1, 2, 3, ..., N_\mathrm{c}, \qquad (4.51)$$

such that

$$T(\tau) = T_\mathrm{w} - (T_\mathrm{w} - T_\mathrm{R})\, e^{-t_{R_0} \mathrm{X}_2 \tau} \qquad \text{for} \qquad \tau < \frac{x}{\mathrm{X}_1} \qquad (4.52a)$$

and

$$T(x) = T_\mathrm{w} - (T_\mathrm{w} - T_\mathrm{R})\, e^{-t_{R_0} \frac{\mathrm{X}_2}{\mathrm{X}_1} x} \qquad \text{for} \qquad x < \mathrm{X}_1 \tau. \qquad (4.52b)$$

To initiate the process of estimating the concentration solution, we begin by introducing the indices $0 \le i \le N_x$ for variable x and $0 \le j \le N_\tau$ for variable τ into the equations mentioned above, i.e.

$$T_j = T_\mathrm{w} - (T_\mathrm{w} - T_\mathrm{R})\, e^{-t_{R_0} \mathrm{X}_2 \tau_j} \qquad \text{for} \qquad \tau_j < \frac{x_i}{\mathrm{X}_1}, \qquad (4.53a)$$

and

$$T_i = T_{\text{w}} - (T_{\text{w}} - T_{\text{R}})\, e^{-t_{R_0}\frac{\text{X}_2}{\text{X}_1}x_i} \qquad \text{for} \qquad x_i < \text{X}_1\tau_j. \tag{4.53b}$$

We know that N_x and N_τ are the number of discretization points for x and τ, respectively. We calculated them in the the beginning of this chapter.

As a result, the component's particular Henry constant, following the insights of (4.7), transforms into the following expression after incorporating the indices i and j, i.e.

$$a_n(T_i^j) = a_n(T_{\text{R}})\exp\left[\frac{-\Delta H_{A,n}}{\text{R}}(\frac{1}{T_i^j} - \frac{1}{T_{\text{R}}})\right], \qquad n = 1, 2, 3, ..., N_{\text{c}}. \tag{4.54}$$

This adjustment also transforms the abbreviations given by (4.13) into the indexed form, as follows

$$\text{b}_n(T_i^j) = \frac{1}{1 + Fa_n(T_i^j)}, \qquad \text{d}_n(T_i^j) = \frac{t_{R_0}\text{D}_x}{1 + Fa_n(T_i^j)}\frac{1}{\Delta x}. \tag{4.55}$$

Next, we establish (4.51) to facilitate the computation process. With a slight rearrangement, introducing the indices i and j, and then putting the values of $(T_i^j)_\tau$ and $a_n(T_i^j)_T$ from (4.52a) and (4.54), respectively, equation (4.51) assumes the following form

$$[1 + Fa_n(T_i^j)]c_{n_\tau} + \frac{F\Delta H_{A,n}a_n(T_i^j)t_{R_0}\text{X}_2\,(T_{\text{w}} - T_{\text{R}})\,e^{-t_{R_0}\text{X}_2\tau_j}}{\text{R}(T_i^j)^2}c_n = -c_{n_x} + t_{R_0}\text{D}_xc_{n_{xx}}. \tag{4.56}$$

To capture the concentration update in cell i and time step $j + 1$, we introduce in the above equation the backward difference terms for convection and central difference terms for dispersion, as in (4.11), i.e.

$$\begin{aligned}[1 + Fa_n(T_i^j)]\frac{c_{n,i}^{j+1} - c_{n,i}^j}{\Delta\tau} + \frac{F\Delta H_{A,n}a_n(T)t_{R_0}\text{X}_2\,(T_{\text{w}} - T_{\text{R}})\,e^{-t_{R_0}\text{X}_2\tau_j}}{\text{R}(T_i^j)^2}c_{n,i}^j \\ = -\frac{c_{n,i}^j - c_{n,i-1}^j}{\Delta x} + t_{R_0}\text{D}_x\frac{c_{n,i-1}^j - 2c_{n,i}^j + c_{n,i+1}^j}{\Delta x^2}.\end{aligned} \tag{4.57}$$

Let us define a new abbreviation g_n in the above equation. Given (4.53a) and (4.53b), it has two possible values since there is the term $(T_i^j)_\tau$, i.e.

$$\text{g}_n(T_i^j) = \begin{cases} \frac{F\Delta H_{A,n}a_n(T_i^j)t_{R_0}\text{X}_2(T_{\text{w}}-T_{\text{R}})e^{-t_{R_0}\text{X}_2\tau_j}}{\text{R}(T_i^j)^2(1+Fa_n(T_i^j))}, & \text{for} \quad \tau_j < \frac{x_i}{\text{X}_1}, \\ 0, & \text{for} \quad x_i < \text{X}_1\tau_j \text{ or } \tau_j > \frac{x_i}{\text{X}_1}. \end{cases} \tag{4.58}$$

After rearrangement and introducing the above abbreviations together with those of (4.55), we get

$$c_{n,i}^{j+1} = c_{n,i}^j - \Delta\tau\text{g}_n(T_i^j)c_{n,i}^j - \Delta\tau\text{b}_n(T_i^j)\frac{c_{n,i}^j - c_{n,i-1}^j}{\Delta x} + \Delta\tau\text{d}_n(T_i^j)\frac{c_{n,i-1}^j - 2c_{n,i}^j + c_{n,i+1}^j}{\Delta x}. \tag{4.59}$$

To represent the equation in a simpler form, we use the (4.15), which after further simplification yields

$$\begin{aligned}c_{n,i}^{j+1} = c_{n,i}^j &- \Delta\tau\,\text{g}_n(T_i^j)\,c_{n,i}^j \\ &- \frac{\Delta\tau}{\Delta x}\left[\left\{\text{b}_n(T_i^j)\,c_i^j - \text{d}_n(T_i^j)\,\Delta_+c_i^j\right\} - \left\{\text{b}_n(T_i^j)\,c_{n,i-1}^j - \text{d}_n(T_i^j)\,\Delta_-c_i^j\right\}\right].\end{aligned} \tag{4.60}$$

Hence, using the fluxes defined by (4.17), we get the PDE in the final form as

$$c_{n,i}^{j+1} = c_{n,i}^j - \Delta\tau g_n(T_i^j)c_{n,i}^j - \frac{\Delta\tau}{\Delta x}\left(F_{i+\frac{1}{2}}^c - F_{i-\frac{1}{2}}^c\right). \tag{4.61}$$

The above PDE, like previous model uses an explicit time-stepping scheme. It depends on the function h_n evaluated at T_i^j. The term $-\Delta\tau g_n(T_i^j)c_{n,i}^j$ accounts for any source or sink of the concentration due to the function g_n and the time step $\Delta\tau$.

Stability condition: The computation of the time step in this model follows a slightly different approach than in the previous section because of the additional term $g_{max}(T)=\max\left(-\Delta\tau g_n(T_i^j)c_{n,i}^j\right)$. Given (4.60), (4.24) will take the form

$$0 \le (1 - \Delta\tau g_{max}(T)) - \frac{\Delta\tau}{\Delta x}\left(b_{max}(T) + 2d_{max}(T)\right), \tag{4.62}$$

$$\frac{\Delta\tau}{\Delta x}d_{max}(T), \frac{\Delta\tau}{\Delta x}\left(b_{max}(T) + d_{max}(T)\right) \le 1.$$

where $b_{max}(T)$ and $d_{max}(T)$ are the convection and dispersion coefficients with maximum values at different temperatures given by (4.20).

$$(1 - \Delta\tau g_{max}(T)) - \frac{\Delta\tau}{\Delta x}\left(b_{max}(T) + 2d_{max}(T)\right) \ge 0. \tag{4.63}$$

The above inequality can also be written as

$$\Delta\tau g_{max}(T) + \frac{\Delta\tau}{\Delta x}\left(b_{max}(T) + 2d_{max}(T)\right) \le 1$$

or

$$\Delta\tau \le \frac{\Delta x}{\Delta x g_{max}(T) + b_{max}(T) + 2d_{max}(T)}. \tag{4.64}$$

This produced a slightly smaller time step than in (4.26), since $g_n(T) \ge 0$ yields $g_{max}(T) > 0$.

Coding in MATLAB (R2017a):   We know for the single-component injection tests, the temperature profile has just one significant change. That is why, in MATLAB code, we provide the value of T_w in (4.53a) simply as follows

$$T_w = \begin{cases} T_R & \text{for} \quad 0 \le x \le x_m, \\ T_k & \text{for} \quad x_m < x \le x_{max}, \end{cases} \tag{4.65}$$

where, $T_k = \{T_R, T_H, T_L\}$. However, when we inject ternary mixture multiple times for productivity calculations, the temperature profile becomes more complex with multiple temperature changes. To find the concentration solutions in this case in MATLAB, we need to assign different values to T_w at each switching time. In segment I, it always stays at T_R, but in segment II, it is given as follows

$$T_w = \begin{cases} T_R & \text{for} \quad 0 \le x \le x_m, & \tau \in [0, \tau_{n,max}^P], \\ T_k & \text{for} \quad x_m < x \le x_{max}, & \tau \in [\tau_k, \tau_{k+1}[, \\ T_{k+1} & \text{for} \quad x_m < x \le x_{max}, & \tau \in [\tau_{k+1}, \tau_{k+2}[, \\ & & k \in \mathbb{N}_0, \tau_k < \tau_{n,max}^P. \end{cases} \tag{4.66}$$

We use the value of T_{w} from the above function in 4.53a to calculate the temperature profile of the column. However, this is not so simple. The reason is that at each switching at τ_k, the temperature stops at a certain value, say $T_{\mathrm{S}}(\tau_k)$, and from there it starts moving in a different direction till another switch at τ_{k+1}. The code needs this value of $T_{\mathrm{S}}(\tau_k)$ as a reference value to calculate the temperature profile. We use the same 4.52a to calculate $T_{\mathrm{S}}(\tau_k)$ for each switching time τ_k. If we replace T_{R} by $T_{\mathrm{S}}(\tau_k)$, τ_j by τ_k in the mentioned equation, the corresponding temperature value $T(\tau_k)$ is given as

$$T(\tau_k) = T_{\mathrm{w}} - (T_{\mathrm{w}} - T_{\mathrm{S}}(\tau_k))\, e^{-t_{R_0}\mathrm{X}_2\tau_k}. \tag{4.67}$$

After few easy steps of simplification, we get the expression for $T_{\mathrm{S}}(\tau_k)$ as

$$T_{\mathrm{S}}(\tau_k) = T_{\mathrm{w}} - (T_{\mathrm{w}} - T(\tau_k))\, e^{t_{R_0}\mathrm{X}_2\tau_k}. \tag{4.68}$$

To calculate the value of $T_{\mathrm{S}}(\tau_k)$ from the above formula, we manually enter the values of $T(\tau_k)$ and τ_k in the code. Then we replace the term T_{R} in the analytical solution 4.53a with $T_{\mathrm{S}}(\tau_k)$ to calculate the actual temperature profile of the segment II for the whole time τ, which is obtained as follows

$$T_j = T_{\mathrm{w}} - (T_{\mathrm{w}} - T_{\mathrm{S}}(\tau_k))\, e^{-t_{R_0}\mathrm{X}_2\tau_j} \qquad \text{for} \qquad \tau_j < \frac{x_i}{\mathrm{X}_1}, \tag{4.69}$$

where $T_{\mathrm{S}}(\tau_k)$ is given by (4.68). In our code, we calculate the switching times τ_k, as mentioned earlier, by monitoring the retention times of particular concentrations. Whenever the concentration at x_{m} and x_{max} reaches a certain threshold of 10^{-2}, we consider it significant and record the corresponding times. Since we plan to address only the optimal design concept using this model, all the switching, cycle, and injection times are calculated as in the previous model, given by equations (4.40), (4.48), and (4.50), respectively.

The outcomes of this model have been elaborated upon in Chapter 5, within Sections 5.2.2 and 5.3.2.

4.3 EDM Coupled with Energy Equation

In this section, we compute solution to the detailed and final model presented in Section 2.2. This advanced model, which incorporates the EDM of the concentration along with the detailed energy equation, describes an advancement in the induced temperature profile. In particular, it addresses not only the effects of external temperature gradients on the propagation of concentration fronts, but also the resulting heat exchange within the column.

Let us discretize the system by again using the explicit finite volume method. As with the previous models, we are dealing with a forward difference in time, the backward difference for the convection terms, and the central difference of order two in the dispersion terms of (2.21), i.e.

$$\begin{bmatrix} 1 + Fa(T_i^j) & c_i^j Fa(T_i^j)_T \\ \mathrm{G}Fa(T_i^j) & 1 + c_i^j \mathrm{G}Fa(T_i^j)_T \end{bmatrix} \begin{bmatrix} \frac{c_i^{j+1} - c_i^j}{\Delta\tau} \\ \frac{T_i^{j+1} - T_i^j}{\Delta\tau} \end{bmatrix} = \\ - \begin{bmatrix} \frac{c_i^j - c_{i-1}^j}{\Delta x} \\ \mathrm{X}_1 \frac{T_i^j - T_{i-1}^j}{\Delta x} \end{bmatrix} + \begin{bmatrix} t_{R_0}\mathrm{D}_x \frac{c_{i-1}^j - 2c_i^j + c_{i+1}^j}{\Delta x^2} \\ t_{R_0}\mathrm{X}_3 \frac{T_{i-1}^j - 2T_i^j + T_{i+1}^j}{\Delta x^2} \end{bmatrix} + \begin{bmatrix} 0 \\ t_{R_0}\mathrm{X}_2(T_{\mathrm{w}} - T_i^j) \end{bmatrix}. \tag{4.70}$$

Since, $\mathbf{J}$ is non-singular, so $\mathbf{J}^{-1}$ exists and we calculate it as

$$\mathbf{J}^{-1} = \frac{1}{\lambda_2} \begin{bmatrix} 1 + c_i^j \mathrm{G}Fa(T_i^j)_T & -c_i^j Fa(T_i^j)_T \\ -\mathrm{G}Fa(T_i^j) & 1 + Fa(T_i^j) \end{bmatrix}. \tag{4.71}$$

In view of (4.71), (4.70) becomes

$$\begin{bmatrix} c_i^{j+1} \\ T_i^{j+1} \end{bmatrix} = \begin{bmatrix} c_i^j \\ T_i^j \end{bmatrix} - \frac{\Delta\tau}{\lambda_2} \begin{bmatrix} 1 + c_i^j \mathrm{G}Fa(T_i^j)_T & -c_i^j Fa(T_i^j)_T \\ -\mathrm{G}Fa(T_i^j) & 1 + Fa(T_i^j) \end{bmatrix}$$
$$\left(\begin{bmatrix} \frac{c_i^j - c_{i-1}^j}{\Delta x} - t_{R_0}\mathrm{D}_x \frac{c_{i-1}^j - 2c_i^j + c_{i+1}^j}{\Delta x^2} \\ \mathrm{X}_1 \frac{T_i^j - T_{i-1}^j}{\Delta x} - t_{R_0}\mathrm{X}_3 \frac{T_{i-1}^j - 2T_i^j + T_{i+1}^j}{\Delta x^2} \end{bmatrix} - \begin{bmatrix} 0 \\ t_{R_0}\mathrm{X}_2(T_\mathrm{w} - T_i^j) \end{bmatrix} \right). \tag{4.72}$$

For simplicity, let us substitute some combinations of constant values as

$$\mathrm{D}_1 = \frac{t_{R_0}\mathrm{D}_x}{\Delta x}, \qquad \mathrm{D}_2 = \frac{t_{R_0}\mathrm{X}_3}{\Delta x} \qquad \text{and} \qquad s = t_{R_0}\mathrm{X}_2\Delta\tau \tag{4.73}$$

and differences as

$$\Delta_{\pm} c_i^j = \pm \left(c_{i\pm 1}^j - c_i^j \right), \tag{4.74a}$$

$$\Delta_{\pm} T_i^j = \pm \left(T_{i\pm 1}^j - T_i^j \right). \tag{4.74b}$$

After introducing the above terms in (4.72) a small rearrangement gives

$$\begin{bmatrix} c_i^{j+1} \\ T_i^{j+1} \end{bmatrix} = \begin{bmatrix} c_i^j \\ T_i^j \end{bmatrix} - \frac{1}{\lambda_2} \begin{bmatrix} 1 + c_i^j \mathrm{G}Fa(T_i^j)_T & -c_i^j Fa(T_i^j)_T \\ -\mathrm{G}Fa(T_i^j) & 1 + Fa(T_i^j) \end{bmatrix}$$
$$\left(\frac{\Delta\tau}{\Delta x} \begin{bmatrix} \left\{ c_i^j - \mathrm{D}_1\Delta_+ c_i^j \right\} - \left\{ c_{i-1}^j - \mathrm{D}_1\Delta_- c_i^j \right\} \\ \left\{ \mathrm{X}_1 T_i^j - \mathrm{D}_2\Delta_+ T_i^j \right\} - \left\{ \mathrm{X}_1 T_{i-1}^j - \mathrm{D}_2\Delta_- T_i^j \right\} \end{bmatrix} - \begin{bmatrix} 0 \\ s(T_\mathrm{w} - T_i^j) \end{bmatrix} \right). \tag{4.75}$$

Let $\mathrm{F}_{i+\frac{1}{2}}^c$ and $\mathrm{F}_{i-\frac{1}{2}}^c$ be right and left fluxes of concentration and $\mathrm{F}_{i+\frac{1}{2}}^T$ and $\mathrm{F}_{i-\frac{1}{2}}^T$ of temperature, respectively, such that

$$\mathrm{F}_{i+\frac{1}{2}}^c = c_i^j - \mathrm{D}_1\Delta_+ c_i^j, \qquad \mathrm{F}_{i-\frac{1}{2}}^c = c_{i-1}^j - \mathrm{D}_1\Delta_- c_i^j,$$
$$\mathrm{F}_{i+\frac{1}{2}}^T = \mathrm{X}_1 T_i^j - \mathrm{D}_2\Delta_+ T_i^j, \qquad \mathrm{F}_{i-\frac{1}{2}}^T = \mathrm{X}_1 T_{i-1}^j - \mathrm{D}_2\Delta_- T_i^j. \tag{4.76}$$

After introducing above fluxes in (4.75), we get

$$\begin{bmatrix} c_i^{j+1} \\ T_i^{j+1} \end{bmatrix} = \begin{bmatrix} c_i^j \\ T_i^j \end{bmatrix} - \frac{1}{\lambda_2} \begin{bmatrix} 1 + c_i^j \mathrm{G}Fa(T_i^j)_T & -c_i^j Fa(T_i^j)_T \\ -\mathrm{G}Fa(T_i^j) & 1 + Fa(T_i^j) \end{bmatrix}$$
$$\left(\frac{\Delta\tau}{\Delta x} \begin{bmatrix} \mathrm{F}_{i+\frac{1}{2}}^c - \mathrm{F}_{i-\frac{1}{2}}^c \\ \mathrm{F}_{i+\frac{1}{2}}^T - \mathrm{F}_{i-\frac{1}{2}}^T \end{bmatrix} - \begin{bmatrix} 0 \\ s(T_\mathrm{w} - T_i^j) \end{bmatrix} \right). \tag{4.77}$$

Stability condition: In this model, in addition to the mass balance, the energy equation is used to determine the time step $\Delta\tau$. This is due not only to the coupling between the two equations, but also to their simultaneous discretization. This results in two time step values, and we select the smallest among them for further computations.

Ignoring the Jacobian matrix in (4.75), the condition (4.22) for the mass balance can be written as

$$\bar{c}_i^{j+1} = \left(1 - \left(\frac{\Delta\tau}{\Delta x} + 2\frac{\Delta\tau}{\Delta x}\mathrm{D}_1\right)\right)c_i^j + \frac{\Delta\tau}{\Delta x}\mathrm{D}_1 c_{i+1}^j + \left(\frac{\Delta\tau}{\Delta x} + \frac{\Delta\tau}{\Delta x}\mathrm{D}_1\right)c_{i-1}^j \geq 0.$$

which implies

$$0 \leq 1 - \left(\frac{\Delta\tau}{\Delta x} + 2\frac{\Delta\tau}{\Delta x}\mathrm{D}_1\right), \frac{\Delta\tau}{\Delta x}\mathrm{D}_1, \frac{\Delta\tau}{\Delta x} + \frac{\Delta\tau}{\Delta x}\mathrm{D}_1 \leq 1$$

or

$$1 - \left(\frac{\Delta\tau}{\Delta x} + 2\frac{\Delta\tau}{\Delta x}\mathrm{D}_1\right) \geq 0. \tag{4.78}$$

After using the value of D_1 from (4.73), the above inequality gives

$$\left(\frac{\Delta\tau}{\Delta x} + 2t_{R_0}\mathrm{D}_x\frac{\Delta\tau}{\Delta x^2}\right) \leq 1$$

or

$$\Delta\tau \leq \frac{\Delta x^2}{\Delta x + 2t_{R_0}\mathrm{D}_x}. \tag{4.79}$$

Similarly, from (4.75), we also can write the condition for temperature as

$$\bar{T}_i^{j+1} = \left(1 - \left(\frac{\Delta\tau}{\Delta x}\mathrm{X}_1 + 2\frac{\Delta\tau}{\Delta x}\mathrm{D}_2 + s\right)\right)T_i^j + \frac{\Delta\tau}{\Delta x}\mathrm{D}_2 T_{i+1}^j + \left(\frac{\Delta\tau}{\Delta x}\mathrm{X}_1 + \frac{\Delta\tau}{\Delta x}\mathrm{D}_2\right)T_{i-1}^j + sT_w \geq 0,$$

which implies

$$0 \leq 1 - \left(\frac{\Delta\tau}{\Delta x}\mathrm{X}_1 + 2\frac{\Delta\tau}{\Delta x}\mathrm{D}_2 + s\right), \frac{\Delta\tau}{\Delta x}\mathrm{D}_2, \frac{\Delta\tau}{\Delta x}\mathrm{X}_1 + \frac{\Delta\tau}{\Delta x}\mathrm{D}_2, sT_w \leq 1$$

or

$$1 - \left(\frac{\Delta\tau}{\Delta x}\mathrm{X}_1 + 2\frac{\Delta\tau}{\Delta x}\mathrm{D}_2 + s\right) \geq 0. \tag{4.80}$$

Hence, again using abbreviations (4.73) in above inequality, we get

$$\left(\frac{\mathrm{X}_1}{\Delta x} + 2t_{R_0}\frac{\mathrm{X}_3}{\Delta x^2} + t_{R_0}\mathrm{X}_2\right)\Delta\tau \leq 1$$

or

$$\Delta\tau \leq \frac{\Delta x^2}{\mathrm{X}_1\Delta x + 2t_{R_0}\mathrm{X}_3 + \Delta x^2 t_{R_0}\mathrm{X}_2}. \tag{4.81}$$

So, both the concentration and energy (temperature) equations have demanded different time step restrictions. It means that we will have to use the smallest among them, i.e.

$$\Delta\tau = \min\left(\frac{\Delta x^2}{\Delta x + 2t_{R_0}\mathrm{D}_x}, \frac{\Delta x^2}{\mathrm{X}_1\Delta x + 2t_{R_0}\mathrm{X}_3 + \Delta x^2 t_{R_0}\mathrm{X}_2}\right) \tag{4.82}$$

and in dimensionlized form, $\Delta t = t_{R_0}\Delta\tau$.

Coding in MATLAB (R2017a): In this model, as discussed in section 4.2, we control the solution in a similar way by setting the target temperature to T_w. This process is even easier to handle if we only consider (4.65) for single-component injections and (4.66) for ternary mixture injections. The additional calculations we performed in the previous section are only due to the adjustment of the analytical solution of temperature to the numerical solution of concentration. No such manual adjustments are required for this model. However, all the switching, cycle, and injection times are calculated here as well using the same equations (4.40), (4.48), and (4.50) as in the previous model.

The outcomes of this model are explained in Chapter 5, Sections 5.2.3 and 5.3.3.

Summery of the Chapter 4: In this chapter, we have estimated the numerical solutions of the Equilibrium Dispersive Model (EDM) coupled with three different types of temperature profiles. The first profile involved temperature step gradients, whose solutions were estimated using the Finite Volume Method (FVM) independently in each segment of the column. Next, we explored a semi-analytical solution where the numerical solution of the EDM was estimated considering a simplified energy equation, which was solved analytically using the Laplace transform. Finally, we estimated the pure numerical solution of the EDM coupled with a detailed energy equation, which was converted into matrix form. In each case, a specific stability analysis was conducted.

Chapter 5

Computation and Results

In this Chapter we apply the results of the numerical analysis carried out in Chapter 4. The selected analytical results of the equilibrium theory were already presented in Chapter 3. The study includes both single-component and ternary mixture injections and provides a comprehensive overview of the effects of different temperature on the retention behavior.

It is important to highlight that in Chapter 4, we have solved all the models using a non-dimensional time (τ) and a normalized space coordinate (x). However, for presentation purposes, we will now present the results in terms of dimensional time (t) in "minutes" and space (z) in "cm".

First, the results of the single component experiments for cycloheptanone C7 are presented to analyze the retention behavior under two different temperature changes for gradient operations: T_R to T_L and T_R to T_H. These results are then compared to those obtained under isocratic (reference) conditions. This comparison allows us to reveal any shifts or improvements in the concentration pulses due to the application of the implemented gradients. The system with some experimental parameters used for these tests is listed in Table 5.1.

Moving on to a more complex scenario, we present the results when we inject several times the ternary mixture of cycloketones C5, C6 and C7. The additional system parameters for these injections are listed in Table 5.2. We will present the improvements in cycle times and associated productivity obtained by implementing gradient operations compared to isocratic conditions in the models discussed in Chapter 4.

At the end of our study, we will perform a brief comparison between the theoretical predictions and available experimental results. The latter results, as already mentioned, were obtained in a parallel PhD thesis project [39]. Most of the parameters used in this work are taken from this project.

5.1 Parameter Studies

Before discussing the results and outcomes of the numerical calculations, we will explain some of the important parameters from the two given tables, which will help especially the readers who are new to the field to understand the importance of these parameters in HPLC processes, especially when using temperature gradients.

Table 5.1: Parameters used in single-component injections (connected to experimental study), ordered as follows

Symbol	Quantity	Value Used in Simulation
$z_{\max}$	Length of the column	20 cm
A	Cross-sectional area of the column	0.166 cm^2 (diameter d = 0.46 cm)
ϵ	Porosity of the column	0.555
ρ^L	Density of the liquid phase	0.894 g/cm^3
C_p^L	Heat capacity of liquid phase	3.46 J/g.K
ρ^S	Density of the solid phase	2.65 g/cm^3
C_p^S	Heat capacity of solid phase	0.703 J/g.K
T_R	Reference temperature	298.41 K
$a_1(T_R)$	Henry constant of C7 at T_R	2.630
$\Delta\bar{H}_{A,1}$	Adsorption enthalpy of C7	-8.180 kJ/mol
M_1	Molecular weight of C7	112.17 g/mol
$\Delta H_{A,1}$	Specific adsorption enthalpy of C7 $\left(\frac{\Delta\bar{H}_{A,1}}{M_1}\right)$	-0.0729 kJ/g
u	Interstitial velocity	3.26 cm/min
t_{R_0}	Retention time of a non-retained solute for mass and energy balances $[\frac{z_{\max}}{u}, 0.5\frac{z_{\max}}{u}]$	[6.142 3.07] min
N_p	Number of the theoretical plates for half of the column	[2871 (Experimental), 1000, 200]
D_z	Axial dispersions corresponding to N_p, Eq. 5.1	[0.006 (Experimental), 0.02, 0.08]
Δt_{inj}	Injection time	5 min
$c_{1,\mathrm{inj}}$	Feed concentration (as in experiments)	0.956 g/L
T_L	Low temperature	283.8 K
T_H	High temperature	313.15 K
X_1	Eq. 2.15c	[0.13(Experimental), 0.5, 1.0]
X_2	Eq. 2.15d	[0.17(Experimental), 0.5, 10] min^{-1}
X_3	Eq. 2.15e	0.000003
α_w	Heat transfer coefficient through the wall	0.7768 J/min.cm^3.K
t_{dead}	Dead time in single component experiments	3.246 min

Table 5.2: In addition to Table 5.1, these parameters are used for ternary mixture injections

Symbol	Quantity	Value Used in Simulation
Δt_{inj}	Injection time	1.33 min
$[a_1(T_R), a_2(T_R), a_3(T_R)]$	Reference Henry constants of [C5, C6, C7] at T_R	[0.693,1.343,2.630]
$[\Delta\bar{H}_{A,1}, \Delta\bar{H}_{A,2}, \Delta\bar{H}_{A,3}]$	Adsorption enthalpies	[-5.481,-6.674,-8.180] kJ/mol
$[M_1, M_2, M_3]$	Molecular weights of [C5, C6, C7]	[84.12, 98.15, 112.17] g/mol
$[\Delta H_{A,1}, \Delta H_{A,2}, \Delta H_{A,3}]$	Specific adsorption enthalpies $\left(\Delta\bar{H}_{A,n}/M_n, n=1,2,3.\right)$	[-0.0652,-0.0680,-0.0729] kJ/g
$[c_{1,\mathrm{inj}}, c_{2,\mathrm{inj}}, c_{3,\mathrm{inj}}]$	Feed concentrations of above comps.	[0.949, 0.948, 0.956] g/L
$[m_{1,\mathrm{inj}}, m_{2,\mathrm{inj}}, m_{3,\mathrm{inj}}]$ Eq.(2.52)	Masses injected of above comps.	3.8 ×10^{-4} g (each)
T_L	Low temperature	278.95 K
T_H	High temperature	332.51 K
t_{dead}	Dead time in ternary mixture experiments	0.25 min

Number of Theoretical Plates (N_p)**:** Theoretical plate numbers are a quantitative measure of the efficiency of a chromatographic column. A higher N_p indicates better separation efficiency because it suggests that the components of a mixture spend more time interacting with the stationary phase and thus have more opportunities to separate.

In our PDEs, we need to specify the value of the axial dispersion D_z. This value is calculated from the number of theoretical plates N_p. The value of N_p for one of the two segments is obtained from the experiments. Thus, the value of D_z is calculated as follows

$$D_z = \frac{u z_{\mathrm{m}}}{2 N_p}. \tag{5.1}$$

Note that for simplicity, the axial dispersion coefficient in the energy equation λ_z is calculated with the same formula, so that $\lambda_z = D_z$.

Henry Constants: In liquid chromatography, Henry's constant is essential for understanding solute partitioning behavior between the liquid mobile phase and the solid or liquid stationary phase. It influences elution times, resolution and selectivity of the separation.

In this work, we use reference Henry constants at reference temperature of cyclo-ketones $(C5, C6, C7)$ estimated in the experimental project mentioned at the beginning. Based on these reference Henry constants, we estimate temperature-dependent Henry constants using Eq. 2.4.

Enthalpy of Adsorption: The enthalpy of adsorption (ΔH_A) is a critical concept in chromatography. It represents the heat energy associated with the adsorption of molecules onto a solid surface, such as a chromatographic column's stationary phase. This phenomenon is crucial because it helps us understand how strongly or weakly solutes are retained by the stationary phase in chromatographic separations.

The enthalpy of adsorption, along with Henry's constant, is a fundamental concept in chromatography that governs the choice of conditions, columns, and temperature control to achieve accurate and efficient separations in analytical chemistry.

The values of adsorption enthalpies associated with the tested components are obtained directly from the experiments. These values act as measurable outcomes that we track during our experimental activity.

Densities and Heat Capacities: In liquid chromatography, knowledge of the densities and heat capacities of the liquid and mobile phases is essential. The following explains why they are so important:

- **Density of mobile phase** (ρ^L)**:** Knowing the density of the mobile phase is critical. It helps us understand how densely packed or distributed the molecules are. Denser mobile phases can affect separation efficiency because they interact differently with the stationary phase.

- **Density of stationary phase** (ρ^S)**:** The density of the stationary phase is equally important. It affects how well the sample adheres to the column. Different compounds may "stick" differently depending on the density of the stationary phase.

- **Heat capacity of mobile phase** (C_p^L)**:** The heat capacity of the mobile phase indicates how much heat energy it can absorb or release. This is important because temperature changes occur frequently during chromatography. Knowing the heat capacity helps control the temperature for optimal separations.

- **Heat capacity of stationary phase** (C_p^S)**:** Similarly, the heat capacity of the stationary phase plays a role in the interaction with the sample. Some compounds require more or less heat to move efficiently through the column.

Segmentation of the Column: In this work, two equal-sized segments of chromatographic columns are considered for the implementation of the so-called segmented temperature gradients. Since only the temperature of segment II is changed while that of segment I is kept constant, we used the segmentation ratio in the energy balance. This means that the value t_{R_0} (see Table 5.1) is multiplied by 0.5 when used in the energy balance. Details of this segmentation can be found in the parallel thesis [39].

Note that along with all the parameters given in the Tables 5.1 and 5.2, the values of N_p, X_1, and X_2 are given in groups of three values each, one of which comes from the experiments, while the other two represent typical values used in the literature. By default, we will use only the experimental values, but in some figures we will show the results for all three values for comparison purposes.

Moreover, in the experiments, the "dead time" was recorded, a short delay during which the measurement system cannot immediately respond to new signals in chromatographic experiments. Dead time is a common feature in chromatography and is critical for data analysis. To match our theoretical results with experiments where dead time was recorded as part of the parallel PhD project, we adjusted all our time-based plots for this "dead time" (t_{dead}).

Now we present the numerical results step by step, starting with the injection of single components and ending with the injections of ternary mixture.

5.2   Results for Single-Component Injections

In this section we will discuss in detail the results of the single-component's injections obtained from all the models solved in Chapter 4. We know that we perform the single-component analysis to better understand the behavior of each component under different temperature regimes, which helps us to plan and select appropriate temperature regimes for the injection of ternary mixtures to increase the productivity of the HPLC columns. We start by showing results of EDM coupled with ideal temperature gradients, and end with results for the same mass balance under more complex temperature regimes (described by a detailed energy equation).

5.2.1   Results of EDM Coupled with Ideal Temperature Step Gradients

In this section, we discuss the results of the model studied in Section 4.1.1. The provided space discretization points N_x are 4000, which is a sufficiently high number to obtain a good resolution of the results. Using the equation (4.26), $\Delta\tau = 0.00041$ is generated, which in dimensional form corresponds to $\Delta t = 0.0025$ min. For a given final simulation time of 50 min, the total number of time discretization points $N_\tau = N_t$ is determined to be 19714.

Figure 5.3a shows chromatograms (or t-plots) illustrating the behavior of the components during both heating and cooling of Type I compared to the isocratic state (see Section 4.1.1 for both Type I and Type II). It can be clearly seen that the retention times differ by more than one minute. Moreover, it was already explained in Chapter 3 that for a Type I temperature change, the mobile phase concentration's peaks remain the same, with the time widths also remaining constant. This serves as the confirmation of mass conservation. Additionally, it proves that the numerical results agree with the theoretical results. The dispersion observed in the pulses arises not only from the prescribed value of $N_p = 2871$ but also from the natural dispersion in the numerical scheme.

Figure 5.3b shows the pulse behavior for the same three implemented temperature regimes, but for Type II. We again see a visible difference in the respective retention times, but as always with the Type II temperature change, both the concentration peaks and the time widths are affected.

To better understand the concentration distribution between phases under different temperature gradients, we analyze the concentration pulses at different times within the column and at different locations versus time t, c.f. Figures 5.4 and 5.5. Within the column, we show the concentrations distribution at three different times t_I, t_{II}, and t_{III}. We remember this plot as z-plot. Recall that in Chapter 3, the z-plots contain four pulses at four selected time points, but here we can plot only three pulses at three different time points due to a broader pulse injection. On the other hand, against time t, we plot the concentration pulses at different positions z_0, z_m and z_{max}, which we call t-plot.

Figures 5.4a and 5.4b are the z-plots in which the concentration of mobile phase c_1 is represented by a dotted line, the concentration of stationary phase q_1 is represented by a solid line, and the total concentration $c_1 + q_1$ is represented by a dashed line. The blue colored pulse at time t_I is plotted when the pulse fully enters the column. The black pulse at time t_{II} is the interesting one, as it clearly shows the transition at the interface. Finally, the pink pulses at time t_{III} are plotted when the adsorption fronts just reach z_{max}. The times t_I and t_{II} are the same for both figures, but t_{III} is different because the pulses reach z_{max} at different times at different temperatures. With this type of temperature change, the concentration peak of the mobile phase remains constant, but the concentration of the stationary phase and the pulse indicating the total concentration vary. Recall that the reasons for these changes in the concentration peaks and their respective widths are explained in detail in Chapter 3 (equilibrium theory). Here we present the results very briefly for comparison purposes.

Figures 5.4c and 5.4d are the corresponding t-plots or chromatograms which shows c_1 at different locations z_0, z_m and z_{max}.

Figure 5.5 shows the results for the same trend of temperature changes, but of Type II. For this type of temperature change, the concentration in mobile and stationary phases varies, but the peaks representing the total concentration remain constant.

Figure 5.6 analyzes the effect of different N_p on the dispersion tendency of the concentration c_1. As expected, the pulse is dispersed to a large extent for small N_p. This raises the concern of increasing the cycle time in experiments with ternary mixtures, which reduces productivity. For the extremely large value, i.e. $N_p = \infty$, the results reduce almost to equilibrium theory. The little dispersion in this case is due to the numerical scheme's inherent dispersion. The numerical dispersion, while minimal, results in a slightly longer cycle time for EDM compared to EM and highlights the effects of numerical approximations. Numerical solutions can lead to numerical dispersion as the model becomes more detailed and the way the calculations are performed. For

this reason, there may be scatter in the upcoming results where $N_p = \infty$ (dispersion coefficient of zero) is used. The results given are demonstrated for the Type II of temperature change. Other types of cooling and heating show a similar trend.
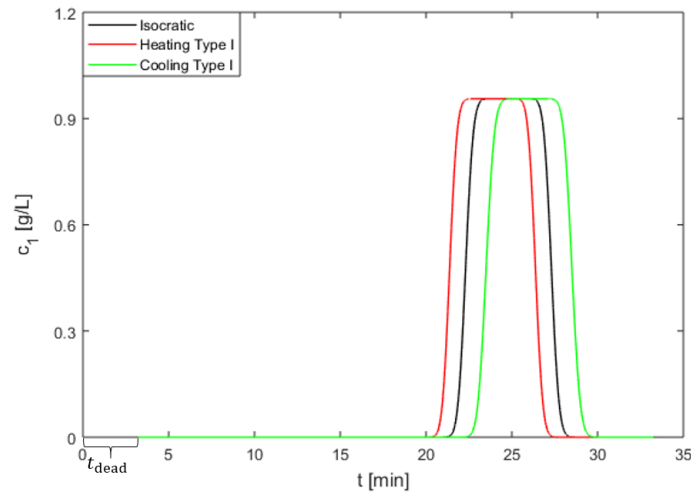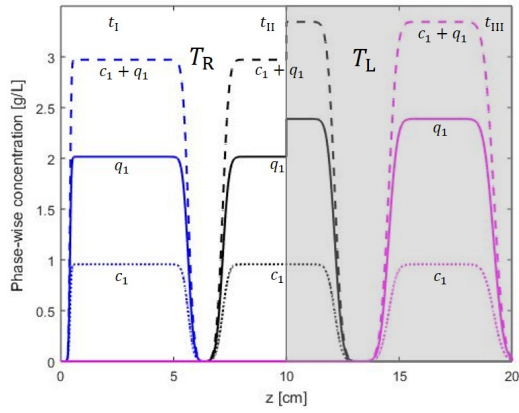

a Type I: When both the segments are kept all the time at different temperatures.
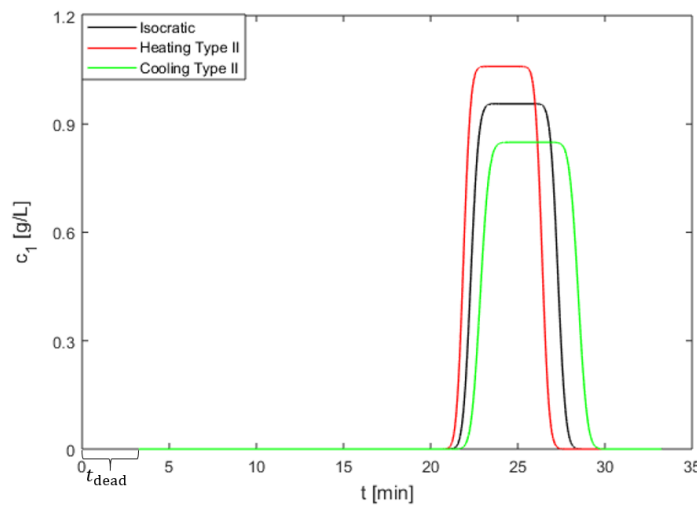
b Type II: When both the segments are at the same temperature initially. Then the temperature in segment II is changed at $t_s = 18$ min.
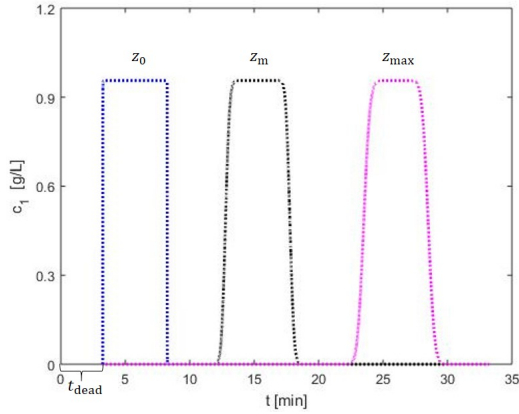
Figure 5.3: Illustration of the single-component results of Type I and Type II plotted at $z = z_{\max}$.

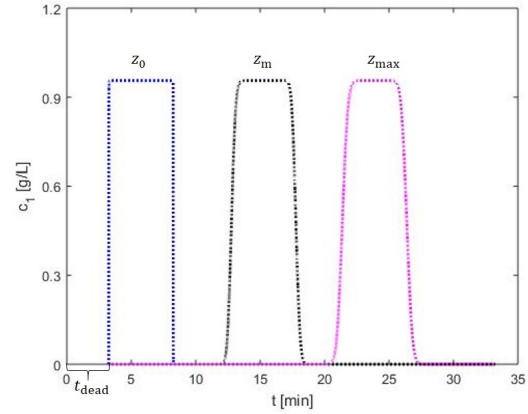a z-plot of cooling: $t_\mathrm{I} = \Delta t_\mathrm{inj}$=5 min, t_II=12 min, and t_III=19.3 min. Dead time must be added to all these times for correct correspondence to the figures.
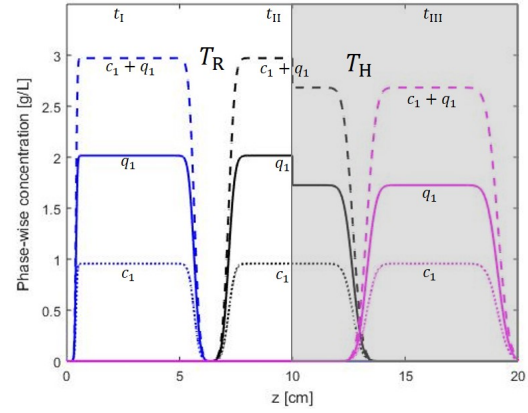
b z-plot of heating: t_III=17.4 min.
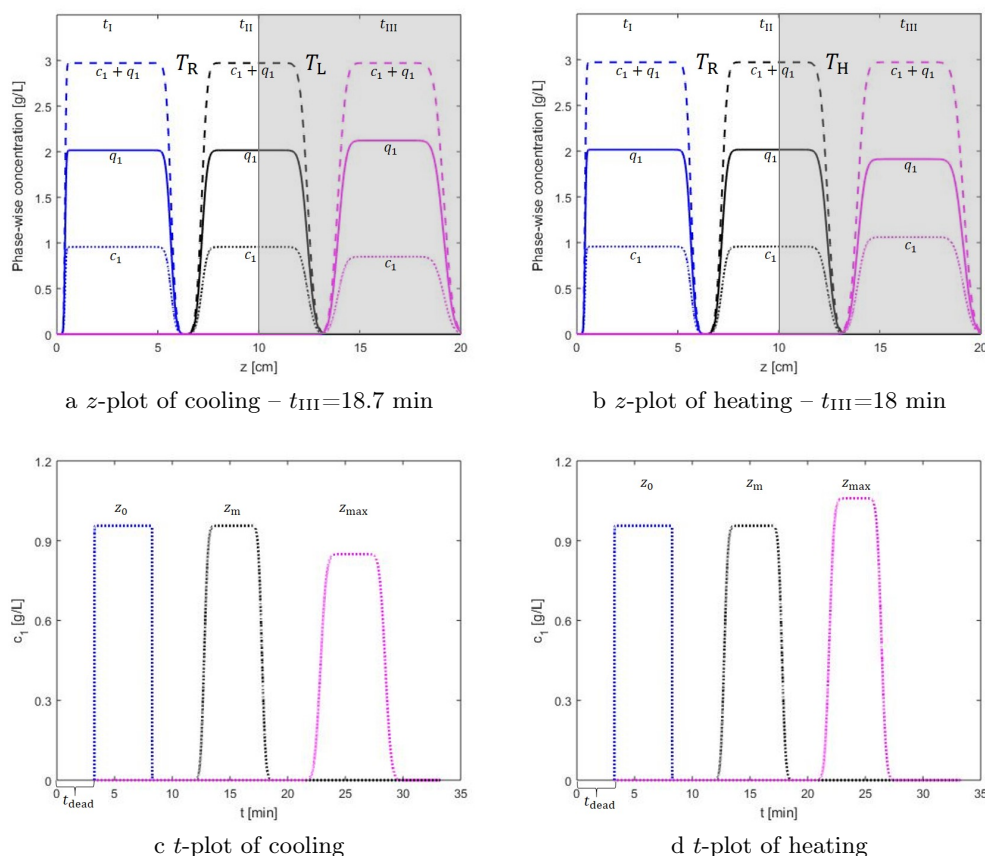
c t-plot of cooling

d t-plot of heating

Figure 5.4: Concentration behavior in both mobile and stationary phases at different times within the column (a and b) and at different locations against time (c and d) under temperature changes of Type I. Left side: T_R to T_L, Right side: T_R to T_H.

a z-plot of cooling – t_{III}=18.7 min

b z-plot of heating – t_{III}=18 min

c t-plot of cooling

d t-plot of heating

Figure 5.5: Concentration behavior in both mobile and stationary phases at different times within the column (a and b) and at different locations against time (c and d) under temperature changes of Type II. Left side: T_{R} to T_{L}, Right side: T_{R} to T_{H}.
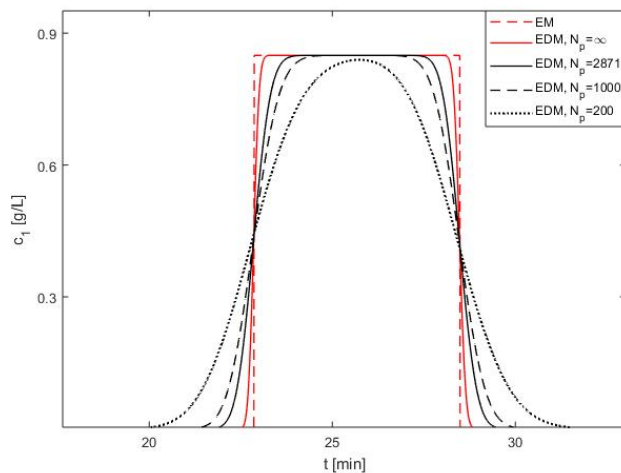

Figure 5.6: Illustration of the effect of the theoretical plate number N_p over the dispersion of the pulses for cooling of Type II. The result of EM is also provided.

5.2.2 Results of EDM Coupled with the Simplified Energy Equation

Now we present the semi-analytical results of the model discussed in Section 4.2. The provided space discretization points N_x are 4000 giving $\Delta x = 0.00025$. Using the equation (4.64), $\Delta \tau = 0.00041$ was generated, which in dimensional form corresponds to $\Delta t = 0.0025$ min. For a given dimensionless simulation time of 10 (61 min in dimensional form), the number of time discretization points in this model $N_\tau = N_t$ is determined to be 24199.

Figure 5.7 is again a plot of single-component tests, but this time we see that the temperature changes slowly instead of jumping stepwise. We have fixed the value of X_1 at 0.13 and vary the value of X_2. The curves in the figure that show different temperatures of segment II are associated with the right axis, while the concentration pulses are associated with the left axis.

The value of X_2 plays a crucial role in determining the rate of temperature change. For the smaller value of X_2 (taken from experiments), a slow temperature change is recorded, causing lesser effect over the propagation of the fronts. The concentration pulse leaves the column before the temperature reaches the wall temperature T_w. On the other hand, higher values of X_2 (chosen from the literature) show a faster impact. Its highest possible value leads to a temperature jump, so that the resulting concentration sees the full wall temperature and the results of temperature and concentration are reduced to those of EDM under ideal step temperature gradients, c.f. Figure 5.3a.

This observation suggests that X_2 plays an important role in influencing the retention behavior by affecting the spacing between concentration pulses during cooling and heating processes.
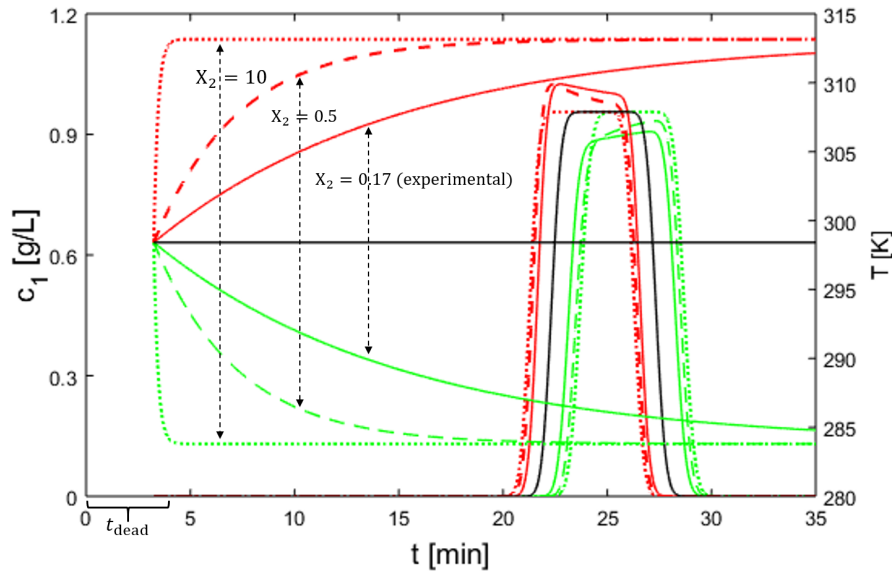

Figure 5.7: The impact of keeping $X_1 = 0.13$ fixed and varying X_2 on the rate of temperature change consequently affecting the retention time of concentration c_1. The red color represents heating, the green color represents cooling, and the black color represents isocratic conditions. Whereas, each concentration and its associated temperature are indicated by a same line that is either solid, dashed or dotted.
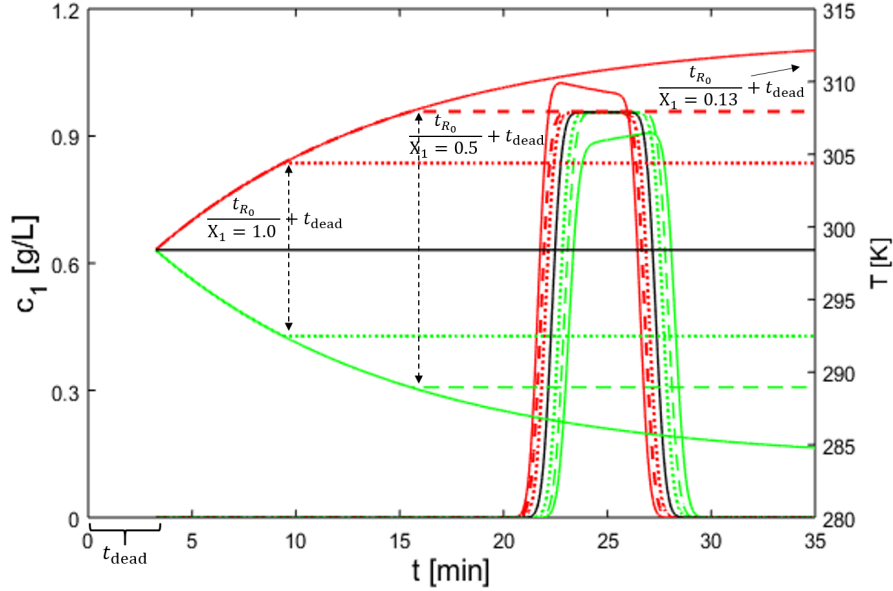
Figure 5.8: The impact of keeping $X_2 = 0.17$ fixed and varying X_1 on the rate of temperature change consequently affecting the retention time of concentration c_1. Colors selection for different conditions are like in the previous Figure.

In Figure 5.8, we fix the value of X_2 to 0.17 and vary the value of X_1, showing an interesting effect on the behavior of the temperature curve. Notably, with each given value of X_1, the temperature curve maintains a consistent temperature level after the time $\frac{1}{X_1}$. The factor t_{R_0} is multiplied to obtain its dimensioned value compatible with the t-axis. For both values 0.5 and 1.0 of X_1, the temperature becomes a straight line without reaching the actual implemented temperature T_{w}. Therefore, the pulse does not pass through the actual temperature regime and have a smaller effect on their velocity. For the lower value of 0.13, we have $\frac{t_{R_0}}{X_1}$=51 min, which is the time before which the temperature has already reached T_{w}, giving the maximum change in concentration velocity. All colors and line styles are consistent with those employed in Figure 5.7.

This observation suggests that X_1 also plays a role, albeit in a different way, in influencing retention behavior by altering the spacing between concentration pulses during cooling and heating processes.

5.2.3   Results of EDM Coupled with Detailed Energy Equation

In this section, we will present the results of the single-component experiments using the solution of the model discussed in Section 4.3. The provided space discretization points N_x are 2000 which generates $\Delta x = 0.0005$. Using the equation (4.82), $\Delta \tau = 0.00037$ was generated, which in dimensional form corresponds to $\Delta t = 0.0022$ min. For a dimensionless simulation time of 10 (about 61 min.), the number of time discretization points in this model $N_\tau = N_t$ is determined to be 26966.

Comparing this model with the previous one, it's noticeable that the energy equation coupled with the EDM incorporates a significant term $G_n q_n(T)$, where G_n and $q_n(T)$ are given by

equations (2.15b) and (2.5). This term plays a crucial role in accounting for the heat exchange phenomena during the adsorption and desorption processes. The energy equation also accounts for the effects of axial dispersion on heat conduction. For simplicity we have taken $\lambda_z = D_z$.

In Figure 5.9, we present the results of the scenario where X_1 remains constant while X_2 is subjected to variation. In order to provide a clearer representation due to the complexity of the temperature curve, we have divided the results into Sub-figures for different values of X_2. The figures use the same colors and line styles for the corresponding temperatures as in Figure 5.8.

The results under isocratic conditions are colored black in the first Sub-figure. The first two Sub-figures clearly show a wave type in the temperature curve above the adsorption and desorption fronts of the concentration. This wave proves exothermic and endothermic processes during adsorption and desorption, respectively. In contrast to the results of the previous model, we observe a stronger concentration tendency to the right edge of the peak. This phenomenon is due to the fact that the temperature, which changes during adsorption/desorption, affect the concentration in the later course. Another fact is that the more we increase the value of X_2, the smoother the exothermic/endothermic wave in the temperature curve becomes, which is clear in the last Sub-figure.

Moreover, the variation of X_2, in terms of retention times, shows a similar trend as in Figure 5.7.

In Figure 5.10, we illustrate, like in Figure 5.8 the influence of keeping X_2 fixed and considering X_1 to be 0.5 and 1.0. For $X_1 = 0.17$, it is already shown in Figure 5.9, on the top.

For $X_1 = 0.5$ we see that the temperature becomes constant after the time $\frac{t_{R_0}}{0.5} + t_{\text{dead}}$ min to about 304 K. This time the adsorption/desorption wave occurs earlier and with larger amplitude. This wave disturbs the straight line that is fixed at 304 K. This causes the pulses to be earlier and more concentrated at the left edge.

For $X_1 = 1.0$, the temperatures become constant early enough that they have little effect on the elution, and it can be seen that the pulses are closer together for both heating and cooling. In addition, the amplitude of the exothermic/endothermic wave becomes smaller so that the peak of the concentration pulse is smooth.

It is evident that variations of the parameter X_2 affect the exothermic and endothermic processes during adsorption and desorption, with higher values of X_2 leading to smoother-like temperature curves. In addition, changing the parameter X_1 has a pronounced effect on the timing of heat exchange, concentration distribution as well as the spacing between pulses.
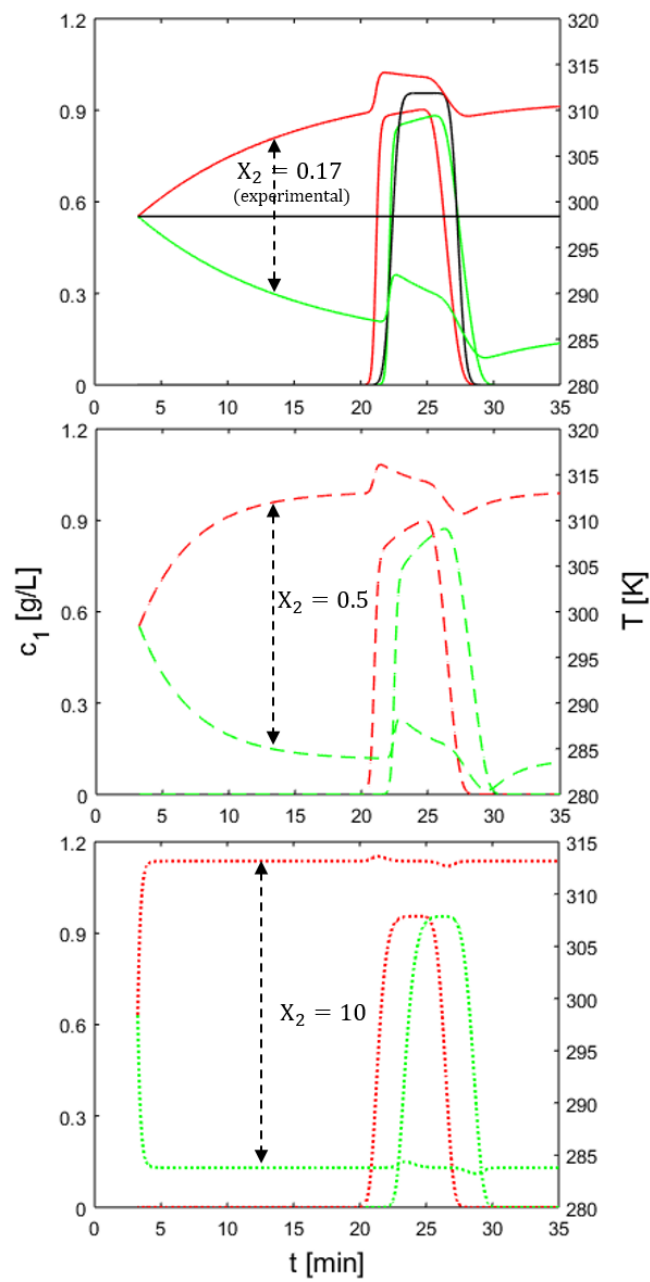
Figure 5.9: The impact of keeping $X_1 = 0.13$ fixed and varying X_2 on the rate of temperature change consequently affecting the retention time of concentration c_1.
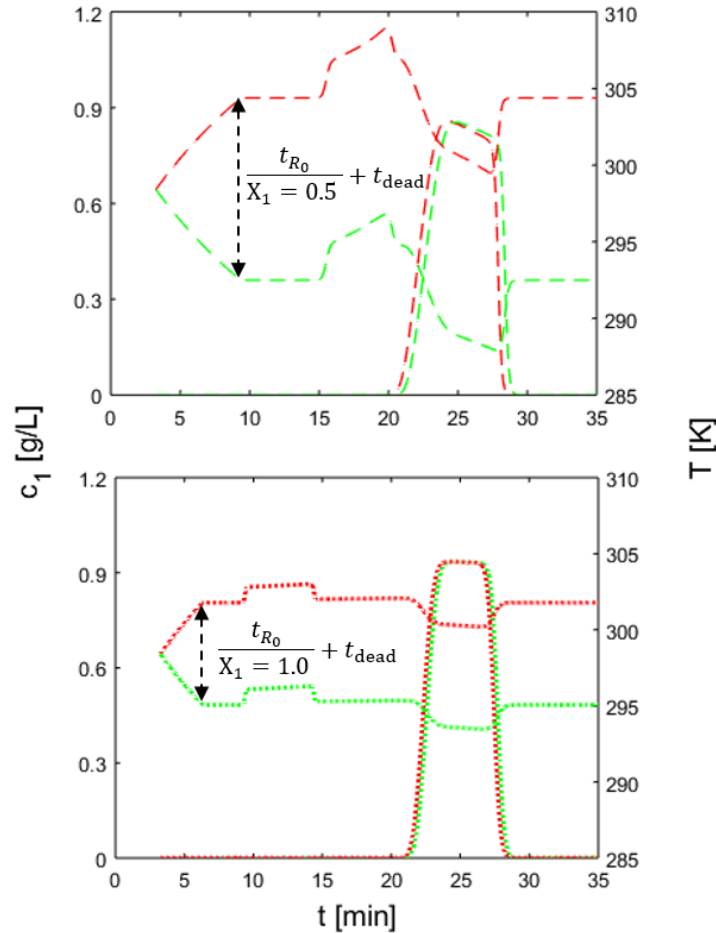
Figure 5.10: The impact of keeping $X_2 = 0.17$ fixed and varying X_1 on the rate of temperature change consequently affecting the retention time of concentration c_1.

Comparison for the Single-Component Injections by All the Models: At the end of the presentation of the interesting single-component results, we would like to make a brief comparison of the results of all three models to see the relationship between them and how the introduction of the new parameters into the models affects the results.

Figure 5.11a shows the agreement of the results of Type I temperature change in the EDM coupled with the ideal step gradients (SG) with the results of the EDM coupled with the simplified energy equation (SEE) and the coupling with the detailed energy equation (EE). The latter two models give similar results for $X_1 = 0.13$, as suggested by experiment, and $X_2 = 10$, which happens to be chosen high. At this value of X_2, the temperature profiles of our last two models take the form of near-ideal step gradients, showing similar retention behavior to the EDM at SG. We see that we have less dispersion in the EDM at SG than in the last two models, with the EDM at EE having the largest dispersion.

On the other hand, 5.11b compares the results of the above models for a different type of temperature change. When the EDM coupled with SG operates under temperature change

of Type II, the results agree with those of the last two models for $X_1 = 0.13$ and $X_2 = 0.17$.
These both values are now from the experiments. This means that this type of temperature
change is closer to the reality. The results of EDM coupling EE are more dispersed compared
to that in Figure 5.11a. Therefore, the concentration peaks are close to each other in both
heating and cooling. The pulse under heating is even less concentrated than under isocratic
conditions. The reason for this scatter is not only the slow temperature change, but also that the
adsorption/desorption process affected the applied temperature and the pulses left the column
before being affected by the fully implemented temperatures. In contrast, the EDM at SEE shows
very good agreement with the EDM at SG.
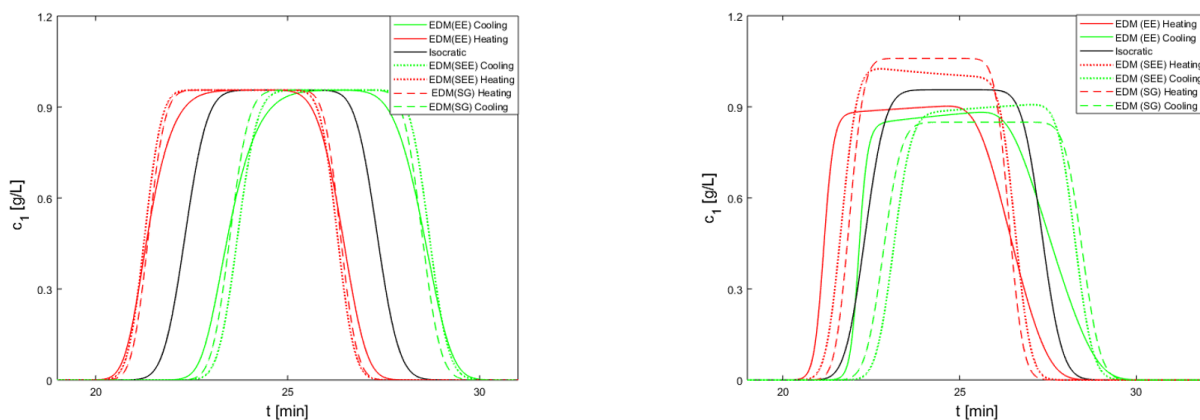
a Comparison of the results of Type I tempera-
ture change by EDM under SG with the results
of EDM under SEE and EE for $X_1 = 0.13$ (exper-
imental) and $X_2 = 10$ (Randomly taken high).

b Comparison of the results of Type II tempera-
ture change by EDM under SG with the results
of EDM under SEE and EE for $X_1 = 0.13$ and
$X_2 = 0.17$ (Both experimental).

Figure 5.11: Comparison of the single-component results by all the three models discussed in
Section 5.2

5.3   Results for Ternary Mixture Injections

As mentioned earlier and as in Chapter 3, we now present the results of the previously discussed
models for the injection of ternary mixtures, i.e. for $N_c = 3$, to see to what extent the numerical
calculations predict the productivity of the column. Recall that we have discussed two scenarios
in the aforementioned chapter, namely "Late Eluter" and "Early Eluter", in order to understand
and present well most of the possible scenarios in the experimental laboratory. Since the concept
was well understood, we have addressed in Chapter 4, the scenario considered in the experiments,
which is not exactly the same as "Late Eluter" one, but a closer one. Because according to the
chosen reference Henry constants given in table 5.2, we have $\alpha_{1,2} \approx \alpha_{2,3}$. Nevertheless, this
scenario could be improved when processed under temperature gradients.

We now start again with the presentation of our results using the simpler model and move
step by step to more detailed models.

5.3.1 Results of EDM Coupled with Ideal Temperature Step Gradients

In this section we present the results of the model for $N_c = 3$ discussed in Sub-section 4.1.2. The provided space discretization points N_x are 2000 and generate $\Delta x = 0.0005$. Using the equation (4.26), $\Delta \tau = 0.0005$ is calculated, which is given in dimensional form as $\Delta t = 0.0032$ min. For the given simulation time of 65 min, the number of time discretization points in this model $N_t = N_\tau$ is set to 19799. Note that different values of N_p result in different time steps and thus different N_t.

Comparison of the Results of EDM With EM: First, we compare the EDM's numerical results under step temperature gradients for $N_p = \infty$ with the equilibrium theory results shown in Figure 5.12. We fit the same parameters given in the Table 5.2 in EM discussed in Chapter 3 and superimpose both results.

In the chromatogram, the rectangular pulses representing the results of EM have a shorter cycle time, reflecting the idealized fast equilibrium between the mobile and stationary phases. In contrast, despite the application of an infinite number of theoretical plates ($D_z = 0$), the EDM results still exhibit numerical dispersion effects. The reason for this dispersion is explained in the text accompanying the Figure 5.6. The resulting dispersion is minimal for the faster eluting components, but increases for the later eluting components. This is because for the latter components, the longer-lasting interaction with the stationary phase also contributes to the dispersion in their pulses.

Recall that we calculate the cycle time using the retention times of c_1 and c_3 while considering a concentration threshold of 0.01.
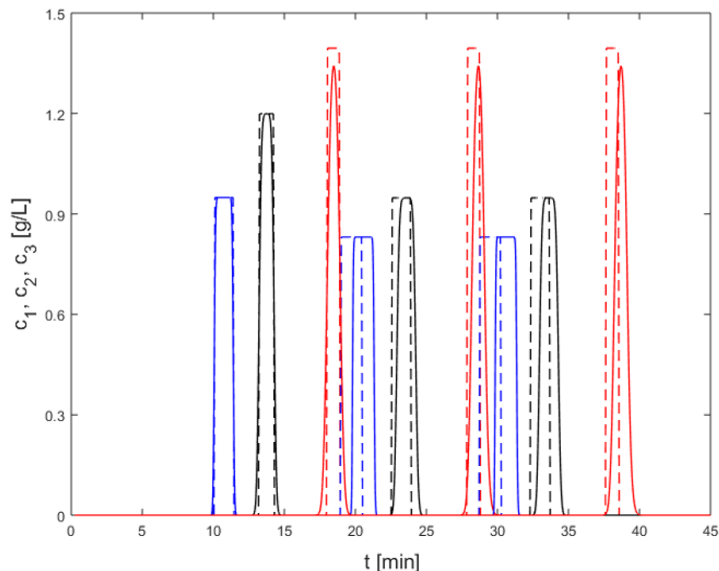

Figure 5.12: Illustration of the shift in cycle time in the results of EDM with $N_p = \infty$ ($D_z = 0$) (shown with bold lines) compared to the analytical solution of EM (shown with dashed lines). The cycle time reported by EM is 9.77 minutes, which is shorter than that of EDM. The cycle time in the latter case is 10.03 minutes.

Now we discuss independent results generated by this model.

Figure 5.13 shows the evolution of the concentration profiles for both the conventional isocratic condition and the conservative concept of gradient operation with safety margins. The results are shown in the latter case for different N_p (or D_z) values. The corresponding N_p value and the resulting cycle time as well as the applied safety margins (times) are given separately for each result. The c_1, c_2 and c_3 components are marked in blue, black and red, respectively.

Each injection is associated with an injection time, two temperature switching times (first cooling and then heating), and a cycle time. The cycle time is the same for each injection because each injection has a uniform temperature regime, i.e. $\Delta t_c^1 = \Delta t_c^2 = \Delta t_c^3$. All injection times Δt_{inj}^p, switching times t_k and cycle times Δt_c^p, with p=3 and k=1,2,...,6, are calculated with the formulas (4.42b), (4.40), and (4.43a), respectively. The first two types of times are listed in the Table 5.14, while the consistent cycle time is given in each figure.

The upper Sub-figure shows that in the case of isocratic conditions, since no safety margin is required, the cycle time of 12.22 is applied. On the other hand, in gradient operation shown in the rest of the Sub-figures, it can be observed that the smaller the value of N_p, the larger the dispersion, and thus the cycle time increases. As can be seen in Table 5.14, all other times also become longer as we decrease the value of N_p. The cycle time Δt_c^3 already takes into account the given safety margin, whose value starts from 15 min for higher N_p and goes to 17 min for smaller N_p. This makes it less productive compared to the isocratic operation. The problem is that when using the cycle time without safety margins, there is a risk of remixing, since the slowest component of each injection requires a different temperature regime than the fastest component of the next injection, as was already made clear in Chapter 3. This fact makes this concept less productive or, in other words, suboptimal. That is why we have introduced an optimal design concept ignoring the safety margins.

In the optimal design concept shown in Figure 5.15, we handle the switching of temperatures in such a way that we make earlier injections without applying the safety margins and still avoid remixing. In the figure, it can be seen that we have achieved the shortest possible cycle time for the largest plate number, i.e. $N_p = \infty$. The reason for the dispersion in the results of this figure is already explained in the text associated to the Figure 5.6. For $N_p = 2871$ and 1000, the applied cycle time is still shorter than that in the isocratic mode, but for N_p=200 it has exceeded the isocratic value, rendering it useless. Therefore, for the application of the concept of this study, it is imperative to consider this range of N_p when selecting a chromatographic column.

The cycle time given in the figure is estimated from the second injection, i.e. Δt_c^2, which is calculated using Eq. (4.48). This is because the cycle times becomes consistent after second injection, i.e. $\Delta t_c^1 \neq \Delta t_c^2 = \Delta t_c^3$. The injection times are calculated using Eq. (4.50). All other important times are given in table 5.16, and if we compare these values with table 5.14, we clearly see a useful reduction.
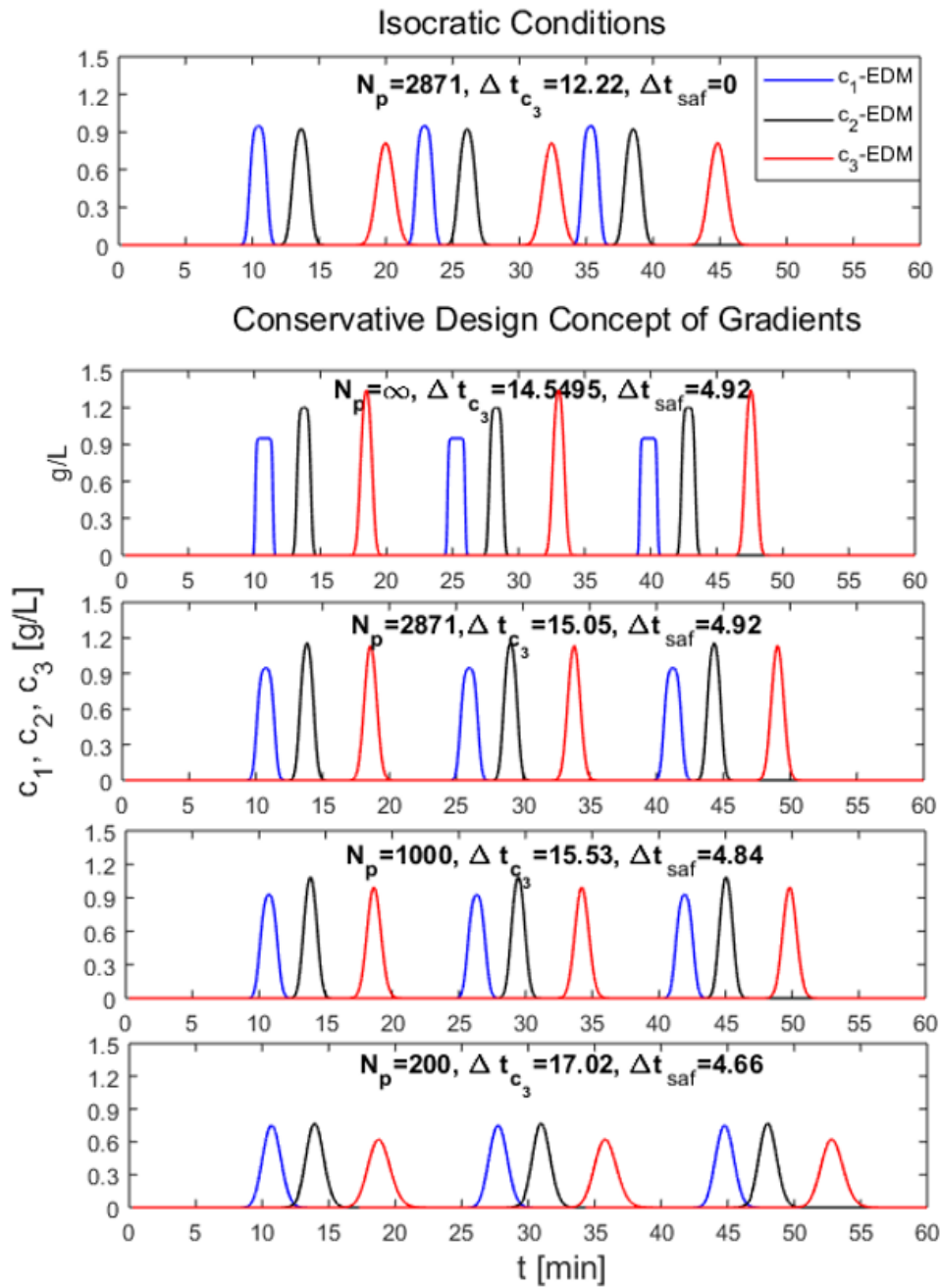
Figure 5.13: Illustration of solution behavior for ternary mixture injections for a conservative design concept that considers safety margins. The mixture is injected three times, with the fastest component c_1 marked in blue, the slower component c_2 in black, and the slowest component c_3 in red. Above is the isocratic reference case, while below are the results for said gradient case for different plate numbers N_p to show its effect on dispersion and consequently on the cycle time.

Table 5.14: These results are linked to the Figure 5.13

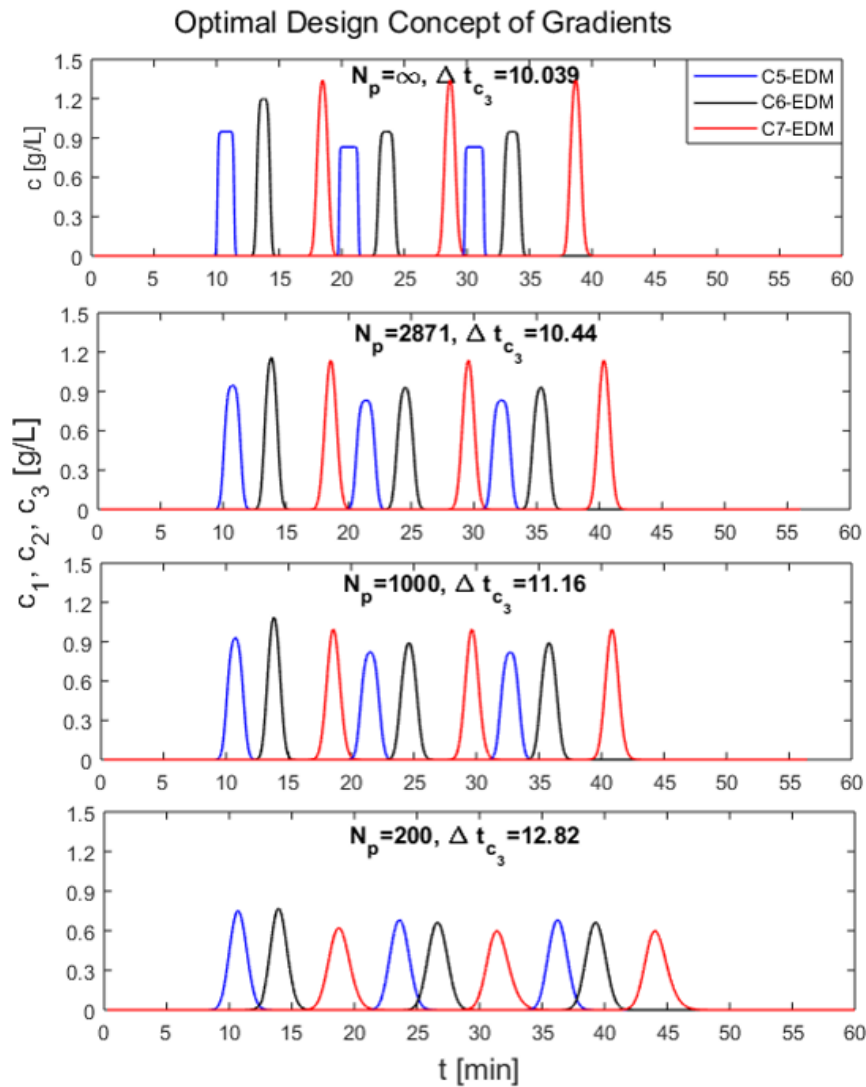| Charac. Times [min]	t_{inj}^1	t_{inj}^2	t_{inj}^3	t_1	t_2	t_3	t_4	t_5	t_6
Isocratic, N_p=2871	0.25	12.47	24.69	-	-	-	-	-	-
Gradients, $N_p = \infty$	0.25	14.79	29.34	11.56	19.47	26.11	34.02	40.66	48.57
N_p=2871	0.25	15.48	30.72	11.93	19.91	27.17	35.15	42.41	50.38
N_p=1000	0.25	15.784	31.32	12.05	20.14	27.59	35.68	43.13	51.22
N_p=200	0.25	17.27	34.30	12.68	21.26	29.70	38.28	46.73	55.31

Figure 5.15: Illustration of the solution behavior of ternary mixture injections for the optimal design concept that does not consider safety margins. As in Figure 5.13, the results are again shown for different plate numbers. The color scheme applied is also the same.

Table 5.16: These results are linked to the Figure 5.15. The given times are in [min].

Charac. Times	t_{inj}^1	t_{inj}^2	t_{inj}^3	t_1	t_2	t_3	t_4	t_5	t_6	Δt_{c}^1	Δt_{c}^2	Δt_{c}^3
Gradients, $N_p = \infty$	0.25	10.56	20.60	11.56	19.47	21.45	29.74	31.49	39.78	9.56	10.03	10.03
N_p=**2871**	0.25	10.83	21.46	11.83	19.79	22.022	30.29	32.65	40.92	10.13	10.44	10.44
N_p=**1000**	0.25	11.25	22.42	12.05	20.14	22.68	31.05	33.85	42.122	10.68	11.16	11.16
N_p=**200**	0.25	13.28	25.93	12.68	21.27	25.71	34.07	38.15	46.72	12.36	12.82	12.82

5.3.2 Results of EDM Coupled with Simplified Energy Equation

In this section, we present the results of the semi-analytical solution of the model for $N_c = 3$, as discussed in Sub-section 4.2. The provided space discretization points N_x are the same as in the previous model: 2000, generating $\Delta x = 0.0005$. Using the equation (4.64), $\Delta \tau = 0.00053$ is calculated, which is given in dimensional form as $\Delta t = 0.0032$ min. For the given non-dimensional simulation time of 16, the number of time discretization points in this model $N_t = N_\tau$ is set to 30477.

Figure 5.17 illustrates the solution behavior for both isocratic and gradient conditions, this time for a slower temperature change. In the previous model, the cycle time becomes constant after two injections, but in this case it becomes constant after five injections, which is why we show seven injections in Figure 5.17. We refer to the first five injections as the start up of the process, which is marked in grey. The last two injections, marked in sky-blue, are the repetition of injection cycles that occur under periodic similar temperature regimes and we call it cyclic steady-state.

The switching strategy remains the same as in the previous model and is given by equation (4.40). The estimation of cycle and injection times is also the same as in the previous model. These formulas are given by the Eqs. (4.48) and (4.50), respectively. Since the temperature change is not so simple, the temperature profile is also shown in green color in connection with the right axis, while the concentration corresponds to the left axis.

As shown via dashed line, we see that seven injections of the so called ternary mixture are processed under isocratic conditions in around 96 minutes with cycle time of 12.23 minute. This is similar to the one given by EDM, shown in the top Sub-figure of Figure 5.13.

On the other hand, if we examine the results of the gradient operation of the optimal design concept, it is completed in about 88 minutes, resulting in an acceptable reduction in cycle time of 11.05 minutes (calculated from the seventh injection). The temperature of the segment II is changed from T_R to T_L immediately with the start of the injections at z_0. After the time $t_1 = t_{1,\text{max}}^1 = 11.68$ min, it is switched to T_H and after the time $t_2 = t_{3,\text{max}}^1 = 21.50$ min, it is switched back to T_L. However, due to the slow temperature exchange, the pulses are not completely cooled or heated. Except for the first few injections, the difference between cooling and heating remains very small and they do not reach the applied values T_L and T_H, respectively. Considering the switching time criteria given in equation (4.40), the temperature profile becomes periodic after 5 injections and then we call it the operating periodic regime. Here, the process become cyclic steady-state rendering a shorter cycle time compared to the isocratic conditions. The components of the first injection are slightly more concentrated compared to the rest of the injections, because for them the temperature difference between the reference and the implemented is comparatively larger.

If we compare the rows belonging to $N_p = 2871$ in the tables 5.18 and 5.16, we see that all times in the latter table are longer than in the former table. Also, the cycle times in the currently applied model are now comparatively longer. This is due to the complexity of this model because of the temperature profile, which is closer to reality.
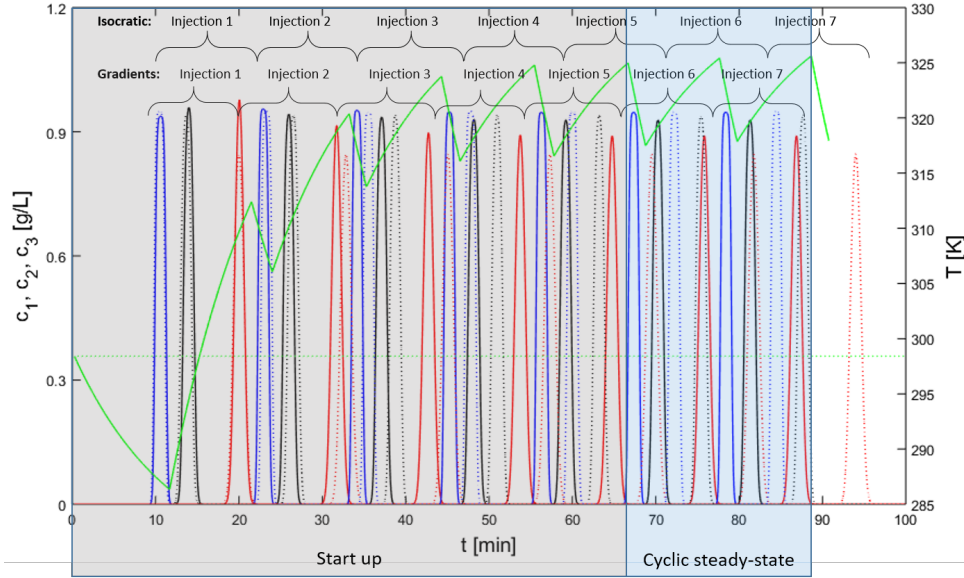

Figure 5.17: Illustration of the results obtained by EDM coupled with the simplified energy equation when $X_1 = 0.13$, $X_2 = 0.17$. The design concept used is optimal which does not consider safety margins. Concentrations are plotted on the left axis, and since we now have complicated temperature regimes, we plot them in green, which corresponds to the right axis. The results of the gradient conditions and the isocratic conditions are overlaid by solid and dashed lines, respectively. The sustained cycle time in isocratic operation according to this model is 12.23 minutes. For gradient operation it is 11.05 minutes. All other characteristic times such as switching, injection and cycle times are given in Table 5.18.

Table 5.18: Results linked to Figure 5.17. All times are in [min]

Charac. Times	t_{inj}^1	t_{inj}^2	t_{inj}^3	t_{inj}^4	t_{inj}^5	t_{inj}^6	t_{inj}^7	Δt_{c}^1	Δt_{c}^2	Δt_{c}^3	Δt_{c}^4	Δt_{c}^5	Δt_{c}^6	Δt_{c}^7
Isocratic	0.25	13.09	25.32	37.55	49.78	62.02	74.25	12.23	12.23	12.23	12.23	12.23	12.23	12.23
Gradients	0.25	12.85	24.23	35.30	46.37	57.42	68.47	11.98	11.33	11.11	11.08	11.06	11.05	11.05

Switch. Times	t_1	t_2	t_3	t_4	t_5	t_6	t_7	t_8	t_9	t_{10}	t_{11}	t_{12}	t_{13}	t_{14}
Gradients	11.68	21.50	24.00	33.23	35.24	44.26	46.37	55.31	57.47	66.38	68.48	77.39	79.49	88.40

5.3.3   Results of EDM Coupled with Energy Equation

In this section we present the results of the final and more detailed model for $N_c = 3$ discussed in Sub-section 4.3. This model consists of the same EDM but is now coupled with a detailed energy

balance. This energy balance determines the implemented temperature, which takes into account the phenomenon of heat exchange during the adsorption/desorption processes. It also takes into account the axial dispersion of the temperature.

The same space discretization points N_x are considered as in the previous model. Using the equation (4.82), the $\Delta\tau$ is now calculated to be 0.00037, which is given in dimensional form as $\Delta t = 0.0022$ min. Since simulation of this model takes more time than the previous model, the dimensionless simulation time is given as 16. The resulting number of time discretization points $N_t = N_\tau$ are then set to 43145.

Figure 5.19 shows the results when the same ternary mixture is again injected seven times under both isocratic and gradient conditions. In comparison with Figure 5.17, we explain this figure, where the cyclic steady-state regime begins operating after the fifth injection. In contrast, Figure 5.19 suggests a cyclic operation following the third injection. Uncertain about this observation, we extended the injections for seven periods and once more identified the final two as the inception of cyclic steady-state operation. This also makes this figure compatible with the previous figure for comparison purposes.

The calculation of injection, cycle and the sequence of switching times stay the same as for the previous model. The difference is that the current model becomes more complex with the introduction of new terms such as $G_n q_n(T)$ and X_3 given by Eqs. (2.15b) and (2.15e). This leads to more delay in the temperature change and causes concentration pulses to be more dispersed. Consequently, all injection, retention, switching and cycle times become larger. Please take a comparative look at the Tables 5.18 and 5.20.

As shown by the dashed line, seven injections with this model are processed in about 96 minutes under isocratic conditions with a cycle time of 12.37 minutes, which is similar to the previous model. The reason is that under isocratic conditions $\Delta H_{A,n}$ becomes 0, which makes the effect of the additional term $G_n q_n(T)$ vanish, see Eq. (2.15b). Thus, under isocratic conditions, the energy equation reduces almost to that shown in the previous figure.

The gradient process takes comparatively longer than its predecessor to process seven injections. The process is completed in 92 minutes with a cycle time of 11.69 minutes. In contrast, the predecessor model required 88 minutes. However, the results of the current model show a shorter cycle time compared to the isocratic model, which is a success compared to the previous models because it takes into account more realistic conditions, especially in the area of temperature gradients within the HPLC process.

Moreover, exothermic/endothermic waves are clearly visible in the temperature profiles of all injections, since they migrate more slowly and have enough time to affect the heat exchange within the column. This fact proves the existence of the term $G_n q_n(T)$ in the model.
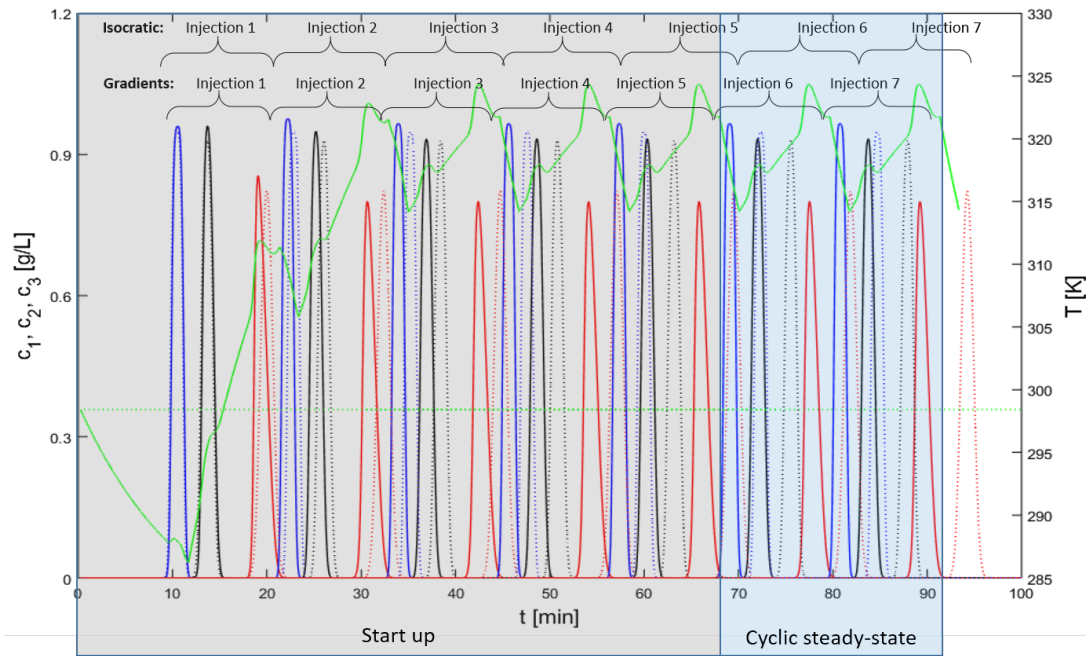
Figure 5.19: Illustration of the results for optimal design concept without safety margins obtained by EDM in conjunction with the detailed energy equation. The parameters applied, colors and axes for the concentrations and temperature are the same as in Figure 5.17. According to this model, the cycle time for isocratic operation is 12.37 minutes, which is almost the same as that of the previous model. For gradient operation, it is 11.69 minutes, which is shorter than the isocratic cycle time. All other important times are again given in tabular form, c.f. Table 5.20.

Table 5.20: These results are linked to Figure 5.19

Charac. Times	t_{inj}^1	t_{inj}^2	t_{inj}^3	t_{inj}^4	t_{inj}^5	t_{inj}^6	t_{inj}^7	Δt_c^1	Δt_c^2	Δt_c^3	Δt_c^4	Δt_c^5	Δt_c^6	Δt_c^7
Isocratic	0.25	12.62	25.00	37.37	49.75	62.12	74.49	12.37	12.37	12.37	12.37	12.37	12.37	12.37
Gradients	0.25	12.16	23.84	35.53	47.22	58.92	70.61	11.91	11.68	11.69	11.69	11.69	11.69	11.69

Switch. Times	t_1	t_2	t_3	t_4	t_5	t_6	t_7	t_8	t_9	t_{10}	t_{11}	t_{12}	t_{13}	t_{14}
Gradients	11.69	21.36	23.48	33.28	35.29	45.12	47.11	56.97	58.92	68.81	70.73	80.66	82.54	92.51

Comparison for the Ternary Mixture Injections by All the Models: At the end of the results of all our models presented in this chapter, we do a very interesting comparison of the three models studied. Figure 5.21 compares the last two Sub-figures showing the seventh injection from Figures 5.19 and 5.17 with the same injection that would look like in EDM with ideal step gradients. That is, if we increase the number of injections in Figure 5.15 to seven, the retention behavior at the seventh injection will look like the Sub-figure above in Figure 5.21. As it was seen in the associated Tables 5.20, 5.18 and 5.16, the EDM has recorded a step by step increase in the cycle time, as much as the coupled temperature profile becomes more detailed.

From the figure, it can be seen that the seventh injection by EDM is completed in about 84 minutes at ideal temperature gradients (Sub-figure above). The same injection given by the same mass balance under the simplified energy equation (middle Sub-figure) terminates in about 88 minutes, while under the detailed energy equation (Sub-figure below) it terminates in about 92 minutes. The different dispersion trends in each model and the associated concentration/dilution are also now well-understood.
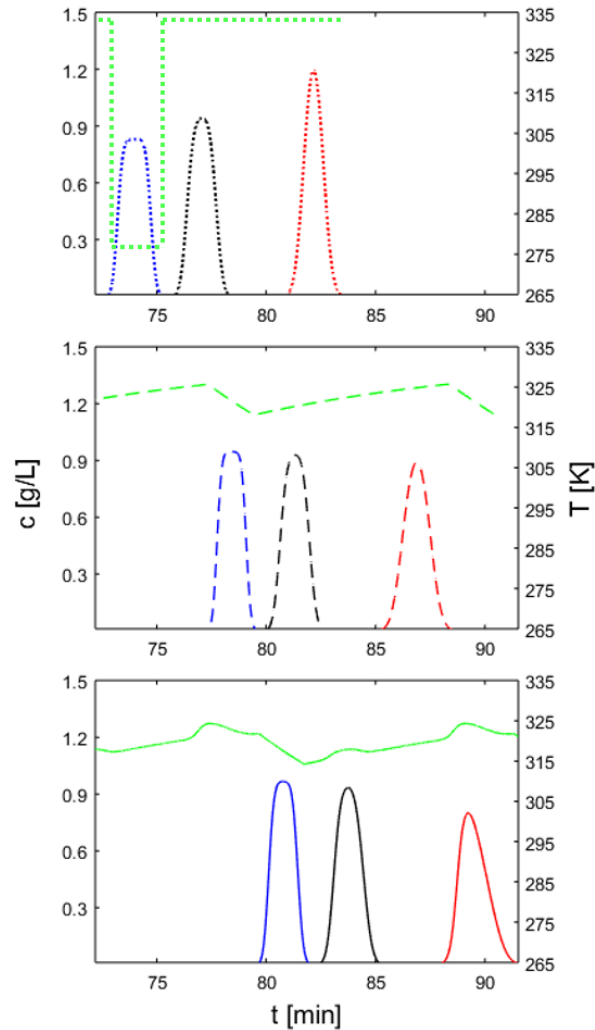

Figure 5.21: Comparison of the retention behavior of the seventh injection. The top Sub-figure shows the results for ideal step temperature gradients, the middle one for the simplified energy equation, and the Sub-figure at the end shows the results for the detailed energy equation. Concentration is always plotted on the left axis, while temperature is plotted in green on the right axis

5.4   Comparison of Computations with Experiments

In the final section of this dissertation, we give a brief overview of the experiments conducted as part of the parallel doctoral project [39] mentioned earlier. We have chosen the results of our last and final model for comparison because they are more appropriate with respect to the conditions applied. In all cases of our prepared theoretical results for comparison, $N_p = 2871$, $X_1 = 0.13$ and $X_2 = 0.17$ are considered, since these values are obtained from experiments themselves. First, we briefly review the material and methods used for the experiments in the laboratory. The details, figures and results are taken from our previously published article [38]. More details are available in the aforementioned thesis.

5.4.1   Material and Methods

In the experimental study, cyclopentanone (C5), cyclohexanone (C6), and cycloheptanone (C7) purchased from Alfa Aesar were employed as solutes of the ternary mixture. Methanol from Sigma-Aldrich and distilled water filtered with 0.45 μm filter paper from Sartorius Stedim Biotech GmbH were used as the mobile phase, while a C18 column (Agilent Zorbax Eclipse XDB, D_c= 4.6 mm, L=100 mm, particle size=5 μm) was employed as the stationary phase (50%/50%, v/v). The matching peaks showed up in the following order under these reverse phase conditions: C5, C6, and C7. The injection concentrations $c_{n,\text{inj}}$ for $n = 1, 2, 3$ used are 0.1 vol%. By demonstrating that the main characteristics of the elution profiles remain constant regardless of the injection volume, the concentrations under consideration were experimentally confirmed in preliminary experiments to be in the linear isotherm range. Syringe and pump injections were used to introduce volumes between 50 and 1500 μL. Using Thiourea (Merck) as a tracer, the column porosity ϵ was calculated. In order to calculate the extra-column dead times (t_{dead}), which differ in single-component and ternary mixture injections, marker experiments were carried out.

Figure 5.22 shows the experimental setup of segmented temperature gradient liquid chromatography. The system consists of a conventional HPLC apparatus (Hewlett Packard 1100) and an extended temperature modulation unit with insulation. In this study, the detector wavelength was set at 280.2 nm. It was found that the detector calibration factors for C5, C6, and C7 were 0.004, 0.005, and 0.005 $\text{gL}^{-1}\text{mAU}^{-1}$, respectively. The so-called segment I and segment II are connected in series, with segment I held in an HPLC oven to maintain the reference temperature of 298.41K, while segment II is held in a cylindrical water jacket. The temperature of segment II is gradually adjusted to the low temperature T_L or the high temperature T_H by circulating the water externally through two thermostats. These values are also different for the injection of single components and ternary mixtures, as shown in the Tables 5.1 and 5.2. Two thermocouples were used to measure the temperatures in the water jacket and at the column exit. The temperature at the outer surface of the outlet of the column was measured, because it is technically difficult to measure the actual internal temperature. The two measured temperatures were recorded in real time. The thermostat assumed that there was an equilibrium between the interior of the column, its wall and the water surrounding it. To ensure a safe operating range of the column, the temperature range was set from 279K to 333K. In the experiments, the heat transfer rate proved to be reasonably quick, allowing for a decent approximation of the expected temperature gradients.
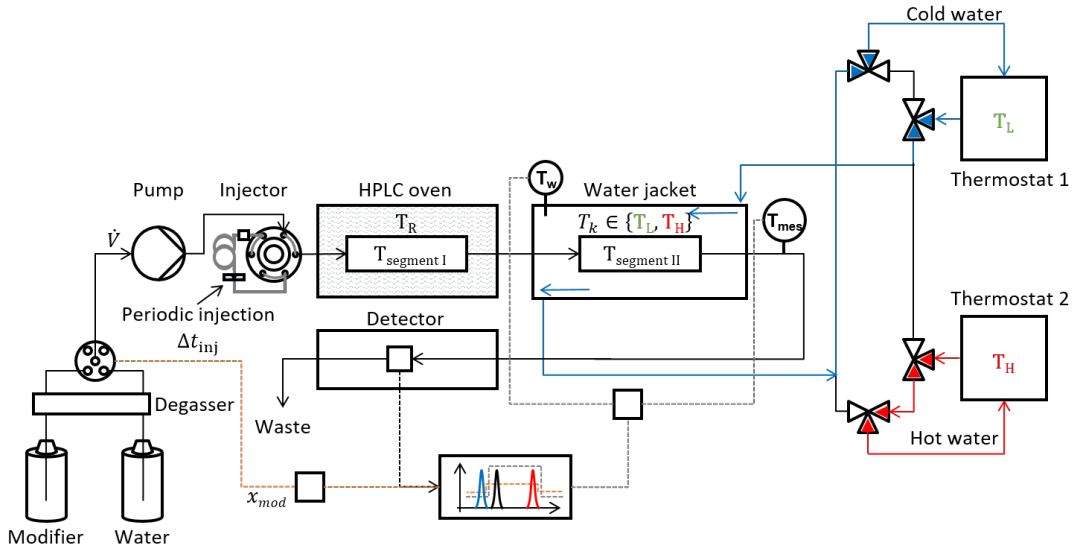
Figure 5.22: Illustration of the liquid chromatography experimental system with imposed segmented temperature gradients. It is made up of thermostats, a water jacket, and an HPLC unit. The pump was programmed with a flow rate of $\dot{V} = u\epsilon A = 0.3$ ml/min. A countercurrent flow of two liquids occurs inside and outside the water jacket. The temperature in the oven was kept as a reference temperature, $T_R = 298.41$K for segment I. Two thermocouples are placed in the water jacket ($T_k = T_L$ or T_H for segment II). The actual temperatures are measured for the water and the outer surface of the outlet tube.

5.4.2 Comparison for Single-Component Injections

In this section, we compare the results of the wide single pulse injection of the experiments and the results of our last detailed model, which are already shown in Section 5.2.3. In the experiments, the result of the Type I temperature change (when both segments are initially kept at different temperatures) agrees with the theoretical results for $X_1 = 0.13$ and $X_2 = 10$ given in the Sub-figure at the top of Figure 5.9. On the other hand, the result of the temperature change of Type II (when both segments are initially kept at the same reference temperature T_R and for segment II it is switched to T_L or T_H at $t_s = 18$ min) agrees with the theoretical results for $X_1 = 0.13$ and $X_2 = 0.17$. The comparisons in both the types are shown in Figures 5.23 and 5.24 respectively.
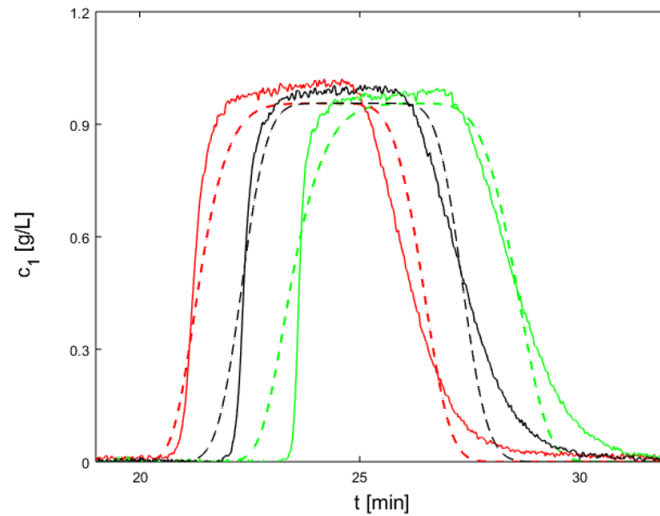
Figure 5.23: Comparison of the theoretical results (dashed lines) of our detailed model discussed in section 5.2.3 with the experimental results (solid lines) for the Type I temperature change. The colors red, green, and black represent heating, cooling, and reference conditions, respectively. In the theoretical results, $X_1 = 0.13$ and $X_2 = 10$ are used.
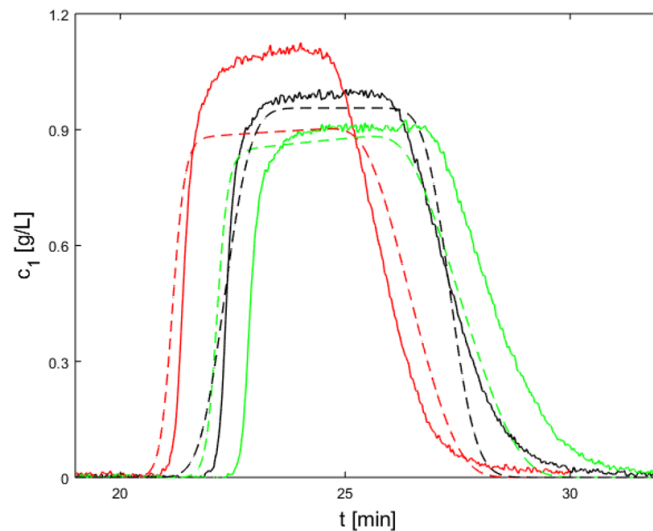

Figure 5.24: Comparison of the theoretical results with the experimental results of the temperature change of Type II. The theoretical results in this figure consider the same values for X_1, but a different value for $X_2 = 0.17$.

The two figures 5.23 and 5.24 show good agreement between the profiles, suggesting that the numerical solution effectively replicates the temperature variations. Nevertheless, there are minor differences. These discrepancies could be due to several factors. One possible reason of these differences is inaccuracies in the Henry constants. Since the temperatures of the two

segments were controlled in different ways, while the Henry constants were calculated based on the temperature of the water jacket, the actual temperatures in the two segments may not match exactly. In addition, the operation of the thermostat itself may cause temperature fluctuations. Last but not least, in addition to axial thermal dispersion, radial thermal dispersion may also play a role in the elution profile, for which a more detailed 2D model should be developed.

5.4.3 Comparison for Ternary Mixture Injections

In this section, the results of the experiments using shorter ternary mixture injections are compared with those obtained with the same detailed model discussed in Section 5.3.3.

Since only two injections are processed in the experiments, Figure 5.25 shows the comparison of the theoretical results for two successive injections. Again, good agreement can be seen, with the exception of component 3 (C7), which is more dispersed and diluted compared to the experiments. EDM results in a slightly longer cycle time than in the experiments, but is still shorter than under isocratic conditions. The slight shift in cycle time for the experiments is due to the different criteria used to determine the cycle time.
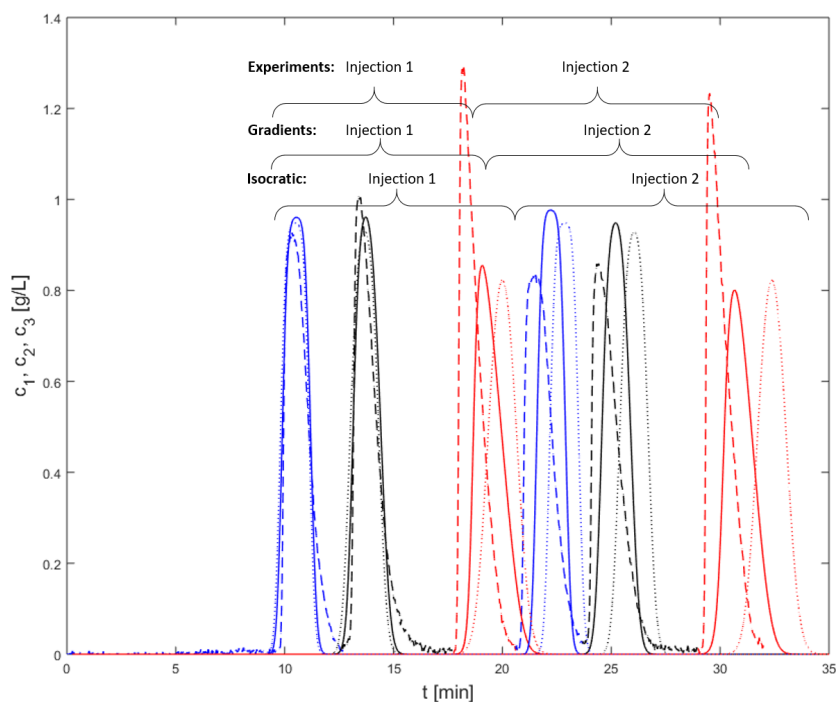

Figure 5.25: Comparison of the theoretical results for ternary mixture injections with the experimental results of the temperature change of Type II. The theoretical results in this figure consider the same values for N_p, X_1 and X_2 as in Figure 5.24. The cycle time in the experiments was reported to be 11.4 minutes, while EDM under detailed energy balances gave a cycle time of 11.7 minutes. Under isocratic conditions, the cycle time is comparatively longer at 12.37 minutes. They all are estimated from the second cycle.

5.5   Predicted Productivity for All Models Compared to Experiments

Finally, we show the increase in productivity achieved in all the models studied. We present from Chapter 3 productivity of a simple and ideal model, the so-called equilibrium model, which considers the ideal rectangular injections of concentration with the ideal temperature step gradients (SG). Then follows the well-known model, EDM. This model is tested under three different temperature profiles in Chapter 4: SG, simplified energy equation (SEE) and with the energy equation (EE). The EM proposed the shortest cycle time, as shown in Figure 5.26. After introducing more parameters into the model and gradually coupling them with the aforementioned temperature profiles, the model become more complex. This leads to more dispersion in concentration pulses and thus to a shift in the cycle time. In the EM at SG and EDM at SG and SEE both, the cycle time remains shorter than in experiments, but in EDM at EE, it exceeds the cycle time recorded in the experiments. Nevertheless, all of these cycle times applied under gradient operations are shorter than the isocratic conditions, making our study a successful initiative in modeling and simulating temperature gradients to increase the productivity of liquid chromatographic columns. The formula for calculating cycle time is given in the previous discussions for all the models, while the corresponding productivities for gradient and isocratic conditions are calculated with the formulas (2.50) and (2.51), respectively. Note that we consider the mass of component C5. To get the value of productivity in gram per hour per liter $(\mathrm{gh}^{-1}\mathrm{L}^{-1})$, we divide the obtained values by column's volume $V_c = z_{\max}\mathrm{d} = 9.2\mathrm{cm}^3$, see Table 5.1.
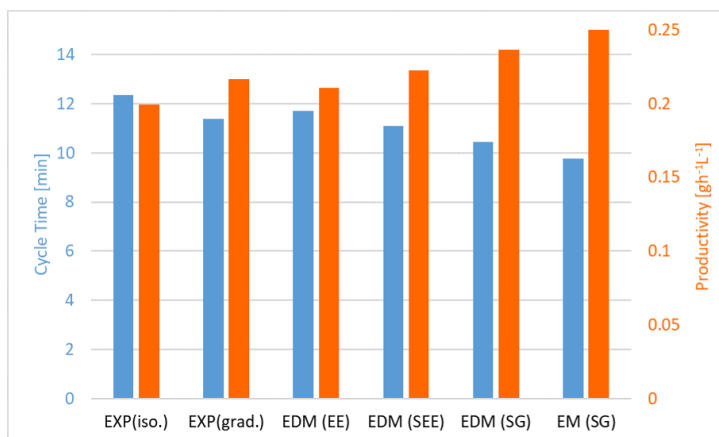

Figure 5.26: Cycle times (in blue) and corresponding predictions of productivity (in orange) for all models studied compared to isocratic conditions and experiments. They correspond to the left and right axes, respectively. Results are compared with experimental data for EM with temperature step gradients (SG), as discussed in Chapter 3 and illustrated in Figure 5.12; EDM with SG, detailed in Section 5.3.1; EDM with simplified energy equation (SEE), described in Section 5.3.2; and EDM with energy equation (EE), outlined in Section 5.3.3. The following experimental parameters are considered: $N_p = 2871$, $X_1 = 0.13$ and $X_2 = 0.17$. For example, when comparing productivity in the case of EE, it is 16% higher compared to the isocratic conditions, where by EM, it is 20%.

Chapter 6

Conclusions and Outlook

Conclusions

In this work, we have investigated a specific new mode of high performance liquid chromatography (HPLC) operation based on the introduction of temperature gradients that can increase performance, e.g. productivity, compared to conventional (isocratic) operation. Our primary focus has been on mathematical methods and analysis, although we have been fortunate to have access to practical experiments conducted by a fellow PhD candidate.

Our research began by considering an HPLC column incorporating two segments of the same properties of the chromatographic system such that the temperature of the second segment can be modulated in a flexible manner.

Distinctly established mass balances describing the front propagation processes in the chromatographic column were examined: the Equilibrium Model (EM) and the Equilibrium Dispersive Model (EDM). These mass balances served to illuminate the complicated behavior of concentrations within the HPLC column. Our objective were to control this behavior using temperature modulations, achieved through an external heat source. This approach was aimed at reducing cycle times. The nature of this heat source's contribution was described by the energy balance we established. This balance took various forms differing in the degree of details captured. Considered were composite and simplified versions, as well as an idealized representation in the form of a step function.

The PDE models were linked to mixed Dirichlet and Neumann boundary conditions. Dirichlet boundary conditions create a rectangular pulse at the column's inlet, while Neumann boundary conditions ensure solution consistency with reality at the outlet.

At the core of our models lies the concept of quantitatively describing the concentration "c" in the mobile phase and "q" in the adsorbed phase over time and position in the column. Their interaction was determined by a thermodynamic function called the adsorption isotherm. The adsorption isotherm considered in this study revealed that changes in "c" prompt a straightforward response, following a linear trajectory. However, when it comes to temperature dependence, the reaction becomes more intricate, deviating from a linear path. The slope of this trajectory is controlled by the component specific Henry constants, which depends on both the implemented temperature and the corresponding enthalpy of adsorption. Essentially, the extent to which a temperature gradient can improve results relies on the specific Henry constants unique to each component.

Building on these fundamental concepts, we proceeded to complement our mass balances step by step with energy balances. Initially, we introduced the idea of ideal temperature step gradients. Then we used more intricate energy balance concepts. This approach provided insights into how an array of factors influences the behavior of concentrations and retention times, whether under the uniform isocratic conditions or dynamic gradient conditions.

First, we considered the Equilibrium Theory of chromatography and the Method of Characteristics. We obtained analytical solutions that have illuminated trajectories for elution profiles, offering a better understanding of the slopes of the trajectories under varying temperatures. This knowledge guided us through our subsequent studies, which have encompassed numerical computations.

We then moved to a semi-analytical approach that focuses on the EDM and a simplified energy balance equation. This type of heat equation takes into account the main guiding principles of heat transfer, but ignores several factors such as the exothermic/endothermic phenomenon of adsorption/desorption and the axial dispersion of temperature. Using the Laplace transform, we reduced the complexity of this equation and used the finite volume method (FVM) with upwind fluxes to practically estimate solute concentrations. This method helped us understand how slower temperature gradients compared to faster gradients affect solute concentrations.

When it comes to numerical solutions, we explored the EDM under two distinct temperature profiles: the temperature step gradients and the detailed energy equation. Ensuring precision, we conducted a stability analysis for each model, determining specific time steps that the tool used to solve the model equations (MATLAB) could effectively manage. This approach enabled us to acquire stable solutions using the FVM. It's worth noting that the final model, which coupled the EDM with the detailed energy balance, yielded particularly more realistic results. In this case, the delayed temperature profile not only exhibited exothermic/endothermic waves but also demonstrated their influence on concentration peaks.

The solutions to above the models were estimated first for single-component injections. Through a range of scenarios, we analyzed how changing factors, such as early switching times and delayed switching times of temperature impact the solution. Then, we studied multi-injections of a ternary mixture, examining how controlled temperature adjustments can shrink cycle times and enhance productivity. Considering various improvement options for testing ternary mixtures, we presented two interesting potential concepts: the "conservative design concept with safety margins" and the "optimal design concept without safety margins". In the first approach, we achieved a hypothetical cycle time shorter than the isocratic one. However, this method necessitates considering safety margins to prevent unintended mixing between consecutive injections, rendering it sub-optimal compared to the isocratic operation. In contrast, a subsequently analyzed optimal design concept eliminates the need for safety margins, resulting in a shorter cycle time. This optimized cycle time obtained by the aforementioned models contributed to an 16-20% increase in productivity for the specific case studies considered. Analyzing profiles before and after the transition to a different temperature regime showed that the conservation of mass is maintained. This is essential to obtaining a useful mathematical method.

A substantial benefit to our research was the fact that we could align our models' predictions with actual experimental results. The results were available thanks to the parallel work conducted in the above mentioned parallel PhD project [39]. A very good resemblance between them, with little differences, validates the significance of our theoretical study. Our theoretical study lead to a better understanding of the experiments. The step by step inclusion of additional parameters in the models has resulted in increased cycle time. The cycle times derived from experimental data

correspond to more realistic conditions, which highlights the discernible discrepancy between idealized scenarios and the complex conditions encountered in practice.

This research provides valuable insights and tools not only on how different temperature changes affect the movement of concentrations in columns, but also for estimating useful cycle times and amplitudes for perturbations in some chromatographic processes. These tools can be used for other specific separation processes, as long as we understand sufficiently well how temperature and certain parameters work together. However, we need to understand that gradient chromatography does not work the same way for all situations. Even though it is effective at speeding up processes and making columns more productive compared to the isocratic conditions, we need to remember that it works best under specific conditions and might not be a universal solution for every case.

In summary, our research bridges the field of numerical computations, mathematical modeling and analysis with empirical reality. It lays the foundation for further improving liquid chromatographic processes capable to solve mixtures of components.

Outlook

- We used linear chromatography in this study because we worked with a diluted solute mixture. However, in future work, non-linear chromatography can be applied to more concentrated systems where solute interactions are significant. This method is particularly useful for studying systems with high solute concentrations, where non-linear effects such as saturation and competitive adsorption become prominent.

- More sophisticated forms of gradients can be used instead of step-like temperature gradients. They are especially useful when dealing with complicated combinations or simulating actual temperature variations in applications such as pharmaceutical stability testing.

- In this work we considered equilibrium models. Non-equilibrium models can be used when dealing with systems that do not comply to the equilibrium assumptions. This is typically the case when substances do not have sufficient time to reach a stable concentration profile due to dynamic transport phenomena.

Bibliography

[1] Guiochon, G.; Golshan-Shirazi, S.; Katti, A. *Fundamentals of Preparative and Nonlinear Chromatography, 1st ed.*; MA: Academic Press, Boston, USA, **1994**

[2] Guiochon, G.; Felinger, A.; Shirazi D.G.; Katti, A.M. *Fundamentals of Preparative and Nonlinear Chromatography, 2nd ed.;* Elsevier Academic Press, New York, USA, **2006**

[3] Schmidt-Traub, H. *Preparative Chromatography, 3rd ed.*; (Eds. Henner Schmidt-Traub, Michael Schulte and Andreas Seidel-Morgenstern), Weinheim: Wiley, **2020**.

[4] Broughton, D.B.; Gerhold, C.G. *Continuous sorption process employing fixed bed of sorbent and moving inlet sand outlets*; US Patent No. 2.985.589, **1961**.

[5] Seidel-Morgenstern, A.; Kessler, L.C.; Kaspereit, M. New developments in simulated moving bed chromatography. *Chem. Eng. Technol.* **2008**, *31*, 826–837.

[6] Kaspereit, M. Advanced operation concepts for simulated moving bed processes. In: *Advanced Chromatography, vol. 47*; (eds. E. Grushka and N. Grinberg), 165–192. Boca Raton, FL: CRC Press, **2009**

[7] Zobel, S.; Helling, C.; Ditz, R.; Strube, J. Design and operation of continuous counter current chromatography in biotechnological production. *Ind. Eng. Chem. Res.* **2014**, *53*, 9169–9185.

[8] Spedding, F.H.; Voigt, A.F.; Gladrow, E.M.; Sleight, N.R.; Powell, J.E.; Wright, J.M.; Butler, T.A.; Figard, P. The Separation of Rare Earths by Ion Exchange. 1, 2 II. Neodymium and Praseodymium. *Journal of the American Chemical Society* **1947**, *69(11)*, 2786-2792.

[9] Mair, B. J.; Gaboriault, A. L.; Rossini, F. D. Assembly and testing of 52-foot laboratory adsorption column. *Industrial & Engineering Chemistry* **1947**, *39(9)*, 1072-1081.

[10] Broughton, D. B. Production-scale adsorptive separations of liquid mixtures by simulated moving-bed technology. *Separation Science and Technology* **1984**, *19(11-12)*, 723-736.

[11] Kroef, E. P.; Owens, R. A.; Campbell, E. L.; Johnson, R. D.; Marks, H. I. Production scale purification of biosynthetic human insulin by reversed-phase high-performance liquid chromatography. *Journal of Chromatography A* **1989**, *461*, 45-61.

[12] Nicoud, R.M.; Fuchs, G.; Adam, P.; Bailly, M.; Küsters, E.; Antia, F.D.; Reuille, R.; Schmid, E. Preparative scale enantioseparation of a chiral epoxide: comparison of liquid chromatography and simulated moving bed adsorption technology. *Chirality* **1993**, *5(4)*, 267-271.

[13] Ching, C. B.; Chu, K. H.; Hidajat, K.; Uddin, M. S. Comparative study of flow schemes for a simulated countercurrent adsorption separation process. *AIChE Journal* **1992,** *38(11)*, 1744-1750.

[14] Frenz, J.; Horváth, Cs.; in: Horváth, Cs. (Ed.), *High-Performance Liquid Chromatography — Advances and Perspectives, Vol. 5*; Academic Press, New York, NY, **1988**, 211-314.

[15] Subramanian, G.; Phillips, M.W.; Jayaraman, G.; Cramer, S.M. Displacement chromatography of biomolecules with large particle diameter systems. *Journal of Chromatography A* **1989,** *484*, 225-236.

[16] Katti, A.M.; Dose, E.V.; Guiochon, G. Comparison of the performances of overloaded elution and displacement chromatography for a given column. *Journal of Chromatography A* **1991,** *540*, 1-20.

[17] Felinger, A.; Guiochon, G. Optimization of the experimental conditions and the column design parameters in overloaded elution chromatography. *Journal of Chromatography A* **1992,** *591(1-2)*, 31-45.

[18] Felinger, A.; Guiochon, G. Comparison of maximum production rates and optimum operating/design parameters in overloaded elution and displacement chromatography. *Biotechnology and Bioengineering* **1993**, *41(1)*, 134-147.

[19] Felinger, A.; Cavazzini, A.; Remelli, M.; Dondi, F. Stochastic-dispersive theory of chromatography. *Analytical Chemistry* **1999**, *71(20)*, 4472-4479.

[20] Carta, G. Exact analytic solution of a mathematical model for chromatographic operations. *Chemical Engineering Science* **1988**, *43(10)*, 2877-2883.

[21] Guiochon, G.; Lin, B. *Modeling for preparative chromatography*, Academic Press., Amsterdam, **2003**

[22] Qamar, S.; Perveen, S.; Seidel-Morgenstern, A. Numerical approximation of a two-dimensional nonlinear and nonequilibrium model of reactive chromatography. *Industrial & Engineering Chemistry Research* **2016**, *55(33)*, 9003-9014.

[23] Qamar, S.; Uche, D. U.; Khan, F. U.; Seidel-Morgenstern, A. Analysis of linear two-dimensional general rate model for chromatographic columns of cylindrical geometry. *Journal of Chromatography A* **2017**, *1496*, 92-104.

[24] Ruthven, D. M. *Principles of adsorption and adsorption processes.* John Wiley & Sons, **1984**.

[25] Giddings, J. C.; Eyring, H. A molecular dynamic theory of chromatography. *The Journal of Physical Chemistry, 59(5)* **2002**, 416-421.

[26] Giddings, J.C. *Unified Separation Science*, Wiley, New York, USA **1991**.

[27] McQuarrie, D. A. On the stochastic theory of chromatography. *The Journal of Chemical Physics* **1963**, *38(2)*, 437-445.

[28] Cruz, P.; Santos, J. C.; Magalhães, F. D.; Mendes, A. Simulation of separation processes using finite volume method. *Computers & chemical engineering* **2005**, *30(1)*, 83-98.

[29] Greibrokk, T. Subcritical water chromatography: A green approach to high-temperature liquid chromatography. *Anal. Chem* **2002**, *74*, 375A-378A.

[30] Osher, S. Convergence of generalized MUSCL schemes. *SIAM Journal on Numerical Analysis* **1985**, *22(5)*, 947-961.

[31] Levenspiel, O. *Chemical Reaction Engineering*; John Wiley & sons, **1998**.

[32] Cussler, E. L. *Diffusion: mass transfer in fluid systems*; Cambridge University Press, **2009**

[33] Patankar, Suhas. *Numerical heat transfer and fluid flow*; Taylor & Francis, **2018**.

[34] Plemmons, R. J., M-matrix characterizations. I—nonsingular M-matrices. *Linear Algebra and its applications* **1977**, *18(2)*, 175-188.

[35] Jandera, P., & Churáček, J. Gradient elution in liquid chromatography: XI. Influence of the adjustable gradient parameters on the chromatographic behaviour of sample compounds. *Journal of Chromatography A* **1980**, *192(1)*, 1-18.

[36] Jandera, P., & Churáček, J. Gradient elution in liquid chromatography: XII. Optimization of conditions for gradient elution. *Journal of Chromatography A* **1980**, *192(1)*, 19-36.

[37] Hayat, A.; An, X.; Qamar, S.; Warnecke, G.; Seidel-Morgenstern, A. Theoretical Analysis of Forced Segmented Temperature Gradients in Liquid Chromatography. *Processes* **2019**, *7*, 846.

[38] An, X.; Hayat, A.; Lee, J. W.; Qamar, S.; Warnecke, G.; Seidel-Morgenstern, A. Analysis and experimental demonstration of temperature step gradients in preparative liquid chromatography. *Journal of Chromatography A* **2022**, *1665*, 462831

[39] An, X. *Exploitation of temperature and solvent gradients in preparative liquid chromatography*. Doctoral Thesis, Submitted, OvGU Magdeburg, Germany, **2023**.

[40] Geankoplis, C. J. *"Transport processes and separation." Process Principles (4th ed.)*; Prentice Hall NJ **2003**.

[41] Haynes, H.W., Jr. An Analysis of Sorption Heat Effects in the Pulse Gas Chromatography Diffusion Experiment. *AIChE J.* **1986**, *32*, 1750–1753. [CrossRef]

[42] Tswett, M.S. On a New Category of Adsorption Phenomena and Their Application to Biochemical Analysis. *Tr. Varshavskogo Obschestva Estestvoispytatelei, Otd. Biolol.* **1905**, *14*, 1-20 (in Russian-Reprinted and Translated in G. Hesse and H. Weil, Michael Tswett's erste chromatographische Schrift, Woelm, Eschwegen, 1954).

[43] Lederer E.; La renaissance de la méthode chromatographique de M. Tswett en 1931. *Journal of Chromatography A.* **1972**, *73(2)*, 361-366.

[44] Martin, A.J.; Synge, R.L. A new form of chromatogram employing two liquid phases: A theory of chromatography. 2. Application to the micro-determination of the higher monoamino-acids in proteins. *Biochemical Journal* **1941**, *35(12)*, 1358.

[45] James, A.T.; Martin, A.J. Gas-liquid partition chromatography: the separation and micro-estimation of volatile fatty acids from formic acid to dodecanoic acid. *Biochemical Journal* **1952**, *50(5)*, 679.

[46] Lathe, G.H.; Ruthven, C.R.J. The separation of substances and estimation of their relative molecular sizes by the use of columns of starch in water. *Biochemical Journal* **1956**, *62(4)*, 665.

[47] Cuatrecasas P.; Anfinsen, C. B. *Methods in Enzymology, Vol. XXII*; (Eds. Colowick, S. P.; Kaplan, N. O.), Academic Press, NY, 1971,345.

[48] Guillaume, Y.; Guinchard, C. Prediction of Retention Times, Column Efficiency, and Resolution in Isothermal and Temperature-programmed Gas Chromatography: Application for Separation of Four Psoalens. *J. Chromatogr. Sci.* **1997**, *35*, 14–18. [CrossRef]

[49] Xiu, G.; Li, P.; Rodrigues, A.E. Sorption-enhanced Reaction Process with Reactive Regeneration. *Chem. Eng. Sci.* **2002**, *57*, 3893–3908. [CrossRef]

[50] Robinson, P.G.; Odell, A.L. Comparison of Isothermal and Non-linear Temperature Programmed Gas Chromatography the Temperature Dependence of the Retention Indices of a Number of Hydrocarbons on Squalane and SE-30. *J. Chromatogr. A* **1971**, *57*, 11–17. [CrossRef]

[51] Kaczmarski, K.; Gritti, F.; Guiochon, G. Prediction of the Influence of the Heat Generated by Viscous Friction on the Efficiency of Chromatography Columns. *J. Chromatogr. A* **2008**, *1177*, 92–104. [CrossRef] [PubMed]

[52] Gritti, F.; Michel Martin, M.; Guiochon, G. Influence of Viscous Friction Heating on the Efficiency of Columns Operated Under Very High Pressures. *Anal. Chem.* **2009**, *81*, 3365–3384. [CrossRef] [PubMed]

[53] Sainio, T.; Kaspereit, M.; Kienle, A.; Seidel-Morgenstern, A. Thermal Effects in Reactive Liquid Chromatography. *Chem. Eng. Sci.* **2007**, *62*, 5674–5681. [CrossRef]

[54] Sainio, T.; Zhang, L.; Seidel-Morgenstern, A. Adiabatic Operation of Chromatographic Fixed-bed Reactors. *Chem. Eng. J.* **2011**, *168*, 861–871. [CrossRef]

[55] Qamar, S.; Sattar, F.A.; Batool, I.; Seidel-Morgenstern, A. Theoretical Analysis of the Influence of Forced and Inherent Temperature Fluctuations in an Adiabatic Chromatographic Column. *Chem. Eng. Sci.* **2017**, *161*, 249–264. [CrossRef]

[56] Brandt, A.; Mann, G.; Arlt, W. Temperature Gradients in Preparative High-performance Liquid Chromatography Columns. *J. Chromatogr. A* **1997**, *769*, 109–117. [CrossRef]

[57] Vu, T.D.; Seidel-Morgenstern, A. Quantifying Temperature and Flow Rate Effects on the Performance of a Fixed-bed Chromatographic Reactor. *J. Chromatogr. A* **2011**, *1218*, 8097–8109 [CrossRef] [PubMed]

[58] Javeed, S.; Qamar, S.; Seidel-Morgenstern, A.; Warnecke, G. Parametric study of thermal effects in reactive liquid chromatography. *Chem. Eng. J.* **2012**, *191*, 426–440. [CrossRef]

[59] Teutenberg, T. *High-temperature Liquid Chromatography: A Users Guide for Method Development*; RSC Chromatography Monographs; Royal Society of Chemistry: London, UK, 2010.

[60] Horváth C.; Melander, W.; Molnar, I. Solvophobic Interactions in Liquid Chromatography with Nonpolar Stationary Phases. *J. Chromatogr. A* **1976**, *125*, 129–156. [CrossRef]

[61] Antia, F.D.; Horvath, C. High-performance Liquid Chromatography at Elevated Temperatures: Examination of Conditions for the Rapid Separation of Large Molecules. *J. Chromatogr. A* **1988**, *435*, 1–15. [CrossRef]

[62] Snyder, D.C.; Dolan, J.W. Initial Experiments in High-performance Liquid Chromatographic Method Development I. Use of a Starting Gradient Run. *J. Chromatogr. A* **1996**, *721*, 3–14. [CrossRef]

[63] Snyder, L.R.; Dolan, J.W.; Lommen, D.C. Drylab® Computer Simulation for High-performance Liquid Chromatographic Method Development: I. Isocratic Elution. *J. Chromatogr. A* **1989**, *485*, 45–89. [CrossRef]

[64] Poppe, H. Some Reflections on Speed and Efficiency of Modern Chromatographic Methods. *J. Chromatogr. A* **1997**, *778*, 3–21. [CrossRef]

[65] Poppe, H.; Kraak, J.C.; Huber, J.F.K.; Van den Berg, J.H.M. Temperature Gradients in HPLC Columns Due to Viscous Heat Dissipation. *Chromatographia* **1981**, *14*, 515–523. [CrossRef]

[66] Lee, H.; Yang, J.; Chang, T. Branching analysis of star-shaped polybutadienes by temperature gradient interaction chromatography-triple detection. *Polymer* **2017**, *112*, 71–75. [CrossRef]

[67] Ahn, S.; Lee, H.; Lee, S.; Chang, T. Characterization of Branched Polymers by Comprehensive Two-Dimensional Liquid Chromatography with Triple Detection. *Macromolecules* **2012**, *45*, 3550–3556. [CrossRef]

[68] Chen, X.; Rahman, M.S.; Lee, H.; Mays, J.; Chang, T.; Larson, R. Combined Synthesis, TGIC Characterization, and Rheological Measurement and Prediction of Symmetric H Polybutadienes and Their Blends with Linear and Star-Shaped Polybutadienes. *Macromolecules* **2011**, *44*, 7799–7809. [CrossRef]

[69] Lee, S.; Lee, H.; Chang, T.; Hirao, A. Synthesis and Characterization of an Exact Polystyrene-graftpolyisoprene: A Failure of Size Exclusion Chromatography Analysis. *Macromolecules* **2017**, *50*, 2768–2776. [CrossRef]

[70] Godunov, S. K.; Ryaben'kii, V. S. Spectral stability criteria for boundary-value problems for non-self-adjoint difference equations. *Russian Mathematical Surveys* **1963**, *18(3)*, 1.

[71] Rhee, H.-K.; Aris, R.; Amundson, N.R. *First-Order Partial Differential Equations, Vol. I*; Prentice-Hall: Englewood Cliffs, NJ, USA, **1986**.

[72] Rhee, H.-K.; Aris, R.; Amundson, N.R. *First-Order Partial Differential Equations, Vol. II*; Prentice-Hall: Englewood Cliffs, NJ, USA, **1989**.

[73] Mazzotti, M.; Rajendran, A. Equilibrium Theory-Based Analysis of Non-linear Waves in Separation Processess. *Annu. Rev. Chem. Biomol. Eng.* **2013**, *4*, 119–141. [CrossRef] [PubMed]

[74] Evans, Lawrence C. *Partial differential equations. Vol. 19*; American Mathematical Society, **2022**.

[75] LeVeque, R. J. *Finite volume methods for hyperbolic problems (Vol. 31)*; Cambridge university press, **2002**.

[76] Durbin, F. Numerical inversion of Laplace transforms: an efficient improvement to Dubner and Abate's method. *The Computer Journal* **1974**, *17(4)*, 371-376.

[77] Shimadzu Corporation, What is HPLC, Shimadzu. [https://www.shimadzu.com/an/service-support/technical-support/analysis-basics/basic/what_is_hplc.html]